Doctoral Dissertation

Title

Computer-aided diagnosis of diffuse lung abnormalities in digital chest radiography

Author

Shoji Kido

Abstract

For evaluation of the reliability of digital radiography for diagnosing subtle interstitial lung abnormalities, the receiver operating characteristic (ROC) analysis was done for determination of differences among radiologists in interpreting screen-film radiography (SFR) and digital radiography (0.2-mm spatial resolution) on patients who had subtle interstitial lung abnormalities and normal chest findings. It was shown that both in storage phosphor radiography (SPR) and film-digitized radiography (FDR), the overall performance with SFR and digital radiography was identical for diagnosing subtle interstitial lung abnormalities. However, there was a significant dependence of the detection performance on the observer's experience. For chest radiologists, critically important information may be lost in generally used digital radiography systems. Also, to determine what compression ratios are acceptable for digital radiography, the effect of data compression on the detection of subtle interstitial lung abnormalities by use of digitized chest radiographs was evaluated. Our results suggest that a 10:1 data compression ratio does not influence the detection of subtle interstitial lung abnormalities. However, information that is lost with a 20:1 data compression ratio might be essential for interpretation by chest radiologists.

We have been developing a computer-aided diagnosis (CAD) system to detect interstitial lung abnormalities in digital radiography. This system uses the processes of four-directional Laplacian-Gaussian filtering and binarization (4LG/B), linear opacity judgment (LOJ), and linear opacity subtraction (LOS). For quantitative analysis, first, the radiographic index (rI), which is the percentage of opacity areas in an ROI, was obtained and evaluated in the images. These opacities

represented the extracted lung abnormalities. Next, we defined normalized radiographic index (RI), and also defined a combined RI [RI(COM)], which was calculated from two RIs obtained by LOJ and LOS. Abnormal interstitial lung abnormalities were well differentiated from normal by the rIs obtained from the images filtered by 4LG/B and from those processed by LOJ. However, honeycomb lesions and other interstitial abnormalities were differentiated from each other only by the rIs obtained from the image processed by LOJ. Moreover, the RI(COM) provided better results in the mild-abnormality group, but it also yielded good results in the severe-abnormality group. These results indicate that this system of combining RIs using LOJ and LOS has improved the detection performance over that using LOJ only. There were no significant differences between the performance of the CAD system and the mean performance of all radiologists. The performance of the CAD system was inferior to the mean performance of chest radiologists. However, the performance of the CAD system was superior to the mean performance of the residents.

We analyzed interstitial lung abnormalities by using fractal geometry. The fractal dimensions (FDs) obtained from the regions of interest (ROIs) in lungs with interstitial abnormalities were significantly higher compared with those of normal lungs. This result indicates that fractal analysis is useful in distinguishing interstitial lung abnormalities from normal lungs. We also evaluated two physical measures, RI and FD, for quantifying interstitial lung abnormalities. The values of RI are considered to reflect the sensitivity in the detection of interstitial lung abnormalities in chest radiographs. On the other hand, the values of FD are considered to reflect specifically the linear opacities processed by LOJ. The values of both RI and FD may be useful for evaluation of

interstitial lung abnormalities on chest radiographs; however, these two physical measures have different features.

We investigated whether our CAD system can be used for estimating the redistribution of pulmonary blood flow in patients with and patients without mitral stenosis (MS). As a measure of pulmonary blood flow redistribution, the upper/lower radiographic index ratio (U/L) was calculated. The U/L values were correlated with pulmonary capillary wedge pressure values. The mean U/L value of the MS group was significantly higher than that of the non-MS group. This result indicates that our system can be used for quantitative estimation of the redistribution of pulmonary blood flow.

In conclusion, our CAD system is useful for the detection and characterization of diffuse lung abnormalities in digital chest radiography.

Key Words

diagnostic radiology
digital radiography
storage phosphor radiography (SPR)
film-digitized radiography (FDR)
data compression
discrete cosine transform (DCT)
receiver operating characteristic (ROC) analysis
comparative study
computer-aided diagnosis (CAD)
image processing
fractal
interstitial lung disease
pulmonary artery
pulmonary blood flow
pulmonary capillary wedge pressure (PCWP)
mitral stenosis (MS)

Nomenclature

ANOVA	analysis of variance
Az	area under the receiver operating characteristic curve
CAD	computer-aided diagnosis
CLABROC	computer program for ROC analysis produced by CE Metz
CORROC2	computer program for ROC analysis produced by CE Metz
CRT	cathode-ray tube
CT	computed tomography
DCT	discrete cosine transform
4LG/B	four-directional Laplacian-Gaussian filtering and binarization
FCR	Fuji computed radiography
FD	fractal dimension
FDR	film-digitized radiography
Group H	Group of honeycombing lung abnormalities
Group O	Group of other interstitial lung abnormalities
HRCT	thin-section computed tomography
LABROC1	computer program for ROC analysis produced by CE Metz
LOJ	linear opacity judgment
LOS	linear opacity subtraction
MS	mitral stenosis
PACS	picture archiving and communication system
PCWP	pulmonary capillary wedge pressure
rI	radiographic index
RI	normalized radiographic index
RI(COM)	combined radiographic index
rI(4LG/B)	rI obtained from the ROI processed by 4LG/B
RI(4LG/B)	RI obtained from the ROI processed by 4LG/B
rI(LOJ)	rI obtained from the ROI processed by LOJ

RI(LOJ)	RI obtained from the ROI processed by LOJ
rI(LOS)	rI obtained from the ROI processed by LOS
RI(LOS)	RI obtained from the ROI processed by LOS
ROC	receiver operating characteristic
ROCFIT	computer program for ROC analysis produced by CE Metz
ROI	region of interest
SD	standard deviation
SEM	standard error of the mean
SFR	screen-film radiography
SPR	storage phosphor radiography
U/L	upper/lower radiographic index ratio

1 Introduction

A computerized method for assisting radiologists in their interpretation of radiographs is called as a computer-aided diagnosis (CAD). The quantitative measures of radiological information provided by a CAD system can be used by radiologists as a "second opinion" to increase their diagnostic accuracy and consistency. This scheme is expanding rapidly in the field of mammography. And also, a number of automated schemes for CAD are being developed which are designed to assist radiologists in their interpretation of radiographs, because chest radiography constitutes a large part of hospital-based diagnostic examinations. These schemes include the detection and classification of pulmonary abnormalities on chest radiographs, such as lung cancer, interstitial lung abnormalities, and pulmonary vascular abnormalities.

Katsuragawa et al (1, 2) developed a classification method for distinguishing between normal lungs and abnormal lungs with interstitial lung abnormalities. They used a power spectrum analysis and a "visual system response" of human observers. They stated that the results were well corresponded to the visual characteristics that radiologists recognized. They selected regions of interest (ROIs) of 6.4 mm x 6.4 mm size situated between ribs in order to avoid the noise caused by rib structures. However, radiologists read chest radiographs not only by looking at opacities between ribs but also by looking at the opacities overlapped with ribs.

We think the CAD system should not only provide the numeric data but also provide the processed images themselves to radiologists to confirm the results on the radiographs. In our approach, we chose a moderate-sized ROI (51.8 mm x 51.8 mm), and extracted diffuse lung abnormalities themselves. So, the processing results were not only given

as the numeric data of physical measures but also confirmed with radiologists' observation on a cathode-ray tube (CRT). The approach, by which the abnormalities themselves are extracted, is good enough. If radiologists wants to confirm the data provided by our CAD system, he can check the processed images on a CRT in visual form. The outputs obtained from our CAD system can be used by radiologists as a "second opinion" to increase their diagnostic accuracy.

In this dissertation, we first evaluated the image quality of digital radiography for appropriate CAD input. And next, we designed and evaluated a CAD scheme for diffuse lung abnormalities. We proposed and evaluated two types of physical measures, and applied our CAD scheme for two types of diffuse lung abnormalities such as interstitial lung abnormalities and pulmonary vascular abnormalities.

1.1 Digital chest radiography

A picture archiving and communication system (PACS) (3) is an inevitable trend as a means of improving organization and communication within a radiology department and hospital. Digital radiography has many advantages, such as flexible image processing, storage, and transmission. Screen-film radiography (SFR) could ultimately be replaced by digital radiography systems. Digital radiography has two types of image acquisition geometry, conventional and scanning (4). Conventional acquisition geometry systems such as storage phosphor radiography (SPR) and film-digitized radiography (FDR) have the advantages of rapid image acquisition and simplicity as compared with scanning systems such as scanned projection radiography. In conventional acquisition geometry, SPR and FDR are promising modalities, and SPR is now widely used in digital radiography. SPR has wide latitude, and the optical density of the printed hard copy can be optimized automatically (5). SPR systems have a

marked technical performance advantage over conventional bedside radiography in the optimization of image density (6). On the other hand, FDR systems are relatively inexpensive as compared with SPR systems. An FDR system, which consists of a laser optical film digitizer and a display system such as a CRT or a laser printer for printing a hard copy, is suitable for clinical use.

One of the most important factors for digital chest radiography is its image quality. The quality of the digital image is limited by the spatial resolution. The digital radiography system which is widely used has a 0.2-mm spatial resolution. The spatial resolution of generally used digital radiography is lower than that of SFR. This may be a serious problem in the diagnosis of subtle lung abnormalities.

There are many reports dealing with the SPR and its spatial resolution. The pixel size of the generally used SPR is 0.2 mm, and the spatial resolution in SPR is inferior to that of SFR. In the detection of mediastinal lesions and pulmonary nodules, the advantages of SPR, such as a wide dynamic range, automatic density optimization, and flexible image processing, have been reported to overcome the disadvantages of SPR such as the lower spatial resolution. Schaefer et al. (7, 8) reported that SPR was superior to SFR in detecting mediastinal lesions and pulmonary opacities more than 2 cm in diameter. In the detection of subtle lung abnormalities such as pneumothoraces and interstitial infiltrates, the relatively lower spatial resolution causes serious problems. Fajardo et al. (9) reported that four of the 8 observers detected pneumothoraces best with SFR, and the other four detected them similarly with SFR and SPR. On the other hand, Schaefer et al. (7, 10) and Elam et al. (11) reported that no significant differences were found between SFR and SPR in detecting interstitial lung abnormalities. Schaefer et al. (10) evaluated the effect of edge enhancement in diagnosing interstitial lung abnormalities

except for ground-glass opacities, and they concluded that moderate edge enhancement at high frequency (enhancement factor = 3, center of frequencies = 1.4 cycles per millimeter) of SPR could improve the detectability of interstitial pulmonary disease to be nearly the same as that with SFR. High-frequency edge-enhanced processing decreases the signal-to-noise ratio, and the quantum mottle of the images increases with high-frequency edge-enhancement. This is thought to be the reason why ground-glass opacities are difficult to recognize even with moderately high-frequency edge-enhanced images. For spatial resolution requirements, Lams et al. (12) reported that the requirement for a septal line was likely to be 0.4 mm. MacMahon et al. (13), reported that 0.2-mm pixel images could be acceptable in clinical use.

The FDR system, which is widely used also has a 0.2-mm spatial resolution. The spatial resolution of FDR is also lower than that of SFR. The image quality of FDR depends on that of the original SFR to be digitized (14). The latitude of FDR is limited by that of SFR, and the latitude of FDR is less than that of SPR. This may be a serious problem in the diagnosis of subtle lung abnormalities. MacMahon et al. reported that the diagnostic accuracy of mild interstitial infiltrates and subtle pneumothoraces with the 0.1-mm pixel FDR was inferior to that of SFR, but that 0.2-mm pixel FDR could be acceptable in clinical use (13). It was also reported that a system with automated density optimization correction of digitized radiographs has been developed, and that this system could compensate for the smaller latitude of FDR (15).

Another important factor for digital radiography is the management of extremely large amounts of digital image data. Digital radiography systems generate a large number of images to be stored and transmitted in PACS systems. In the Osaka University Hospital, approximately 350,000 radiographs are obtained per year. If the mean

size of images is 8 megabytes (2000 x 2000 pixels; 10 bits per pixel; 2 bytes are used for storage), approximately 2,800 gigabytes of image data would be generated each year. Image data compression is one possible solution to the problem of storing and transmitting such large data sets. However, the image deterioration that occurs at high compression ratios might make subtle changes, such as interstitial lung abnormalities, more difficult to diagnose.

Image data compression techniques can be divided into two categories: reversible and irreversible. Reversible compression allows perfect reconstruction of the original image and provides compression ratios of between 2:1 and 3:1 (16). Irreversible compression provides higher compression ratios, but degrades the quality of the image (17). Several investigations have attempted to determine the highest acceptable compression ratio for chest radiography. Ishigaki et al. (18) reported that images compressed at a 25:1 ratio were inferior to images compressed at a 20:1 ratio for detection of nodules and linear shadows on chest radiographs. They concluded that the highest acceptable compression ratio was 20:1. MacMahon et al. (19) suggested that compression ratios as high as 25:1 might be acceptable for primary diagnosis in chest radiography. Aberle et al. (20) proposed that compression ratios of 20:1 might be acceptable. Two discrete cosine transform (DCT) image compression techniques are commonly used: the "full-frame" and the "block" technique. In full-frame DCT, the size of the image must be in powers of 2, and a large amount of memory is required for processing. However, block artifact will not occur (21). In block DCT, images of any size can be input, and less memory is required for processing. However, a block artifact can occur because compression is performed block by block (22). Recently, an adaptive algorithm that

reduces block artifact in block DCT (23-25) has been developed. When this algorithm is used, adaptive DCT is superior to other DCT methods.

1.2 CAD for interstitial lung abnormalities

For diagnosis of interstitial lung abnormalities, chest radiography remains the most common of imaging procedures, which is used as an indicator for the necessity of further imaging examinations such as computed tomography (CT) (26). Interpretation of interstitial lung abnormalities in chest radiographs is one of the important and difficult problems in radiologists' daily clinical work. However, evaluation of interstitial lung disease with chest radiographs is quite difficult. One reason is that various kinds of radiographic patterns are observed, and their changes are often subtle (27). The other reason is that the descriptions of radiographic findings by radiologists often lack objectivity and quantitativeness. If radiographic patterns of interstitial lung disease seen on chest radiographs can be quantitatively analyzed by a computerized system, these objective data may improve the diagnostic accuracy.

Many investigators have reported computer-aided methods for evaluating interstitial lung diseases in chest radiography. The method of texture-analysis is often used for quantitative analysis of interstitial lung abnormalities (1, 2, 28-30). In texture-analysis of the lung zone, a statistical approach has often been used. The density variation and the optical Fourier spectrum were used as physical measures for classifying lungs with interstitial disease. As to an application domain of quantitative analysis, quantification of the severity of pneumoconiosis is frequently reported (31-35). Other than in pneumoconiosis, there are many reports in which the authors have distinguished normal lungs from abnormal lungs with interstitial diseases by classification of the abnormality by using their texture analysis methods (1, 2, 28-30).

1.3 Fractal analysis for interstitial lung abnormalities

Fractal geometry can be used for investigating complicated objects such as clouds, coastlines, and anatomic structures (36). Fractal characteristics are evaluated quantitatively in terms of the fractal dimension (FD) (37). Objects with a higher FD appear more complex compared to those with a lower FD. Thus, the value of the FD seems to reflect the complexity of the objects (36). Some reports showed that fractal geometry was useful in evaluating radiographic patterns. Majumdar et al. (38) reported that fractal geometry was useful in distinguishing osteoporotic bone structures from normal bone, and Caligiuri et al. (39) reported that fractal geometry was helpful for better determination of fracture risk in osteoporosis. Honda et al. (40, 41) noted that the fractal pattern was useful as a numeric grading of the complexity of the ductal patterns and the progression of parotid gland disease. Caldwell et al. (42) characterized mammographic breast tissue patterns by using FD. Regarding lung structure analysis, Mandelbrot suggested that the airway in the lung has fractal structures (36). We consider it reasonable to analyze complexities of lung anatomical structures by using fractal geometry.

1.4 CAD for pulmonary blood flow

Interpretation of vascular structure abnormalities in chest radiography is another important problem, because redistribution of pulmonary blood flow on chest radiographs is a good indicator by which one can evaluate pulmonary venous hypertension in congestive heart disease, such as valvular disease (43-45). The earliest recognizable level of redistribution occurs when there is equal perfusion of the upper and lower lung zones (32). As redistribution becomes more pronounced, the size and number of vessels in the upper lung zone may actually exceed

those seen in the lower lung zones. The physiologic mechanism for redistribution of pulmonary blood flow is subject to controversy (45-47). It has been reported that the degree of pulmonary blood flow redistribution is more sensitive to small elevations in pulmonary capillary wedge pressure (PCWP) than are other radiographic signs of pulmonary hypertension, such as pulmonary vascular blurring and alveolar edema (32). Baumstark et al. (48) reported a positive correlation between the presence of radiographic signs of congestive heart failure and elevation of the PCWP values. However, in daily clinical practice, the diagnosis of redistribution is based on the observer's experience in analyzing the size and number of vessels normally seen in the upper lung zone. Thus, we think that the CAD system would improve the diagnostic accuracy in radiologists' interpretations.

2 ROC analysis of digital radiography system

2.1 Storage phosphor radiography

To evaluate the reliability of SPR for diagnosing subtle interstitial lung abnormalities, we evaluated the differences among radiologists in interpreting SFR and SPR by using subtle interstitial lung abnormalities (49).

2.1.1 Study group

Our study group consisted of 80 patients who were referred to the Osaka University Hospital between May 1990 and May 1991. All patients underwent thin-section CT (HRCT) of the chest due to clinical indications, and posteroanterior SFR and SPR within one week of the HRCT examination. Forty of the 80 had subtle interstitial lung abnormalities, and the other 40 had normal lung parenchyma. The average age of the 40 patients with interstitial lung abnormalities was 48.0 ± 14.0 years (range of 23 - 75 years; 16 men and 24 women), and the average age of the 40 patients with normal lung parenchyma was 37.3 ± 14.0 years (range of 18 - 70 years; 16 men and 24 women). The HRCT examinations consisted of multislice (1.5 or 2.0 mm thick) scans at 10- or 20-mm intervals through the chest. The images were reconstructed with the bone algorithm (a GE9800 scanner, General Electric Medical Systems, Milwaukee, or a Quantex scanner, Yokogawa Medical Systems, Tokyo, Japan). The presence or absence of subtle interstitial abnormalities was evaluated on HRCT images, and the HRCT findings were used as the standard of reference. Two radiologists who did not participate as observers selected these 40 patients from more than 200 patients with interstitial lung abnormalities. Although all interstitial lung diseases included in this study group were judged as subtle, the severity and extent of abnormalities

observed on HRCT were divided into 2 groups: minimal (n = 17) and mild (n = 23). Minimal interstitial pulmonary abnormalities observed on HRCT were thought to be very difficult to detect on chest radiographs, and mild changes seen on HRCT were thought to be relatively easy to detect on chest radiographs.

The radiographic patterns found on HRCT in the 40 patients consisted of fine reticular opacities (n = 19), ill-defined, faint, small nodular opacities up to 3 mm in diameter (n = 13), and ground-glass opacities (n = 11). Three patients had both fine reticular opacities and ground-glass opacities. Fine reticular opacities were caused by peribronchovascular interstitial thickening, interlobular septal thickening, intralobular linear opacities, subpleural thickening, or small honeycombing. Faint small nodular opacities were either interstitial nodules or air-space nodules less than 3 mm in diameter. Cases with nodules more than 4-5 mm in diameter were discarded. Ground-glass opacities reflected minimal interstitial thickening (thickening of the alveolar wall) or subtle air-space disease. The observers were instructed to ignore the following abnormalities that were present in some patients: old tuberculous changes such as pleural thickening and calcification (n = 3) and bullous emphysema (n = 1). In 34 patients, the cause of the interstitial lung abnormalities was known: collagen vascular disease (n = 16), hypersensitivity pneumonitis and diffuse panbronchiolitis (n = 10), metastatic calcification (n = 2), sarcoidosis (n = 2), alveolar proteinosis (n = 2), and eosinophilic granuloma (n = 2). In the remaining 6 patients, interstitial lung abnormalities were of unknown cause.

2.1.2 Image acquisition

All SFR and SPR images were obtained with a conventional chest unit under the conditions of 130 kVp, 1.0-mm nominal focus, 200-cm

film-focus distance, and 12:1 Bucky. The SFR images were obtained with Du Pont C-4D (Du Pont Corp., Wilmington, DE) and the BF-III screens (Kasei Optonix Corp., Tokyo, Japan). The speed of the SFR was 100 (relative speed). The SPR images were obtained with storage phosphor imaging plates (ST III; Fuji Photo Film, Tokyo, Japan). The size of these imaging plates was 14 x 14 inches. The imaging plates were read by Fuji computed radiography (FCR7000; Fuji Photo Film, Tokyo, Japan), and the digital data (spatial resolution = 0.2 mm, 1760 x 1760 pixels, 10 bits) were stored on an optical disk cartridge.

In order to study the effect of different film formats, we used two formats of laser-printed SPR hard copies; one was a full-size SPR image (same size as the SFR image, 14 x 14 inches) with a default mode, and the other was a minified SPR image (2/3 size of the SFR image, 9 x 9 inches) with a default mode. However, a full-size image (14 x 14 inches) could not be directly printed onto a hard copy by this FCR system, because the maximum size of the hard copy was 9 x 9 inches. Therefore, we took one lung from each full-size image and placed it onto two hard copies, so that different portions of the chest image were printed onto each hard copy and then the hard copies were manually reconnected. A default mode approximated the appearance of a conventional radiograph, so that the density and contrast of the two formats of SPR were closely matched to those of SFR. In practice, SPR images were processed with a sigmoid, long-contrast Hurter and Driffield curve and very slight, density-dependent edge enhancement at high frequencies (enhancement factor = 0.3, with enhanced frequency range greater than about 0.1 cycle per millimeter. The values of the parameters are as follows; GT = E, GA = 0.9, GC = 1.6, GS = -0.2, RT = R, RE = 0.3, RN = 0 (GT: gradient type, GA: gradient angle, GC: gradient center, GS: gradient shift, RT: response type, RE: response enhancement, RN: response rank). A pair of

SPR images (7 x 7 inches, 1760 x 1760 pixels, 0.2-mm spatial resolution, 10 bits) is usually printed on a hard copy in commercially available FCR systems; one is the image without image processing or with a default mode, and the other is the image with an edge-enhanced mode. However, the purpose of this study was to estimate whether the quality of SPR was enough for clinical use in the cases of subtle interstitial pulmonary abnormalities, and not to estimate the mediastinal abnormalities. Of course, some of the pulmonary abnormalities, such as mediastinal lesions and pulmonary opacities greater than 2 cm in diameter, were easily detected with an edge-enhanced mode (7), but the abnormalities we dealt with in this study were quite different. For theses reasons, we used only one SPR image (14 x 14 inches or 9 x 9 inches) with a default mode for the readings.

2.1.3 Reading methods

For two reasons, we used only one lung (either the right or the left lung) of each patient for the reading sessions. One reason was that the maximum hard-copy size that we could obtain was 9 x 9 inches. In order to obtain a full-size SPR image (14 x 14 inches), we had to use four 9 x 9-inch hard copies, onto which different portions of the chest image were printed, and these had to be connected skillfully. It was because this was so complicated that we used either the right lung or the left lung instead of both lungs for each patient. A hard copy of one lung could be obtained from two 9 x 9-inch hard copies. The other reason was that a single lung was thought to minimize the educational effect or the effect of practice from the reading sessions. Three image sets (SFR set, full-size SPR set, and minified SPR set) of the right lung (n = 42) and left lung (n = 38) were divided into two reading subsets (right lung session and left lung session). When the right lung was evaluated, the left lung was covered

with black paper. Two reading sessions were carried out with at least a 2-week interval between sessions. To minimize reading order bias, all images in each image set were randomly intermingled for each session, and the order of the three image sets was changed for each session. Three different images of the same patient were evaluated in each reading session.

The reading sessions were carried out by 14 observers. Seven of the 14 were experienced practicing chest radiologists (whom we have called "chest radiologists"), and the other 7 were senior residents (whom we have called "residents"). All of the chest radiologists had more than 10 years' experience in reading SFR images in their daily practice, whereas residents did not have much experience in reading SFR images (average, was 3.6 years). In terms of familiarity with SPR, there was no significant difference between the two groups, because SPR was confined to portable images for intensive-care radiology and emergency radiology in our hospital.

Before each session, three image sets of three educational cases that were not included in the study were shown. Each observer was instructed that lung abnormalities in this series were subtle interstitial abnormalities, and asked to describe separately the presence of abnormalities using a five-level scale of confidence (1: definitely negative, 2: probably negative, 3: possibly positive, 4: probably positive, 5: definitely positive). No other clinical information was supplied, and the observers did not know the percentage of normal cases. No limit was imposed on the reading time.

2.1.4 Data analysis

Observer performance for the three image modalities (sets) was tested by receiver operating characteristic (ROC) analysis (50-52). Perceptual accuracy was described by the area under the ROC curve (Az)

(53). The average Az and the standard error of the mean (SEM) were obtained by individual fitting of ROC curves to the confidence ratings of each observer and averaging of the estimated areas for all observers. Composite ROC curves were calculated by averaging of the slope parameters and the intercept parameters of the observer curves. However, for statistical analysis, averaged Az values were obtained from the individually fitted ROC curves to the confidence ratings of each observer and averaging of the estimated areas across the observers. We used Az values to test the significance of the differences by means of the paired t-test.

2.1.5 Results

For subtle interstitial-infiltrate detection, no significant differences in observer performance for the 14 observers were observed among SFR, full-size SPR, and minified SPR **(Figure 2.1). Table 2.1a-b** shows the results of ROC analysis for the two groups (7 chest radiologists and 7 residents) for each modality. SFR was significantly superior to the two formats of SPR in the observer performance of the 7 chest radiologists ($P < 0.01$).**(Figure 2.2)**. For the 7 residents, on the other hand, there were no significant differences in observer performance with SFR and full-size SPR, but SFR was significantly inferior to the minified SPR ($P < 0.05$) **(Figure 2.3)**. The perceptual accuracies of each modality obtained from the 7 chest radiologists was superior to those obtained from the 7 residents. The perceptual accuracy of the 7 chest radiologists was superior to that of the 7 residents in conventional SFR ($P < 0.001$) and in minified SPR ($P < 0.05$), but no significant differences were observed in full-size SPR **(Figure 2.4)**. The best perceptual accuracy was obtained with SFR as evaluated by the 7 chest radiologists from among the three modalities evaluated by each group ($P < 0.01$). As to the difference between full-size

SPR and minified SPR, no significant differences were observed by both the 7 chest radiologists and the 7 residents.

2.1.6 Summary

The results obtained for all 14 observers indicated that no significant differences between SFR and the two formats of SPR were observed. However, the results obtained for the 7 chest radiologists indicated that the two formats of SPR showed a loss of diagnostic accuracy in the detection of subtle interstitial lung abnormalities. For the 7 residents, on the other hand, SFR was significantly inferior to minified SPR, but there were no significant differences with full-size SPR.

As to the image size, for the 14 observers, no significant differences were observed in our study among full-size SPR (0.2-mm pixel size), minified SPR (0.13-mm pixel size), and SFR. However, for the 7 chest radiologists, significant differences were observed between the two formats of SPR and SFR. On the other hand, there were no significant differences between full-size SPR and minified SPR. After the reading session, eleven of the 14 observers (79%) commented on the impression of superiority of the full-size images, but our results indicated that size may not be a critical factor for storage phosphor images.

The important result of this study is that the best perceptual accuracy was obtained with SFR as evaluated by chest radiologists among the perceptual accuracies of each modality as evaluated by each group. This indicates that some critically important information for diagnosing subtle interstitial lung abnormalities could be lost in the SPR (0.2-mm pixel size, 10 bits) which is generally used today.

2.2 Film-digitized radiography

To evaluate the reliability of FDR for diagnosing subtle interstitial lung abnormalities, we evaluated the differences among radiologists in interpreting SFR and FDR by using subtle interstitial lung abnormalities (54).

2.2.1 Image acquisition

We used same SFR as in the comparative study of SFR and SPR. The FDR images were obtained from the SFR images with a laser optical film digitizer (KFDR-S; Konica Corp, Tokyo, Japan). This device was capable of reproducing a radiograph in digitized form with density and contrast accurately matched to those of the original radiograph. The output data (10 bits) are proportional to the optical density. Optical density 0 corresponds to the output data 0, and optical density 3.0 corresponds to the output data 1023. The time required to digitize a 14 x 14-inch (35 x 35 cm) film was about 20 seconds. A hard copy of digital data (spatial resolution = 0.175 mm, 2000 x 2000 pixels, 10 bits) was obtained by use of a prototype laser printer. The size of the FDR hard copies was the same as that for SFR, 14 x 14 inches. In order to obtain the same size hard-copy FDR image as that for SFR, we employed an interpolation method to expand the original image matrix. In our FDR system, the printed matrix size was smaller than the acquired matrix size (printed matrix size, 0.1 mm; acquired matrix size, 0.175 mm). The interpolation we used was performed by expanding each pixel as twice in the x- and y-axes.

2.2.2 Reading methods

We used two image sets (SFR set and FDR set) of the right lung (n = 42) and left lung (n = 38). Two reading sessions were carried out by 10 observers. All observers read the SFR set first and then the FDR set. The

interval between the two sessions (SFR session and FDR session) was at least 3 months. Five of the 10 observers were chest radiologists, and the other five were residents. The images in each image set were divided into two reading subsets (right-lung subset and left-lung subset). All images in each image subset were randomly intermingled for each observer. Each observer read the two subsets separated by at least a 1-week interval. When the right lung was being evaluated, the left lung was covered with black paper.

Before each session, three images not included in this study were shown as educational cases. All observers were told that lung abnormalities in this series were subtle interstitial abnormalities, and they were asked to rate the presence of abnormalities by using a five-level scale of confidence (1: definitely negative, 2: probably negative, 3: possibly positive, 4: probably positive, 5: definitely positive). No other clinical information was given, and the observers did not know the percentage of normal cases. No time limit was imposed on the reading sessions.

2.2.3 Results

There were no significant differences in the overall performance of all observers in the detection of subtle interstitial lung abnormalities between SFR and FDR (**Figure 2.5**). The results of ROC analysis of chest radiologists and residents for SFR and FDR are shown in **Table 2.2**. For the chest radiologists, SFR was superior to FDR (P = 0.003) (**Figure 2.6**). For the residents, on the other hand, there were no significant differences between SFR and FDR (**Figure 2.7**). Both in SFR and FDR, the observer performance of chest radiologists was superior to that of residents (SFR, P = 0.001, and FDR, P = 0.021) (**Figure 2.8**). The best observer performance was obtained with SFR evaluated by chest radiologists.

2.2.4 Summary

The overall performance with SFR and FDR was identical when they were used for the detection of subtle interstitial lung abnormalities. The observer performance was, however, significantly dependent on observer experience. For chest radiologists, SFR was significantly superior to FDR. For residents, no significant differences were observed between SFR and FDR. The observer performance was significantly better in both SFR and FDR for chest radiologists than for residents. The ability of chest radiologists to diagnose subtle interstitial lung abnormalities was greater than that of residents. The chest radiologists, who have more diagnostic ability, can extract more information from SFR than from FDR in the diagnosis of subtle interstitial lung abnormalities. Thus, that the best observer performance was obtained with SFR read by chest radiologists in this study is reasonable. We believe the reason for this is as follows: In the diagnosis of subtle interstitial lung abnormalities, careful observation of the peripheral lung parenchyma and sufficient experience with such subtle abnormalities is mandatory. For residents, their concentration and experience is insufficient.

2.3 Image data compression

To determine what degree of compression is acceptable, we studied the accuracy with which subtle interstitial lung abnormalities were detected on digitized chest radiographs, which were uncompressed and compressed at various ratios (55).

2.3.1 Image acquisition

We selected 78 SFR images from our image data base. Thirty-eight of the 78 had subtle interstitial lung abnormalities (mean age, 47.7 ± 14.0

years, 16 men and 22 women); the other 40 had normal lung parenchyma (mean age, 37.3 ± 14.0 years, 16 men and 24 women). Interstitial lung abnormalities on chest radiographs were caused by collagen vascular disease (n = 16), hypersensitivity pneumonitis and diffuse panbronchiolitis (n = 10), metastatic calcifications (n = 2), sarcoidosis (n = 2), eosinophilic granulomas (n = 2), and unknown causes (n = 6).

The digitized data were compressed at ratios of 10:1, 20:1, and 30:1, after which images were reconstructed from the compressed data. The compression method used in this study is based on the adaptive DCT coding technique (17, 56) and is irreversible. First, an original digital image is divided into 16 x 16 image blocks, each of which is converted to transform coefficients by the DCT. Next, quantification and frequency cut-off are performed, the parameters of which determine the compression ratio and image quality. For obtaining digital radiographs with minimal image degradation, the combination of these two parameters should be optimized in each block for the selected compression ratio. The larger the quantification interval, the higher the compression ratio; the lower the cutoff frequency, the higher the compression ratio. Finally, coding is performed, and the image data are compressed at a given ratio.

Because, this compression method is irreversible, the reconstructed image is inferior in quality to the original image. The image quality deteriorates further because compression is performed block by block (22), causing prominent boundaries to be formed between blocks in the reconstructed image. To reduce this "block artifact," we employed adaptive processing based on the properties of the blocks (57).

The hardware for data compression and decompression used in this study was a prototype module designed by the Konica Corporation. Approximately 4 seconds are required for compression or decompression of an image (spatial resolution = 0.175 mm, 2000 x 2000 pixels, 10 bits).

Uncompressed FDR images and images compressed at three compression ratios were printed with a prototype laser printer (Konica Corporation). The digital chest images and the original radiographs were of the same size (14 x 14 inches).

Uncompressed and compressed images of the right (n = 41) and left (n = 37) lungs were placed in random order and divided into four right-lung and four left-lung reading subsets. In each subset, images from the same chest did not appear more than once.

2.3.2 Reading methods

Ten radiologists participated as observers. Five were chest radiologists and five were residents. Each observer read each of the eight subsets with at least a 1-week interval between readings. To minimize reading-order bias, the order in which the subsets were read was different for each observer and the images in each subset were placed in random order before each reading session. At the beginning of each reading session, three images not included in this study were shown as educational cases. Each observer was asked to examine each image and to indicate separately, using a five-level scale of confidence (1: definitely negative, 2: probably negative, 3: possibly positive, 4: probably positive, 5: definitely positive), whether he believed that a subtle interstitial abnormality was present. No other clinical information was given, and the observers did not know the ratio of normal to abnormal cases or the ratio of uncompressed to compressed images. No time limit was imposed on the reading sessions.

Observer response data were analyzed by ROC techniques. We compared uncompressed images with each of the three compressed images to determine the threshold for acceptable compression when there were no detectable differences between uncompressed and compressed images.

For statistical analysis, we used the jackknife method described by Dorfman et al. (58), which takes into account the sampling of both images and readers. The pseudo-values obtained from the jackknife method were tested by the analysis of variance (ANOVA) technique.

2.3.3 Results

For all observers, the detection of subtle interstitial lung abnormalities with 30:1 compressed images was less accurate than that with uncompressed images ($P < 0.05$; **Figure 2.9**). For chest radiologists, the detection of subtle interstitial lung abnormalities with 20:1 and 30:1 compressed images was less accurate than that with uncompressed images ($P < 0.05$; **Table 2.3**, **Figure 2.10**). For the residents, however, there was no significant difference in the detection of subtle interstitial lung abnormalities with uncompressed images and that with images at any of the three compression ratios ($P \geq 0.05$; **Figure 2.11**). The most accurate reading was that by chest radiologists using uncompressed images. For each set of uncompressed and compressed images, chest radiologists performed as well as or better than residents.

2.3.4 Summary

For all observers, there was a significant difference between the detection of subtle interstitial lung abnormalities with uncompressed images and that on 30:1 compressed images, but no significant difference was found between interpretations of uncompressed images and those of 20:1 compressed images. However, for chest radiologists, the detection of abnormalities with 20:1 compressed images was less accurate than that with uncompressed images. For residents, however, no significant differences were observed between interpretations of uncompressed images and those of images compressed at ratios of 30:1 or less.

Our results suggest that interstitial lung abnormalities would be diagnosed as accurately with images compressed at a 10:1 ratio as with uncompressed images, because no significant difference was found between interpretations of uncompressed images and images compressed at a 10:1 ratio by either chest radiologists or residents ($P \geq 0.05$). For all observers as a group, there was no statistical difference in detection when 20:1 compressed images were used. However, for experienced chest radiologists, the detection of subtle interstitial lung abnormalities with use of 20:1 compressed images was significantly less accurate than with uncompressed images. This result suggests that clinically important information needed for diagnosis of subtle interstitial lung abnormalities might be lost in 20:1 compressed images.

3 CAD for interstitial lung abnormalities

3.1 Laplacian-Gaussian filtering and linear opacity judgment

Various kinds of interstitial radiographic patterns are observed in chest radiographs of patients with interstitial lung disease. However, it is difficult to extract all patterns. Four basic roentgenographic patterns of interstitial diseases are presented: #1 reticular, #2 nodular, #3 reticulonodular, and #4 linear (59). These patterns are correlated with their CT findings. These four basic patterns were thought to consist of two patterns. One is "nodular" (mainly from #2 and #3), and the other is "linear" (mainly from #1, #3, and #4). We roughly divided these radiographic patterns into two groups, a nodular opacity group and a linear opacity group. A CAD system that we have developed can selectively extract the linear opacities processed by Laplacian-Gaussian filtering and binarization (4LG/B) and by linear opacity judgment processing (LOJ) (60).

3.1.1 CAD scheme

The overall scheme of our computer-analyzing system is shown in **Figure 3.1**. First, chest radiographs were digitized, and ROIs were selected in the right upper and lower lung zones. In order to extract linear opacities selectively, we performed 4LG/B and LOJ processing for each ROI. Finally, the radiographic index (rI), which is a percentage of opacity areas in an ROI, was defined for evaluating the chest radiographs as a physical measure.

3.1.2 Digitization of chest radiographs

Conventional posteroanterior chest radiographs were digitized to a 2000 x 2000 matrix with 1024 gray levels by a laser scanner [Konica

Corp., Tokyo, Japan]. In order to select ROIs for image processing and analyzing, we displayed the digitized image of the full chest radiograph on a CRT. Two ROIs with a 296 x 296 matrix size (51.8 mm x 51.8 mm) were selected manually in a right upper and a right lower lung zone.

One ROI was selected at the level of the upper pulmonary hilum in the right upper zone, and the other was selected above the diaphragm. In order to avoid hilar anatomic structures, we selected both ROIs apart from the hilum (**Figure 3.2**). When we had selected an ROI in the left lower lung zone, the ROI overlapped the cardiac opacity, which caused poor image processing results. Therefore, we excluded this area in this evaluation. There was no such problem in the left upper lung zone. However, in order to evaluate our system by as many cases as possible and to avoid the bias based on the upper or lower lung zone, we selected one ROI in the right upper lung zone and one ROI in the right lower lung zone of each case. In our study, no significant differences were found between the upper and lower ROIs. Therefore, we did not discriminate between ROIs according their positions.

3.1.3 Four-directional Laplacian-Gaussian filtering

In order to extract linear opacities in the selected ROI, we chose the Laplacian-Gaussian filter, which reflected the human visual perception (61). This filter is described

$$\nabla^2 G(r) = \frac{2\sigma^2 - r^2}{2\pi\sigma^6} e^{-\frac{r^2}{2\sigma^2}},$$

where G(r) is the Gaussian distribution, r is the distance from the center of the filter, and σ is the spatial spread parameter, which corresponds to the standard deviation. This filter enhances elements of linear opacities in all directions. For this reason, we employed a new directional one-dimensional Laplacian-Gaussian filter, which enhances specific directional elements. This filter is described

$$\nabla^2 G(x) = \frac{1}{\sqrt{2\pi}\sigma^5}(x^2-\sigma^2)\, e^{-\frac{x^2}{2\sigma^2}},$$

where x is the coordinate axis perpendicular to a specific direction α_i. We changed i from 1 to 4 ($\alpha_1 = 0$, $\alpha_2 = \pi/4$, $\alpha_3 = \pi/2$, $\alpha_4 = 3\pi/4$) and obtained four processed images by using these four directional Laplacian-Gaussian filters. The matrix size of this filter was 15 x 15 pixels (2.625 mm x 2.625 mm), and a width of the line at the center of this filter was set to 5 pixels (0.875 mm). The width (2σ; σ = standard deviation) of the center line of the filter corresponds to the range between the 1/e points of both sides of the maximum of the Gaussian function. In this study, we used the same Laplacian-Gaussian filter for all images.

In the image after processing, some peripheral part of the ROI became ineffective. Therefore, the following processing was carried out in a submatrix of 256 x 256 (44.8 mm x 44. 8mm).

The Laplacian-Gaussian filter has a band-pass characteristic with a peak at $1/(\sqrt{2}\pi\sigma)$. The spatial frequency to be detected can be adjusted by taking a suitable σ. This enables us to detect interstitial lung abnormalities well with the reduced noise. Moreover, this filter corresponds to a physiologic model of human vision (61). Therefore, we could expect the results to be similar to the interpretations of the radiologists. We set σ at 0.438 mm in this system, because there was a relation of $w = 2\sigma$, where w was the width of the line at the center of the filter. Because a suitable diameter of peripheral vessel opacities was thought to be about 0.5-1.0 mm, the value of w had to be set below this value. However, the noise will increase if σ is reduced. Therefore, we decided to keep w at the above-mentioned value.

Another advantage of the Laplacian-Gaussian filter was that the correction of the background trend caused by normal anatomic structures

and the exposure condition was not required, because the background trend frequency was low enough compared with $1/(\sqrt{2}\pi\sigma)$.

The original Laplacian-Gaussian filter does not have a specific directionality, but emphasize in all directions equally. However, in order to extract linear elements of interstitial chest abnormalities, it was necessary for the filter to have various directions on the image plane. Therefore, in our system, filters with four directions, horizontal, vertical, and two diagonal directions ($\alpha_1 = 0$, $\alpha_2 = \pi/4$, $\alpha_3 = \pi/2$, $\alpha_4 = 3\pi/4$), were used. This filter is not a pure Laplacian-Gaussian filter, since though Laplacian means the sum of the 2nd-order derivatives in the horizontal and vertical axes, our filter is only the 2nd-order derivative in one direction. However, we called this filter a directional Laplacian-Gaussian filter or simply a Laplacian-Gaussian filter. The Laplacian-Gaussian filter used in our system could extract a opacity in a specific direction. However, other elements as well as the linear opacities were also extracted. Moreover, the extracted linear opacity elements were not necessarily continuous, and the output image contained scattered pixel patterns. For extracting the linear opacities selectively well, further judgment processing of linear opacities was required. We could understand that the first 4-directional Laplacian-Gaussian filters extracted very short linear opacities or candidate pixels of linear opacities, and the second LOJ processing selected long opacities or true linear opacities from these pixels. Theoretically, similar results can be obtained if the linear opacities are extracted by use of a large-scale Laplacian-Gaussian filter with many directions. However, such a method is actually impossible because of it requires a large amount of calculations.

3.1.4 Binarization

Binarization was done for each image which had been processed with the 4-directional Laplacian-Gaussian filter. Then the summation image was

obtained by addition of the four binary images. As to selecting a suitable threshold of binarization that can extract only interstitial lung opacities, we have no conclusive method. One reason is that various kinds of radiographic patterns are included and their changes are often subtle (27), and the other reason is that the descriptions of radiographic patterns that radiologists use often lack objectivity and quantitativeness. So, at first, we selected 5 candidates of the threshold for 20 cases, based on the observations of radiologists. Next, we decided one threshold for this system based on the results of the preliminary study. This same threshold was applied to all images.

3.1.5 Linear opacity judgment

In order to extract linear opacities selectively, we carried out a method of LOJ for the four binary filtered images **(Figure 3.3)**. In this method, we choose a search line method (62) which detects linear opacity elements.

The search line method used in the LOJ is a method of detecting straight line segments directly on the image plane. This method was applied separately to each of the binary images obtained by 4LG/B, and finally the summation image was obtained by addition of the four LOJ images. This was because, if the judgment processing was done after summing of the 4LG/B output, specification of the linear opacity direction became difficult. This might result in errors in LOJ.

First, a search line of θ and Ls is selected on all pixels within the ROI, where θ is a certain direction and Ls is the length of the search line. Next, the number (N) of pixels (pixels with values greater than zero) on the search line is counted. If N is greater than a threshold, Ts, these pixels are determined to be elements of the linear opacity. In addition, if pixels do not continuously distribute, pixels between the pixels which are

determined as elements of the linear opacity are interpolated. For each pixel in the image, this process is repeated for θ at every $\pi/36$ interval within the range from $\alpha_i - \pi/4$ to $\alpha_i + \pi/4$.

In each case of i ($\alpha_1 = 0$, $\alpha_2 = \pi/4$, $\alpha_3 = \pi/2$, $\alpha_4 = 3\pi/4$), the processed image of LOJ is obtained. Finally, the summation image is obtained by addition of the four processed images of LOJ. In this study, we decided that Ls was 30 pixels (5.25 mm) and Ts was 24 pixels (4.2 mm). These values were determined from the results of a preliminary study using some cases.

In **Figure 3.4**, LOJ images obtained from a normal case and an abnormal case correspond, respectively, to the normal case and the abnormal case in **Figure 3.2**. Figures (a) and (b) are the processed images of the normal case, and (c) and (d) are the processed images of the abnormal case. Figures (a) and (c) are the summation images of 4LG/B, and (b) and (d) are the summation images of LOJ.

3.1.6 Radiographic index

In order to evaluate interstitial lung opacities, we defined a radiographic index (rI) already introduced as a physical measure. The rI is the percent area of extracted opacities to the area of the ROI. This physical measure was thought to be one of the most simple index as in order to evaluate our method, and it correlated well with the extent of interstitial lung abnormalities. The rI was obtained from the summation image of the four images processed with 4LG/B, and from that of the four processed images of LOJ.

3.1.7 Image data base

The image data base consisted of 50 patients with interstitial lung abnormalities and 50 patients with normal lung parenchyma. We used the

right lungs of the chest radiographs. All 100 patients underwent HRCT of the chest. In this study, all of the 50 patients with interstitial lung abnormalities had abnormalities both in a right upper and a right lower lung zone, and all of the 50 patients with normal lung parenchyma had no abnormalities in a right upper and a right lower lung zone. The average age and one standard deviation (SD) of the 50 patients with interstitial lung abnormalities was 57.5 ± 11.8 years (27 men and 23 women), and that of the 50 patients with normal lungs was 38.6 ± 13.2 years (24 men and 26 women). In each case, an HRCT scan of the chest was carried out within one week of the chest radiographic examination. The interstitial lung abnormalities were evaluated on the HRCT images, and HRCT findings were used as the standard of reference for this study.

For evaluating our system, interstitial lung opacities found on HRCT were classified into the following two patterns: #1. Honeycomb lesions (group H): honeycomb opacities were found to be dominant on HRCT. This group often represents typical linear opacities in chest radiographs. #2. Others (group O): abnormal opacities were found on HRCT, but these were excluded from #1. This group included pulmonary abnormalities such as small nodular opacities and ground-glass opacities. Each ROI selected in the chest radiographs was classified according to its corresponding HRCT findings in two groups (#1: group H; n=21; #2: group O; n=79).

3.1.8 Results

The results of the radiographic indices, rI(4LG/B) obtained from the ROIs processed by 4LG/B, and rI(LOJ) obtained from the ROIs processed by LOJ, are shown in **Figure 3.5a**. Significant differences in each of the radiographic indices were observed between the normal group and the abnormal group ($P < 0.001$) **(Table 3.1)**.

The results of the radiographic indices, rI(4LG/B) and rI(LOJ), between group H and group O, are shown in **Figure 3.5b**. **Table 3.2** shows that significant differences were observed in rI(LOJ) between group H and group O (P = 0.37), whereas no significant differences were observed in rI(4LG/B) between group H and group O (P = 0.58).

3.1.9 Summary

We defined two types of rIs as physical measures. One was obtained from the images only processed by 4LG/B, and the other was obtained from the images processed by LOJ. Our CAD system could detect and classify interstitial lung abnormalities on digitized chest radiographs which were confirmed with HRCT. The results of evaluating whether this system was able to detect and to classify interstitial lung abnormalities from the digitized chest radiographs were as follows: Both rI(4LG/B) and rI(LOJ) made it possible to distinguish between normal cases and abnormal cases. Therefore, this system was able to detect interstitial lung abnormalities seen by digital chest radiography. Only in rI(LOJ), significant differences were observed between group H and group O. This indicated that more linear opacities were extracted with LOJ than with the corresponding images of 4LG/B.

3.2 Linear opacity judgment and linear opacity subtraction

The main feature of LOJ was the extraction of linear opacities, because extracting various other types of radiographic patterns seen in chest radiographs was thought to be difficult. This method could differentiate abnormal lungs from normal lungs, and honeycombing lesions in the interstitial lung abnormalities from other interstitial lung abnormalities (interstitial changes other than honeycombing) (60). In this method, other elements in addition to linear opacities were also extracted

in the first image processed with 4LG/B; however, these elements were ignored in the LOJ processing. Therefore, we made an attempt to use these extracted elements for the improvement of our CAD system.

In this section, we added, as a third stage, a process that subtracts the second image, which is processed by LOJ, from the first image, which is processed by 4LG/B. Moreover, we defined a new physical measure, which we called the "combined radiographic index," calculated from the rIs obtained from the images of the LOJ process and its subtraction process (63).

3.2.1 Modified CAD scheme

In our modified scheme, we added three processes to our previous method: a process that subtracts the image processed by LOJ from the image processed by 4LG/B, normalization of the radiographic index, and calculation of the combination of physical measures. The overall scheme of our new algorithm is shown in **Figure 3.6**.

3.2.2 Linear opacity subtraction

In LOJ, short linear elements below the threshold of the filtered image could not be extracted. For evaluation of the degree of severity of interstitial lung disease, which included various types of radiographic patterns, another method that used short linear elements was needed. To use the short linear elements that were not extracted by the search line method, we employed the linear opacity subtraction (LOS) technique. The subtraction image C(i,j) is defined by the following expression:

$$C(i,j) = A(i,j) - B(i,j);$$

$$\text{if } C(i,j) < 0, \text{ then } C(i,j) = 0,$$

where A(i,j) is the image obtained from 4LG/B, and B(i,j) is the image obtained from LOJ. To eliminate the linear opacities of anatomic

structures, we used a greater length Ls for the search line and a higher threshold Ts than were used for the previous LOJ method. The value of Ls was 50 pixels (8.75 mm), and that of Ts was 40 pixels. The LOS images in **Figure 3.7**, obtained from a normal case and an abnormal case, correspond, respectively, to the normal case and the abnormal case in **Figure 3.2**.

3.2.3 Normalized radiographic index

To evaluate interstitial lung opacities quantitatively, we have already defined an rI. With this method, we were able to obtain three different rIs as physical measures. One was rI(4LG/B), expressing the percent area of the binary summation image A(i,j) in the ROI obtained by 4LG/B. The second was rI(LOJ), expressing the percent area of the LOJ summation image B(i,j) in the ROI, and the last was rI(LOS), expressing the percent area of the subtraction image C(i,j) in the ROI.

We defined a new index calculated from the rIs obtained from the LOJ outputs and LOS outputs. To define the new index, we normalized these rIs by using the average and standard deviation of the rIs obtained from the normal control group, which was not included in the study population. We used 25 cases for the normal control group. We defined the normalized radiographic index (RI) by the following expression:

$$RI = (rI - rI'_m) / \sigma'_m ,$$

where rI'_m is the average value of the rIs in the control group and σ'_m is the standard deviation of those. This normalization was performed for the right upper lung zone and for the right lower lung zone. The RI(4LG/B), RI(LOJ), and RI(LOS) were obtained from the ROIs processed by 4LG/B, LOJ, and LOS, respectively.

3.2.4 Combined radiographic index

To detect interstitial lung abnormalities in both mild- and severe-abnormality cases, we defined a new quantitative physical measure which we called the "combined radiographic index, RI(COM)," which was obtained from RI(LOJ) and RI(LOS). This is defined by the following expressions:

$$RI(COM) = \text{minimum } [RI(LOJ), RI(LOS)] \quad \text{for } RI(LOJ) < 1 \text{ and } RI(LOS) < 1,$$

$$RI(COM) = \text{maximum } [RI(LOJ), RI(LOS)] \quad \text{for } RI(LOJ) \geq 1 \text{ and } RI(LOS) \geq 1,$$

$$RI(COM) = [RI(LOJ) + RI(LOS)] / 2 \quad \text{otherwise.}$$

3.2.5 ROC analysis

The ability to detect interstitial lung abnormalities on chest radiographs with these physical measures was evaluated by ROC analysis. To produce ROC curves, we used a five-level scale of confidence which described the presence of abnormalities. The classification of severity for each index was defined as follows:

$T = 0$ for $RI < 0.5$

$T = \text{int } (RI)$ for $0.5 \leq RI < 3.5$

$T = 4$ for $RI \geq 3.5$,

where T is the number of categories and represents the degree of severity (0 is minimum and 4 is maximum). The "int" is the operator which makes RI into an integer. To compare the performance of RIs, we compared the Az values by use of the CORROC2 computer program (CE Metz, Department of Radiology, University of Chicago, Chicago, IL).

3.2.6 Results

Figure 3.8(a) and Table 3.3 show the results for the normal group and for the entire interstitial lung abnormality group. The RI(COM) (Az = 0.96 ± 0.16), was significantly better than the RI(4LG/B) (Az = 0.94 ± 0.21; P = 0.027), RI(LOJ) (Az = 0.87 ± 0.35; P = 0.002), and the RI(LOS) (Az = 0.90 ± 0.04; P = 0.005).

Figure 3.8(b) and Table 3.3 show the results for the normal group and the mild-abnormality group. The RI(COM) (Az = 0.94 ± 0.02) was significantly better than the RI(4LG/B) (Az = 0.89 ± 0.03; P = 0.011) and the RI(LOJ) (Az = 0.81 ± 0.05; P = 0.0004). However, there were no significant differences between RI(COM) and RI(LOS) (Az = 0.90 ± 0.04; P = 0.26).

Figure 3.8(c) and Table 3.3 show the results for the normal group and the severe-abnormality group. There were no significant differences between RI(COM) (Az = 0.98 ± 0.01) and RI(4LG/B) (Az = 0.99 ± 0.01; P = 0.71), and RI(COM) and RI(LOJ) (Az = 0.99 ± 0.01; P = 0.27). However, RI(COM) was significantly better than RI(LOS) (Az = 0.83 ± 0.06; P = 0.0072).

For RI(COM), RI(4LG/B), and RI(LOJ), the detection of interstitial lung abnormalities in the severe-abnormality group was better than that in the mild-abnormality group [RI(COM): P = 0.022, RI(4LG/B): P = 0.0009, RI(LOJ), P = 0.0001]. For RI(LOS), however, there were no significant differences between the normal group and the severe-abnormality group (P = 0.30).

3.2.7 Summary

To improve the performance of our CAD system, we attempted to utilize short extracted linear opacity elements that were ignored in the LOJ method. For this reason, we added a third-stage process that subtracted the second image, processed by LOJ, from the first image,

processed by 4LG/B. Furthermore, to evaluate interstitial lung opacities quantitatively, we defined an RI.

In the mild-abnormality group, RI(LOS) performed better than did RI(LOJ). On the other hand, in the severe-abnormality group, RI(LOJ) performed better than did RI(LOS). The reason for these results can be explained as follows:

Fewer extracted opacities were processed by LOJ in the mild-abnormality group than in the severe-abnormality group. However, in both groups, similar numbers of extracted opacities were normal anatomic structures, such as ribs and vessels. Therefore, in cases involving mild abnormalities, a higher proportion of extracted opacities were normal anatomic structures than in cases involving severe abnormalities. These results suggest that RI(LOJ) was less quantitative in the mild-abnormality group than in the severe-abnormality group, because the effect of normal anatomic structures was relatively greater in the former group. On the other hand, RI(LOS) performed better in the mild-abnormality group. The proportion of elements not judged to be linear opacities was relatively greater, and, as a result of the LOJ, the effect of normal anatomic structures could be ignored.

With 4LG/B, extracted elements were more densely distributed in severe than in mild abnormalities. With the search line method in the LOJ process, the more densely the extracted elements are distributed, the more easily they are judged as elements of linear opacities, and the greater is the number of pixels interpolated as elements of linear opacity. Therefore, the extracted elements in severe abnormalities tended to be more easily judged as elements of linear opacities than were the more sparsely distributed elements in mild abnormalities. After LOS, more opacities were obtained in the severe-abnormality group than in the mild-abnormality group; however, fewer opacities were obtained than were

expected when compared with cases involving mild abnormalities. This difference degraded the performance of RI(LOS) compared with that of RI(LOJ) in the severe-abnormality group.

Our results suggest that, in the mild-abnormality group, it would be better to use RI(LOS), obtained from the LOS; however, in the severe-abnormality group, it would be better to use RI(LOJ), obtained from the LOJ. A physical measure that is useful in cases with both mild and severe abnormalities would be desirable. We thought that we could get better performance by combining the two indices. The new single index, RI(COM), provided better results in the mild- than in the severe-abnormality group, but also showed good results in the severe-abnormality group. This index was superior to either RI(LOJ) or RI(LOS) alone.

As a result of adding LOS to our LOJ method, we could employ RI(COM). The performance of RI(COM) was significantly superior compared with the performance of RI(4LG/B) and of RI(LOJ) in the mild-abnormality group. The performance of RI(COM) is equivalent to the performance of RI(4LG/B) and of RI(LOJ) in the severe-abnormality group. Thus, we were able to improve the performance of our CAD system compared with the system using LOJ only, especially in the mild-abnormality group.

3.3 Performance of CAD versus radiologists

We have proposed a CAD system for detecting and classifying interstitial lung abnormalities (60, 63). We evaluated the performance of our CAD system compared with that of radiologists, using normal cases and abnormal cases that had interstitial lung abnormalities (64).

3.3.1 Study group

The study group consisted of 40 patients who underwent conventional radiography and HRCT of the chest within one week. Twenty of the 40 had interstitial lung abnormalities (average age, 46.5 ± 12.6 years, 10 men and 10 women), and the other 20 had a normal lung parenchyma (average age, 38.5 ± 1.3 years, 9 men and 11 women).

3.3.2 Analysis by CAD

Our CAD system consists of 4LG/B, LOJ, and LOS. For quantitative analysis, we defined RI(COM) as a physical measure. For each patient, two RI(COM) were obtained from the right upper and right lower lung zones. We used the larger of these two indices as a measure of the severity of the interstitial lung abnormality in a patient.

3.3.3 Observations by radiologists

Observations of chest radiographs were carried out by 14 radiologists. Seven of the 14 observers were chest radiologists, and the other seven were residents. The observers read 40 images of right lungs on a view box. The left lungs were covered with black paper. All images in the reading set were randomly intermingled for each observer. Before each session, three images not included in this study were shown as educational cases. All observers were told that lung abnormalities in this series were subtle interstitial abnormalities, and they were asked to rate separately the presence of abnormalities by using a five-level scale of confidence (1: definitely negative, 2: probably negative, 3: possibly positive, 4: probably positive, 5: definitely positive). No other clinical information was given, and the observers did not know the percentage of normal cases. No time limit was imposed on the reading sessions.

3.3.4 Data analysis

Both the performance of our CAD system and that of the radiologists in detecting interstitial lung abnormalities on chest radiographs were evaluated by ROC analysis. Az values for the 14 observers were obtained by use of the ROCFIT computer program (CE Metz, Department of Radiology, University of Chicago, Chicago, IL). The Az values of RI(COM) were calculated directly on the continuous data. Az values were obtained by use of the LABROC1 computer program (CE Metz).

3.3.5 Results

Figure 3.9 shows the results for four kinds of RIs. The performance of RI(LOS) (Az = 0.89) and RI(COM) (Az = 0.88) was superior to that of RI(4LG/B) (Az = 0.80) and RI(LOJ) (Az = 0.77). The performance of RI(COM) was significantly superior to that of RI(4LG/B) and RI(LOJ) (P = 0.018 and 0.015, respectively). However, the performance of RI(LOS) was not significantly superior to that of RI(4LG/B) and RI(LOJ) (P = 0.13 and 0.096, respectively). There were no significant differences between the performance of RI(COM) and that of RI(LOS) (P = 0.45).

Table 3.4 and **Figures 3.10a-b** show the results obtained by the 14 radiologists and RI(LOS) and RI(COM). There were no significant differences between the performance of RI(LOS) and the mean performance of the 14 radiologists (Az = 0.89 and 0.89 ± 0.06, respectively; P = 0.89). The performance of RI(LOS) was inferior to the mean performance of the 7 chest radiologists (Az = 0.89 and 0.94 ± 0.03, respectively; P = 0.0074). However, the performance of the CAD system was superior to the mean performance of the 7 residents (Az = 0.89 and 0.84 ± 0.03, respectively; P = 0.0024) **(Figure 3.10a)**. On the other hand, there were no significant differences between the performance of

RI(COM) and the mean performance of the 14 radiologists (Az = 0.88 and 0.89 ± 0.06, respectively; P = 0.68). The performance of RI(COM) was inferior to the mean performance of the 7 chest radiologists (Az = 0.88 and 0.94 ± 0.03, respectively; P = 0.035). However, the performance of RI(COM) was superior to the mean performance of the 7 residents (Az = 0.88 and 0.84 ± 0.03, respectively; P = 0.0060) **(Figure 3.10b)**.

3.3.6 Summary

The performance of our CAD system was superior to that of the residents. However, the performance did not exceed that of the chest radiologists. Thus, the performance of the CAD system was at an intermediate level between that of the chest radiologists and that of the residents.

In this study, we did not determine the threshold of the CAD system, because many more cases were required for determining an appropriate threshold for distinguishing between normal and abnormal lungs. However, if we had set the threshold of the CAD system at 3.0, this system may have discerned 17 of the 20 normal cases correctly (N1 - N17) and 18 of the 20 abnormal cases (A3 - A20) (**Table 2a, b**). The sensitivity of the system may be 0.90, and its specificity may be 0.85. On the other hand, if the threshold of the radiologists were set at 3.0, in the normal lungs, the chest radiologists may have discerned 15 normal cases correctly, and the residents may have discerned 17 normal cases correctly (**Table 3.5a**). Also, in the abnormal lungs, the chest radiologists may have discerned 19 abnormal cases correctly, and the residents may have discerned 15 abnormal cases correctly (**Table 3.5b**).

The mean sensitivity of the chest radiologists may be 0.92 ± 0.02, and that of the residents may be 0.84 ± 0.06. Also, the mean specificity

of the chest radiologists may be 0.80 ± 0.16, and that of the residents may be 0.79 ± 0.17 (**Table 3.6**). Both this system and the radiologists may have misdiagnosed three cases (N19, N20, A2). However, the CAD system may have discerned three cases correctly that the chest radiologists misdiagnosed (N8, N13, N15), and five cases that the residents misdiagnosed (N8, A3, A4, A5, A14). In these cases, the CAD system would aid both chest radiologists and residents. Similarly, the computerized analysis system may have misdiagnosed one case that both chest radiologists and residents diagnosed correctly (A1). In this case, the reliance of radiologists on the CAD system would have reduced their accuracy. Considering the performance of the CAD system combined with radiologists' judgment, we think that the use of computerized outputs as a "second opinion" can improve the detectability by both chest radiologists and residents. Thus, we believe that we should determine an appropriate threshold for the diagnosis by using more cases in future studies.

4 Fractal analysis for interstitial lung abnormalities

4.1 Quantification by fractal dimension

We attempted to quantify interstitial lung abnormalities which were confirmed on HRCT by using fractal geometry (65).

4.1.1 Fractal geometry

The fractal dimension (FD) can be obtained in several different ways. We used a box-counting method for determining the FDs (37, 66, 67). If the box size d which covers an object changes, then the number of boxes N(d) required to cover the object will change. For example, **Figure 4.1** shows that a closed curve is covered with boxes of size d. In the case illustrated, N(d) is 16. Likewise, for each ROI, we counted N(d) for different sizes of d.

For a fractal object, it is assumed that the number of boxes N(d) is proportional to d^{-FD}. The relationship between d and N(d) is defined as,

$$N(d) = \mu d^{-FD},$$

where μ is a constant. From this relationship, the FD is determined as follows,

$$\ln N(d) = -FD \ln d + \ln \mu .$$

We applied this box-counting method to the output of 4LG/B and LOJ. In this output, linear opacities of interstitial lung abnormalities on chest radiographs were selectively extracted. These extracted linear opacities were intended to be interstitial lung abnormalities themselves.

First, for a given size d, a grid of boxes that covered the whole ROI was generated by computer. It counts the number of boxes N(d) required to cover the extracted linear opacities in the ROI. This process was repeated by variation of d. In this study, the number of boxes d in a side of an ROI was selected as 3m+15, where m ranged from 0 to 9. Thus, for

each ROI, we obtained ten sets of d and N(d). Next, by plotting ln d and ln N(d) on a log-log scale, we calculated the FD as the slope of the regression line by the least-squares method.

4.1.2 Results

Examples of the double logarithmic curves of box d versus the number of boxes N(d) are shown in **Figure 4.2**. The upper line was obtained from the ROI in a lung with interstitial abnormalities, and the lower line was obtained from the ROI in a normal lung. The value of the FD was calculated from the slope of the curve. In this case, the value FD for the case involving interstitial lung abnormalities was calculated as 1.75, and that for the normal lung was calculated as 1.26.

The results for the FDs obtained from our image data base (100 ROIs in lungs with interstitial abnormalities and 100 ROIs in normal lungs) are shown in **Table 4.1**. The mean value of the FDs obtained from the ROIs in the lungs with interstitial abnormalities was 1.67 ± 0.10, and that in the normal lungs was 1.44 ± 0.12. The FDs obtained from the ROIs in the lungs with interstitial abnormalities were significantly higher than those of the normal lungs ($P < 0.001$). The mean value of the FDs obtained from the ROIs in the upper lobes of the lungs with interstitial abnormalities was 1.68 ± 0.08, and that in the lower lobes was 1.65 ± 0.11. However, the mean value of the FDs obtained from the ROIs in the upper lobes of the normal lungs was 1.46 ± 0.12, and that in the lower lobes was 1.42 ± 0.12. In both the upper and lower lungs, there were significant differences in the FDs between the ROIs of lungs with interstitial abnormalities and those of normal lungs ($P < 0.001$).

4.1.3 Summary

Many anatomic and physiologic processes of the human body, including the lung structure, may be explained by means of fractal concepts. In particular, the tracheobronchial tree structure is an example of anatomic fractals (68, 69). In this study, two-dimensional fractal analysis was able to distinguish interstitial lung abnormalities from normal lungs on digitized chest radiographs. However, lung structure is three-dimensional, and thus three-dimensional fractal geometry may be required. However, two-dimensional fractal analysis is correlated with the complexity of radiographic patterns of interstitial lung abnormalities on chest radiographs.

4.2 Comparison of radiographic index and fractal dimension

To evaluate quantitatively the outputs obtained with our CAD system, we defined two physical measures. One was a normalized radiographic index (RI) (60, 63), and the other was a fractal dimension (FD) (65). In section 3.2, the combination of values of RI obtained from LOJ and LOS was shown to have high sensitivity in distinguishing a group of interstitial lung abnormalities from a normal group, especially in the case of mild interstitial lung abnormalities (63). FDs also proved to be useful in distinguishing an interstitial lung abnormality group from a normal lung group (65).

In this study, we evaluated the performance of these two physical measures obtained from our CAD system (70).

4.2.1 Calculation of physical measures

We selected 50 ROIs with mild interstitial lung abnormalities, 50 ROIs with severe interstitial lung abnormalities, and 50 ROIs with normal lung parenchyma from our data base of digitized chest radiographs. In each group, the number of ROIs selected from the upper lung zones and

that of ROIs selected from the lower lung zones were the same. The average age and gender of the individuals were closely matched among the three groups.

The values of RI were obtained as the normalized percent area of extracted opacities in selected ROIs. The values of FD were calculated with a box-counting algorithm.

The performance of these physical measures was evaluated by ROC analysis. To describe the observer performance, we calculated the Az directly on the continuous data of values of RI and FD. The significance of the differences between Az values was evaluated by use of the CLABROC computer program (CE Metz).

4.2.2 Results

In the normal and mild-abnormality groups, the values of RI performed less well in the LOJ images (Az = 0.812 ± 0.042) than in the LOS images (Az = 0.912 ± 0.028; $P < 0.05$), and the values of FD performed better in the LOJ images (Az = 0.867 ± 0.037) than in the LOS images (Az = 0.750 ± 0.048; $P < 0.05$). The values of FD (Az = 0.864 ± 0.036) performed better than those of RI (Az = 0.814 ± 0.042; $P < 0.05$) in the LOJ images. On the other hand, the values of RI (Az = 0.912 ± 0.028) performed better than those of FD (Az = 0.752 ± 0.048; $P < 0.0001$) in the LOS images (**Table 4.2**). In the normal and severe-abnormality groups, both values of RI and FD performed better in the LOJ images (RI: Az =0.992 ± 0.007; FD: Az = 0.968 ± 0.016) than in the LOS images (RI: Az = 0.883 ± 0.034; $P < 0.001$, FD: Az = 0.767 ± 0.047; $P < 0.0001$), and the values of RI performed better than those of FD in LOJ images (RI: Az =0.992 ± 0.006; FD: Az = 0.964 ± 0.018; $P < 0.05$) and LOS images (RI: Az =0.883 ± 0.034; FD: Az = 0.767 ± 0.047; $P < 0.01$) (**Table 4.3**).

4.2.3 Summary

The values of FD performed better in LOJ images than in LOS images in both the mild- and severe-abnormality groups. In the normal and severe-abnormality groups, the values of RI performed better than those of FD in both LOJ and LOS images. On the other hand, in the normal and mild-abnormality groups, the values of RI performed better than did those of FD in LOS images. However, the values of FD performed better than those of RI in LOJ images. This indicates that the values of FD may correlate better with the amounts of extracted linear opacities than do the values of RI, especially in the mild-abnormality group.

5 CAD for pulmonary vasculature

We investigated whether our CAD system can be used for estimating the redistribution of pulmonary blood flow on chest radiographs. We carried out an evaluation of the redistribution of pulmonary blood flow in patients with mitral stenosis (MS) and in patients without MS (71).

5.1 Study group

The study group consisted of 15 male patients with MS and 15 male patients without MS. MS is the most common cause of chronic pulmonary vascular hypertension. Of the 15 male patients without MS, six had normal hearts, and the remaining 9 patients had coronary artery disease. All of the non-MS patients in this study underwent cardiac catheterization because of a suspicion of coronary artery disease. As a result of the cardiac catheterization studies, some were diagnosed as having coronary artery disease, and the others were diagnosed as normal. Erect posteroanterior chest radiographs were taken of each patient immediately before cardiac catheterization. Pulmonary capillary wedge pressure (PCWP) was measured in the supine position. We used the right lungs of the chest radiographs for this analysis. The average age of the 15 patients with MS was 57.0 ± 6.3 years, and that of the 15 patients without MS was 56.4 ± 7.7 years. The mean PCWP values of the 15 patients with MS was 26.1 ± 8.4 mmHg, and that of the 15 patients without MS was 13.1 ± 4.0 mmHg **(Figure 5.1)**.

5.2 CAD scheme

The overall scheme of our CAD system is shown in **Figure 5.2**. First, chest radiographs were digitized, and ROIs were selected in the right upper and lower lung zones. In order to enhance linear opacities

selectively, we performed 4LG/B for each ROI. As a measure of the pulmonary blood flow redistribution, the upper/lower radiographic ratio (U/L) was calculated.

5.3 Upper/lower radiographic index ratio

To measure the pulmonary blood flow redistribution, we defined the U/L as the ratio of the percent area of extracted opacities to the area of the ROI. Cephalization of pulmonary vascular flow is visible toward the upper lung zones. In non-MS patients, the vessels in the lower lung zones carry a greater blood flow than do those in the upper lung zones, due to the effect of gravity, and they are therefore visibly larger than the upper lung zone vessels on chest radiographs. On the other hand, in MS patients, the blood flow in the upper lung zones increases because of raised intravascular pressure and the blood flow in the lower lung zones is diminished because of vasoconstriction or interstitial edema. Thus, a blood flow pattern that is inverted compared to the normal one is seen in erect chest radiographs. Based on these results, the U/L values for MS patients are expected to be greater than those of non-MS patients.

5.4 Results

The output images shown in **Figure 5.1**, obtained from a normal case and an abnormal case, correspond, respectively, to the non-MS case and the MS case in **Figure 5.3**. Figures (a) and (b) are the processed images of the non-MS case, and Figures (c) and (d) are the processed images of the MS case.

The overall correlation between the U/L values and the PCWP values for the 30 male patients is shown in **Figure 5.4**. In all patients, the U/L values were correlated with the PCWP values (mean PCWP value, 20.3 ± 9.5; mean U/L value, 1.10 ± 0.13; $r = 0.405$; $P = 0.025$).

In the 12 patients whose PCWPs were below or equal to 15 mmHg (non-MS, 11; MS, 1), the U/L values were well correlated with PCWP values (mean PCWP value, 11.5 ± 2.5; mean U/L value, 1.06 ± 0.13; r = 0.689; P = 0.011). In the 18 patients whose PCWPs were above 15 mmHg (non-MS, 4; MS, 14), the U/L values were not correlated with PCWP values (mean PCWP value, 25.7 ± 8.8; mean U/L value, 1.14 ± 0.12; r = 0.313; P = 0.210) (**Table 5.1**).

The mean U/L value for the 15 male patients without MS was 1.05 ± 0.09, and the mean U/L value for the 15 male patients with MS was 1.16 ± 0.14. The mean value for the MS group was significantly higher than that of the non-MS group (P = 0.016) (**Table 5.2**).

5.5 Summary

We used computer-aided analysis based on 4LG/B to evaluate the redistribution of pulmonary blood flow in digital chest radiographs. In our study, the U/L values were correlated with the PCWP values, especially in the cases whose PCWP values were below or equal to 15 mmHg. The U/L values are thus thought to reflect the distribution of the pulmonary vasculature.

As determined in this section, MS and non-MS groups had statistically different mean values of the U/L index; however, there was much overlap of individual values. Thus, this analysis can be useful in a CAD scheme where high values of U/L are used to raise the suspicion level of the radiologist as to the presence of MS.

6 Conclusion

The possibility of automated diagnosis has been discussed in the field of medical image processing, and many trials have been done. However, the image diagnosis by radiologists is based on a highly sophisticated ability of pattern recognition that requires experience and knowledge. It is reported that, although completely automated computer interpretation of complex images such as chest radiographs is unlikely to be achieved in the foreseeable feature, CAD is a realistic goal. A computerized diagnostic program could assist the radiologist by identifying probable areas of abnormality (4).

With our CAD system, the processing results are not only obtained as numerical data, but a radiologist can check the processed images on a CRT screen in visual form. The outputs obtained from the CAD system can be used by radiologists as a "second opinion" to increase their diagnostic accuracy. Also, our CAD system could be especially useful for obtaining quantitative data for follow-up of known diffuse lung abnormalities.

Concerning the spatial resolution requirement, despite the fact that the overall performance with SFR and with 0.2-mm spatial-resolution digital radiography is identical, our results suggest that spatial resolution is a very important factor, and that 0.2-mm spatial-resolution digital images may be inadequate when used in the detection of subtle interstitial lung abnormalities. We currently use high-resolution SPR images and high-resolution FDR images. These images have a 0.1-mm or lower spatial resolution. Ikezoe et al. (72) reported that there were no significant differences between SFR and 0.1-mm spatial-resolution SPR in the detection of simulated subtle interstitial lung abnormalities. However, with the status of today's computer technology, extremely large amounts

of data cannot be managed in a short time. For this reason, data from digital radiography systems are somewhat difficult to manage without lower spatial resolution or without data compression. As to what data compression ratios are acceptable, our results suggest that a 10:1 compression ratio does not influence the detection of subtle interstitial lung abnormalities. However, in situations in which early detection of subtle abnormalities is important, our results indicate that 20:1 compression may be inappropriate.

From the viewpoint of designing a CAD system, it is difficult to use images of extremely large size and with data compression for processing directly. We used uncompressed digital images in our CAD system. The pixel size of the digitized chest radiographs which we used was 0.175 mm. This spatial resolution is generally used in digital radiography. Concerning the spatial-resolution requirement, Katsuragawa et al. (73) reported that 0.2-mm pixel images were acceptable in lung texture analysis. For experienced radiologists and for subtle abnormal cases, 0.2-mm spatial-resolution digital radiography may be insufficient; however, the overall performance with SFR and 0.2-mm spatial-resolution digital radiography is identical. Therefore, we think that this spatial resolution is reasonable for the design of a CAD system.

Also, for designing a CAD system, it is important to choose suitable physical measures which represent, both quantitatively and objectively, the results obtained with that system. We have proposed two physical measures. One is a radiographic index and the other is a fractal dimension. We evaluated these two physical measures by using the same outputs obtained from our CAD system. Both physical measures are useful for evaluation of diffuse lung abnormalities on chest radiographs; however, these two physical measures have different features. So, we can

use these physical measures for the classification of diffuse lung abnormalities on chest radiographs.

In general, for radiologists who do not have much experience in reading chest radiographs, the CAD system is useful for improving their diagnosis. On the other hand, for chest radiologists who have considerable experience in reading chest radiographs, CAD may not improve their diagnosis. However, the results of our study indicate that the CAD system would aid chest radiologists, also, in making a diagnosis.

The new points of our dissertation are the diagnostic physical measures for detection of diffuse lung abnormalities whose performances are superior to the detectabilities of residents, and the new method for the displaying the CAD results.

Our CAD system may become the basis for the construction of a CAD system of diffuse lung abnormalities in digital chest radiography.

Acknowledgment

The author thanks Professor Shinichi Tamura for his kind advice and encouragement.

Table 2.1a

Az Values for 7 Chest Radiologists According to Image Modality

Observer	SFR	SPR x 1	SPR x 2 /3
1	0.933	0.918	0.891
2	0.926	0.913	0.921
3	0.911	0.879	0.882
4	0.953	0.902	0.929
5	0.859	0.831	0.847
6	0.912	0.887	0.886
7	0.927	0.925	0.874
Mean ± SEM	0.917 ± 0.004	0.893 ± 0.005	0.890 ± 0.004

SFR: Screen-film radiography, SPR x 1: full-size storage phosphor radiography, SPR x 2/3: minified storage phosphor radiography, SEM: standard error of mean.

Table 2.1b

Az Values for 7 Residents According to Image Modality

Observer	SFR	SPR x 1	SPR x 2/3
1	0.875	0.920	0.893
2	0.814	0.798	0.860
3	0.821	0.815	0.870
4	0.791	0.805	0.868
5	0.854	0.870	0.829
6	0.803	0.925	0.852
7	0.798	0.836	0.835
Mean ± SEM	0.822 ± 0.004	0.853 ± 0.008	0.858 ± 0.003

SFR: Screen-film radiography, SPR x 1: full-size storage phosphor radiography, SPR x 2/3: minified storage phosphor radiography, SEM: standard error of mean.

Table 2.2

Az Values for Chest Radiologists and Residents According to Image Modality

Observer	SFR	FDR
Chest Radiologists		
1	0.93	0.92
2	0.93	0.91
3	0.87	0.86
4	0.91	0.89
5	0.95	0.93
Mean ± SEM	0.92 ± 0.01	0.90 ± 0.01
Residents		
1	0.93	0.92
2	0.93	0.92
3	0.93	0.92
4	0.93	0.92
5	0.93	0.92
Mean ± SEM	0.84 ± 0.01	0.85 ± 0.01

SFR: Screen-film radiography, SPR: storage phosphor radiography, SEM: standard error of the mean.

Table 2.3

Az Values for Chest Radiologists and Residents for Uncompressed and Compressed Images

		Compressed		
Observer	Uncompressed	10:1	20:1	30:1
Radiologists				
1	0.93	0.93	0.89	0.86
2	0.92	0.88	0.89	0.86
3	0.91	0.91	0.87	0.87
4	0.88	0.92	0.88	0.85
5	0.85	0.83	0.81	0.83
Mean ± SEM	0.90 ± 0.01	0.89 ± 0.02	0.87 ± 0.02	0.86 ± 0.01
Residents				
1	0.88	0.88	0.87	0.85
2	0.86	0.88	0.84	0.78
3	0.86	0.87	0.90	0.87
4	0.85	0.87	0.90	0.87
5	0.80	0.79	0.73	0.60
Mean ± SEM	0.85 ± 0.01	0.86 ± 0.02	0.85 ± 0.03	0.79 ± 0.05

SEM: Standard error of mean

Table 3.1

Radiographic Indices of Normal and Abnormal Lungs

	Normal	Abnormal	P-value
rI(4LG/B)	25.6 ± 6.1	39.3 ± 4.8	$P < 0.001$
rI(LOJ)	16.6 ± 6.4	30.4 ± 6.3	$P < 0.001$

Each value is mean ± one standard deviation.

rI(4LG/B): rI processed by 4LG/B

rI(LOJ): rI processed by LOJ

Table 3.2

Comparison of Radiographic Indices and Image Features of HRCT

	Honeycombing	Others	P-value
rI(4LG/B)	41.1 ± 2.7	38.8 ± 5.2	P = 0.058
rI(LOJ)	33.0 ± 3.4	29.8 ± 6.8	P = 0.037

Each value is mean ± one standard deviation.

rI(4LG/B): rI processed by 4LG/B

rI(LOJ): rI processed by LOJ

Table 3.3

Az Values for Interstitial Lung Abnormalities

	Total	Mild	Severe
RI(4LG/B)	0.94 ± 0.21	0.89 ± 0.03	0.99 ± 0.01
RI(LOJ)	0.87 ± 0.35	0.81 ± 0.05	0.99 ± 0.01
RI(LOS)	0.90 ± 0.04	0.90 ± 0.04	0.83 ± 0.06
RI(COM)	0.96 ± 0.16	0.94 ± 0.02	0.98 ± 0.01

Each value is the mean ± one standard deviation.

RI: Normalized radiographic index

4LG/B: Four-directional Laplacian-Gaussian filtering and binarization

LOJ: Linear opacity judgment

LOS: Linear opacity subtraction

COM: Combined radiographic index

Table 3.4

Az Values for Radiologists for Detection of Interstitial Lung Abnormalities

Chest radiologists	Az
1	0.94
2	0.96
3	0.92
4	0.94
5	0.88
6	0.95
7	0.97
Mean ± SD	0.94 ± 0.03

Residents	Az
1	0.87
2	0.85
3	0.85
4	0.84
5	0.86
6	0.83
7	0.79
Mean ± SD	0.84 ± 0.03

Table 3.5a

Five-Level Scale of Scores for Normal Lungs Obtained from CAD System and by Radiologists

	Mean ± SD		
Case	#1	#2	#3
N1	-0.71	1.43 ± 0.49	1.14 ± 0.35
N2	0.81	2.00 ± 1.07	2.71 ± 1.58
N3	1.05	1.29 ± 0.45	1.57 ± 1.05
N4	1.16	1.14 ± 0.35	1.57 ± 1.05
N5	1.21	2.29 ± 0.88	2.00 ± 0.76
N6	1.36	2.57 ± 1.40	1.71 ± 0.70
N7	1.37	2.43 ± 0.90	2.29 ± 1.48
N8	1.55	3.57 ± 0.90*	3.29 ± 1.48*
N9	1.78	1.29 ± 0.45	1.43 ± 0.49
N10	1.78	3.00 ± 1.31	2.57 ± 1.05
N11	1.94	2.14 ± 0.99	2.57 ± 1.18
N12	2.09	2.14 ± 0.83	2.29 ± 1.48
N13	2.23	3.43 ± 1.18*	3.00 ± 1.51
N14	2.31	1.29 ± 0.45	1.00 ± 0.00
N15	2.37	3.29 ± 0.70*	2.86 ± 0.83
N16	2.44	1.86 ± 0.83	2.00 ± 1.07
N17	2.46	1.71 ± 0.70	2.00 ± 1.07
N18	3.14*	3.00 ± 0.76	2.86 ± 0.83
N19	3.87*	3.57 ± 1.18*	4.00 ± 0.76*
N20	3.96*	3.14 ± 0.99*	3.71 ± 0.45*

SD: Standard deviation,; #1: CAD system, #2: chest radiologists (n = 7); #3: residents (n = 7); * : incorrectly identified normal cases (scores > 3.0).

Table 3.5b

Five-Level Scale of Scores for Abnormal Lungs Obtained from CAD System and by Radiologists

	Mean ± SD		
Case	#1	#2	#3
A1	1.39*	4.29 ± 0.88	3.86 ± 0.64
A2	1.59*	2.14 ± 0.99*	1.57 ± 0.49*
A3	3.05	4.00 ± 1.07	2.86 ± 1.25*
A4	3.07	3.86 ± 1.12	2.57 ± 1.50*
A5	3.11	3.43 ± 1.05	2.86 ± 1.25*
A6	3.21	4.71 ± 0.45	4.57 ± 0.49
A7	3.36	4.71 ± 0.45	4.71 ± 0.45
A8	3.53	5.00 ± 0.00	4.43 ± 0.49
A9	4.01	4.00 ± 0.53	3.71 ± 0.70
A10	4.36	5.00 ± 0.00	5.00 ± 0.00
A11	4.43	4.14 ± 0.83	4.00 ± 0.53
A12	4.51	5.00 ± 0.00	5.00 ± 0.00
A13	4.62	5.00 ± 0.00	4.71 ± 0.45
A14	4.65	3.29 ± 1.28	1.14 ± 0.35*
A15	4.75	4.86 ± 0.35	4.14 ± 0.83
A16	5.31	5.00 ± 0.00	5.00 ± 0.00
A17	5.38	4.86 ± 0.35	4.71 ± 0.45
A18	5.64	5.00 ± 0.00	5.00 ± 0.00
A19	5.67	4.86 ± 0.35	4.57 ± 0.49
A20	5.83	5.00 ± 0.00	5.00 ± 0.00

SD: Standard deviation; #1: CAD system; #2: chest radiologists (n = 7); #3: residents (n =7); * : incorrectly identified abnormal cases (scores ≤ 3.0).

Table 3.6

Sensitivity and Specificity Results for CAD System and Observers

Chest radiologists	Sensitivity	Specificity
1	0.90	0.95
2	0.90	0.95
3	0.90	0.70
4	0.95	0.55
5	0.90	0.70
6	0.95	1.00
7	0.95	0.75
Mean ± SD	0.92 ± 0.02	0.80 ± 0.16

Residents	Sensitivity	Specificity
1	0.90	0.85
2	0.75	0.90
3	0.75	0.80
4	0.85	1.00
5	0.90	0.85
6	0.85	0.75
7	0.90	0.40
Mean ± SD	0.84 ± 0.06	0.79 ± 0.17

Sensitivity: number of correctly identified abnormal cases (scores > 3.0) ÷ total number of abnormal cases. Specificity: number of correctly identified normal cases (scores ≤ 3.0) ÷ total number of normal cases. SD: Standard deviation.

Table 4.1

Fractal Dimension Obtained from Normal and Abnormal Lungs

	Lung	FD
Abnormal	Upper	1.68 ± 0.08
	Lower	1.65 ± 0.11
	Mean	1.67 ± 0.10
Normal	Upper	1.46 ± 0.12
	Lower	1.42 ± 0.12
	Mean	1.44 ± 0.12

Each value is mean ± one standard deviation

Table 4.2

Az Values of RIs and FDs in Normal and Mild-Abnormality Groups

	LOJ		LOS	P-value
RI	0.812 ± 0.042	<	0.912 ± 0.028	P < 0.05
FD	0.867 ± 0.037	>	0.750 ± 0.048	P < 0.05

	RI		FD	P-value
LOJ	0.814 ± 0.042	<	0.864 ± 0.036	P < 0.05
LOS	0.912 ± 0.028	>	0.752 ± 0.048	P < 0.0001

Each value is the mean ± one standard deviation.

RI: Normalized radiographic index

FD: Fractal dimension

LOJ: Linear opacity judgment

LOS: Linear opacity subtraction

Table 4.3

Az Values of RIs and FDs in Normal and Severe-Abnormality Groups

	LOJ		LOS	P-value
RI	0.992 ± 0.007	>	0.883 ± 0.034	P < 0.001
FD	0.968 ± 0.016	>	0.767 ± 0.047	P < 0.0001

	RI		FD	P-value
LOJ	0.992 ± 0.006	>	0.964 ± 0.018	P < 0.05
LOS	0.883 ± 0.034	>	0.767 ± 0.047	P < 0.01

Each value is the mean ± one standard deviation.

RI: Normalized radiographic index

FD: Fractal dimension

LOJ: Linear opacity judgment

LOS: Linear opacity subtraction

Table 5.1

Correlation between PCWP Values and U/L Values

	Mean PCWP (mmHg)	Mean U/L value	r	P
≤ 15 mmHg	11.5 ± 2.5	1.06 ± 0.1	0.689	0.011
> 15 mmHg	25.7 ± 8.8	1.14 ± 0.12	0.313	0.210
Total	20.3 ± 9.5	1.10 ± 0.13	0.405	0.025

Each value is mean ± one standard deviation.

Table 5.2

Mean PCWP Value and Mean U/L Value in Patients without and Patients with MS

	Mean PCWP (mmHg)	Mean U/L value
Without MS	13.1 ± 4.0	1.05 ± 0.09
With MS	26.1 ± 8.4	1.16 ± 0.14

Each value is mean ± one standard deviation.

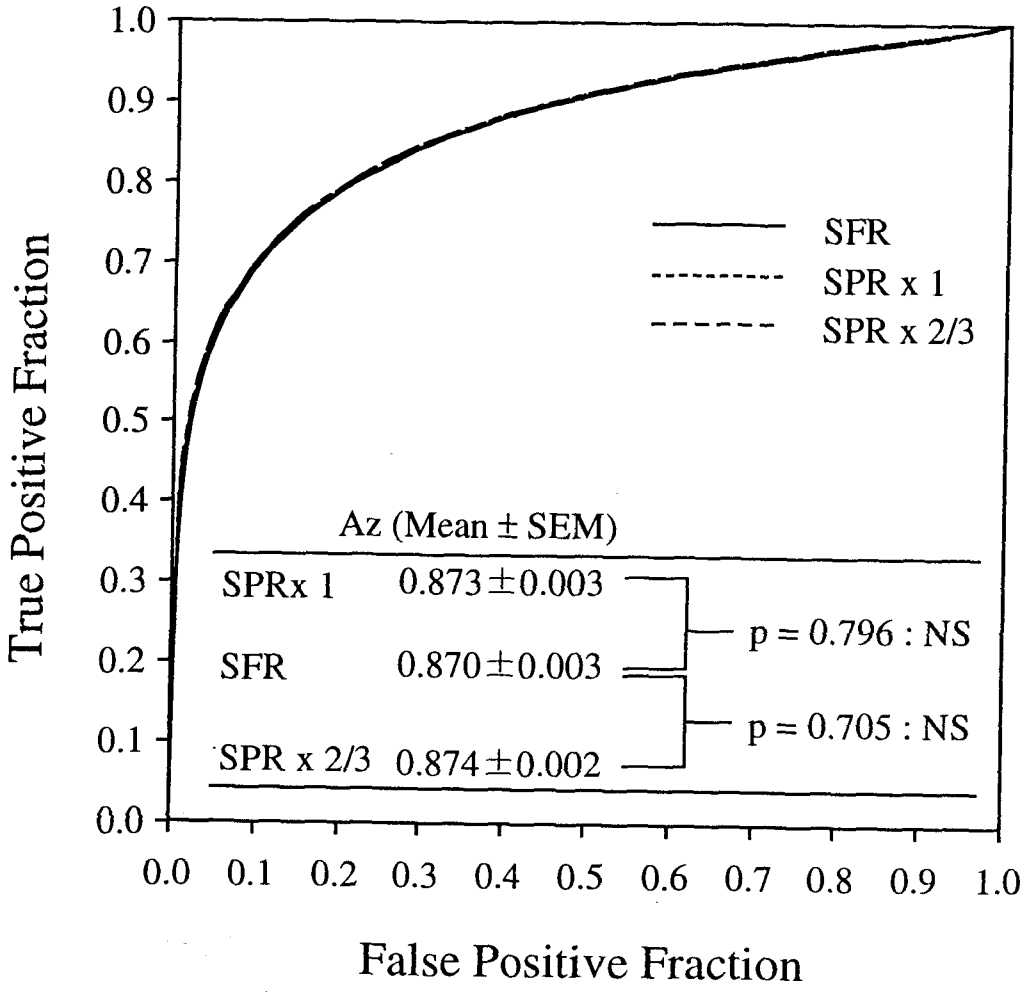

Figure 2.1

Composite ROC curves for the 14 observers. No significant differences in observer performance for the 14 observers were noted among SFR, full-size SPR, and minified SPR.

SFR = Screen-film radiography, SPR x 1 = full-size storage phosphor radiography, SPR x 2/3 = minified storage phosphor radiography, SEM = standard error of mean, NS = not significant.

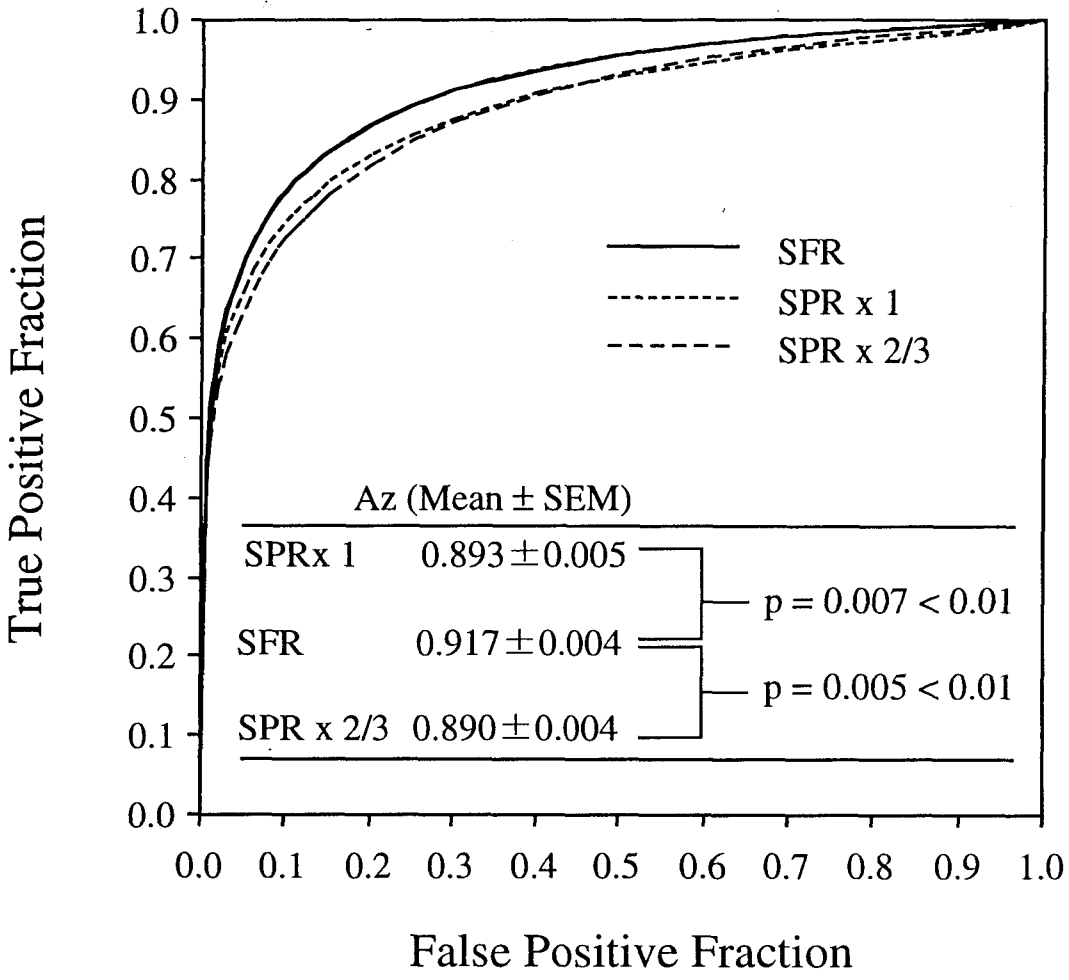

Figure 2.2

Composite ROC curves for the 7 chest radiologists. Significant differences in observer performance for the 7 chest radiologists were observed between SFR and the two formats of SPR ($P < 0.01$).

SFR = Screen-film radiography, SPR x 1 = full-size storage phosphor radiography, SPR x 2/3 = minified storage phosphor radiography, SEM = standard error of mean.

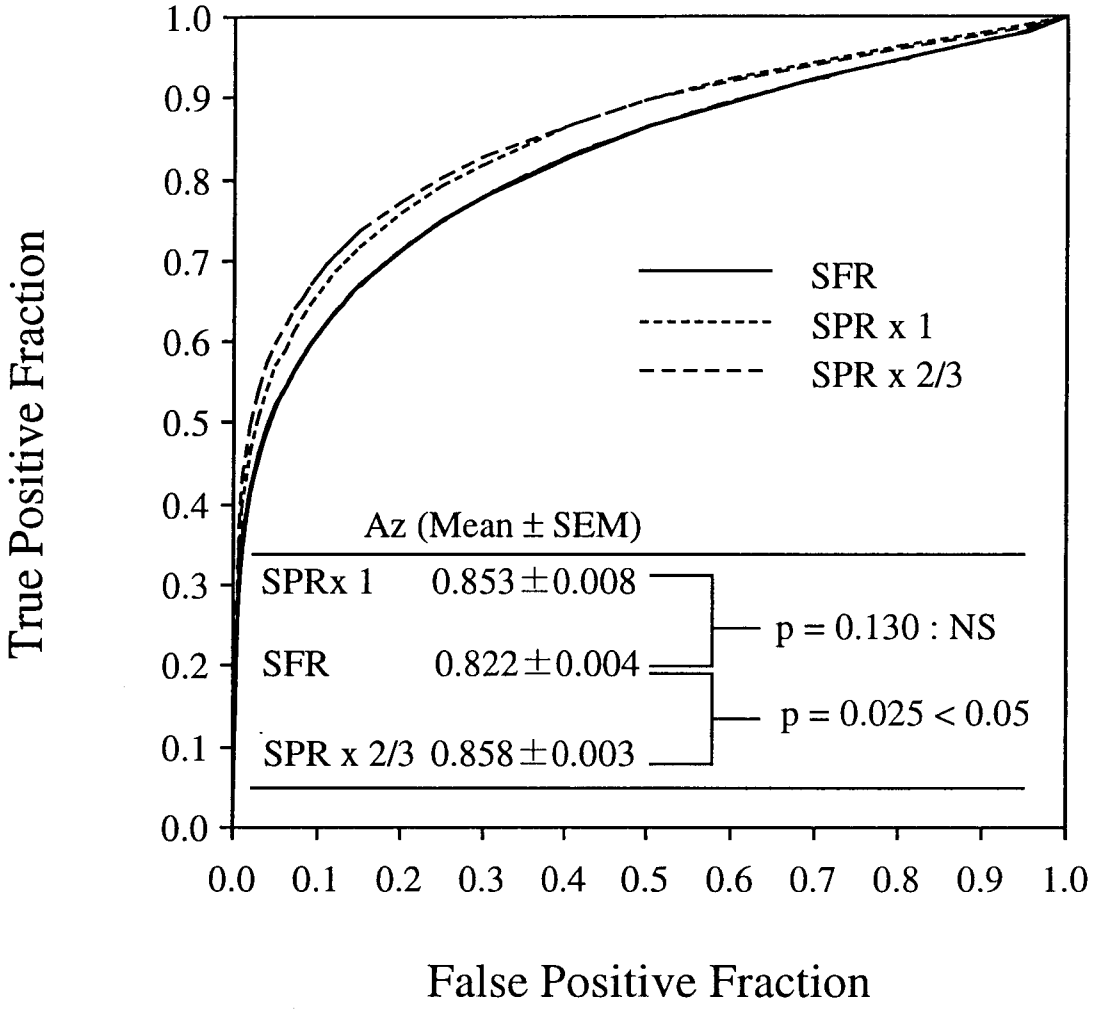

Figure 2.3

Composite ROC curves for the 7 residents. Significant differences were observed between SFR and minified SPR ($P < 0.05$); however, no significant differences in observer performance with SFR and full-size SPR were observed.

SFR = Screen-film radiography, SPR x 1 = full-size storage phosphor radiography, SPR x 2/3 = minified storage phosphor radiography, SEM = standard error of mean, NS = not significant.

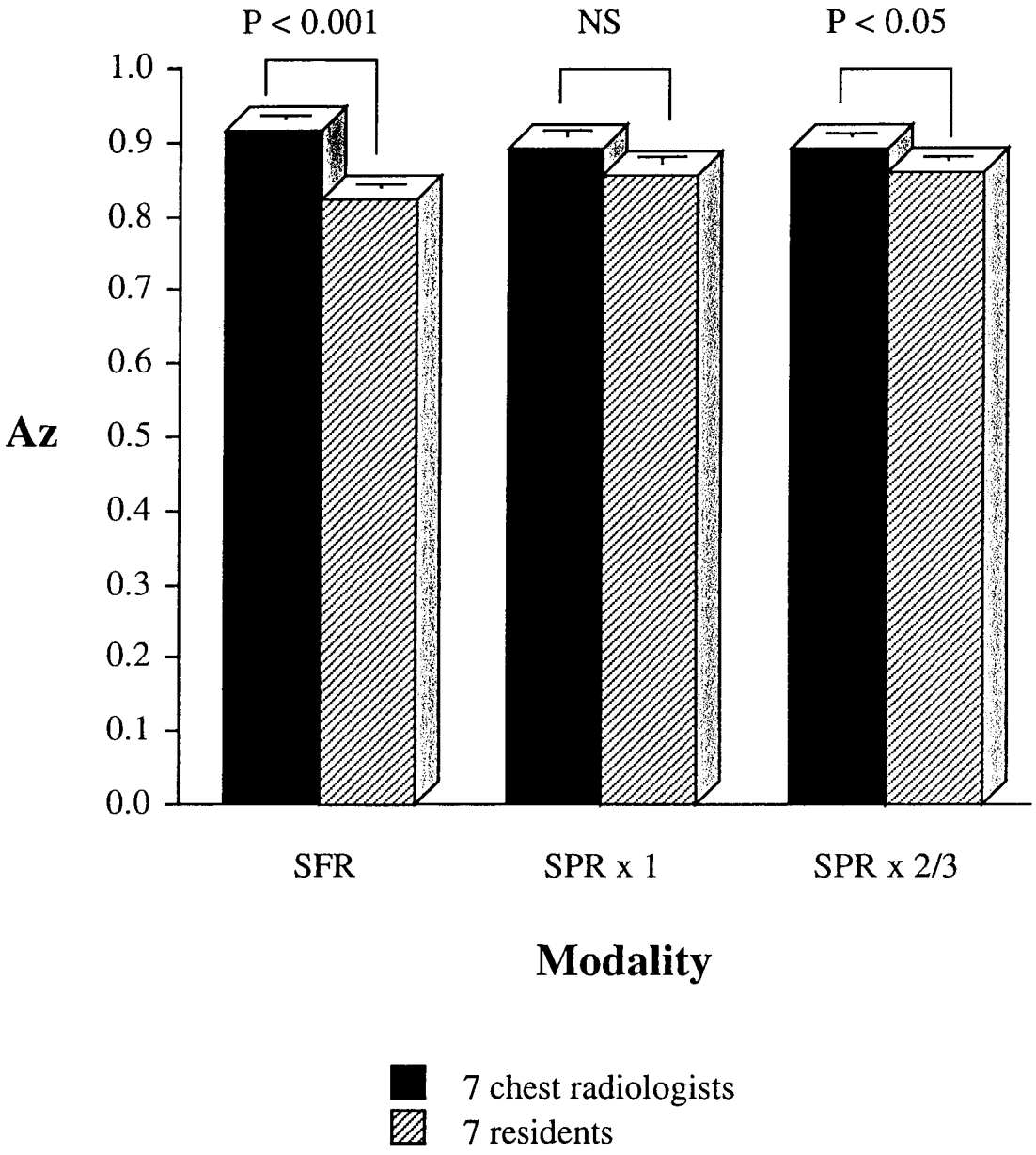

Figure 2.4

Areas under the ROC curves for the 7 chest radiologists and the 7 residents for each image modality. Significant differences in the perceptual accuracy of each modality between the 7 chest radiologists and the 7 residents were observed in SFR ($P < 0.001$) and minified SPR ($P < 0.05$), but no significant differences were observed in full-size SPR.
SFR = Screen-film radiography, SPR x 1 = full-size storage phosphor radiography, SPR x 2/3 = minified storage phosphor radiography, NS = not significant.

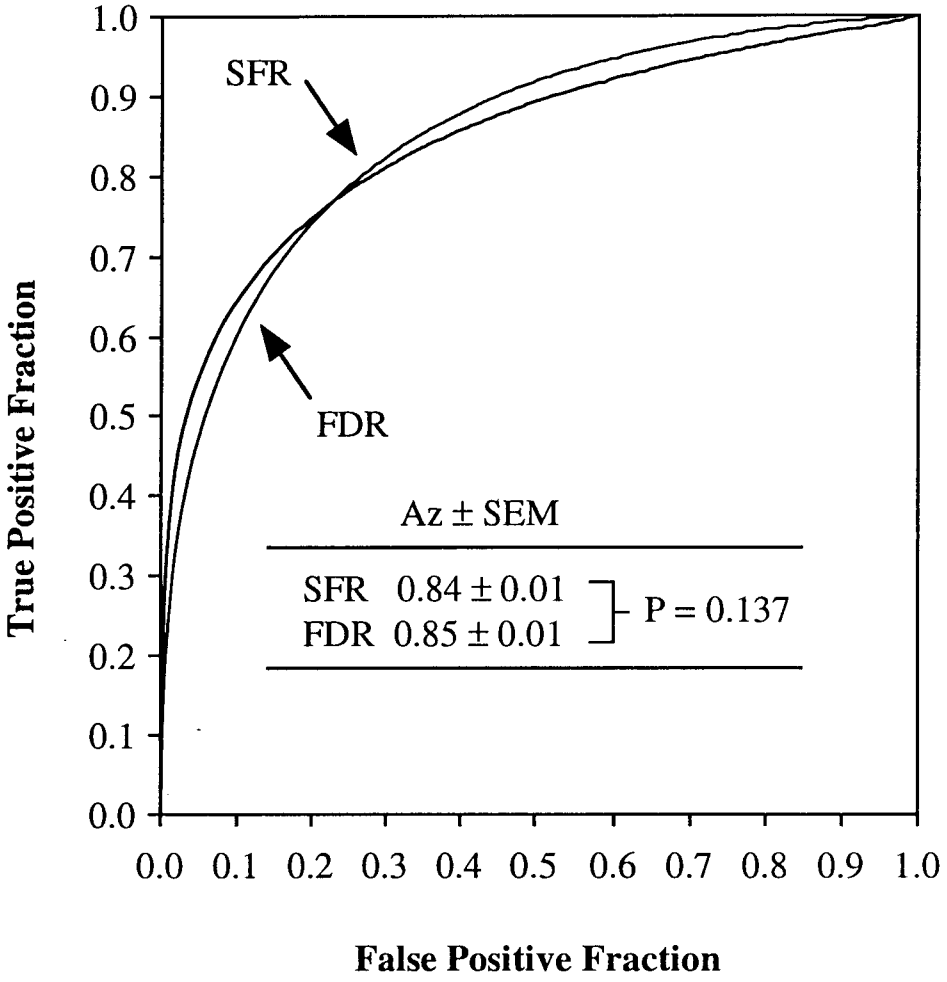

Figure 2.5

Composite ROC curves for the 10 observers. No significant differences in observer performance were found between SFR and FDR (P = 0.137).

SFR = Screen-film radiography, FDR = film-digitized radiography.

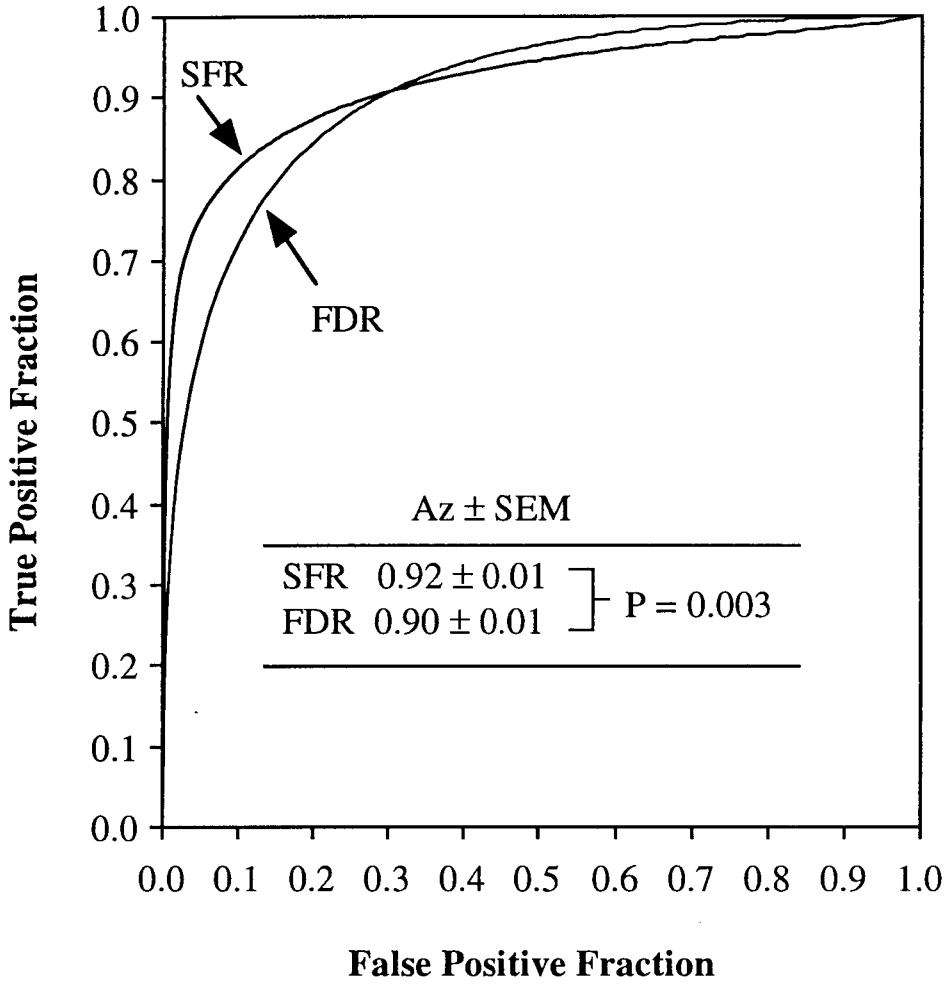

Figure 2.6

Composite ROC curves for the five chest radiologists. Significant differences in observer performance were found between SFR and FDR (P = 0.003).

SFR = Screen-film radiography, FDR = film-digitized radiography.

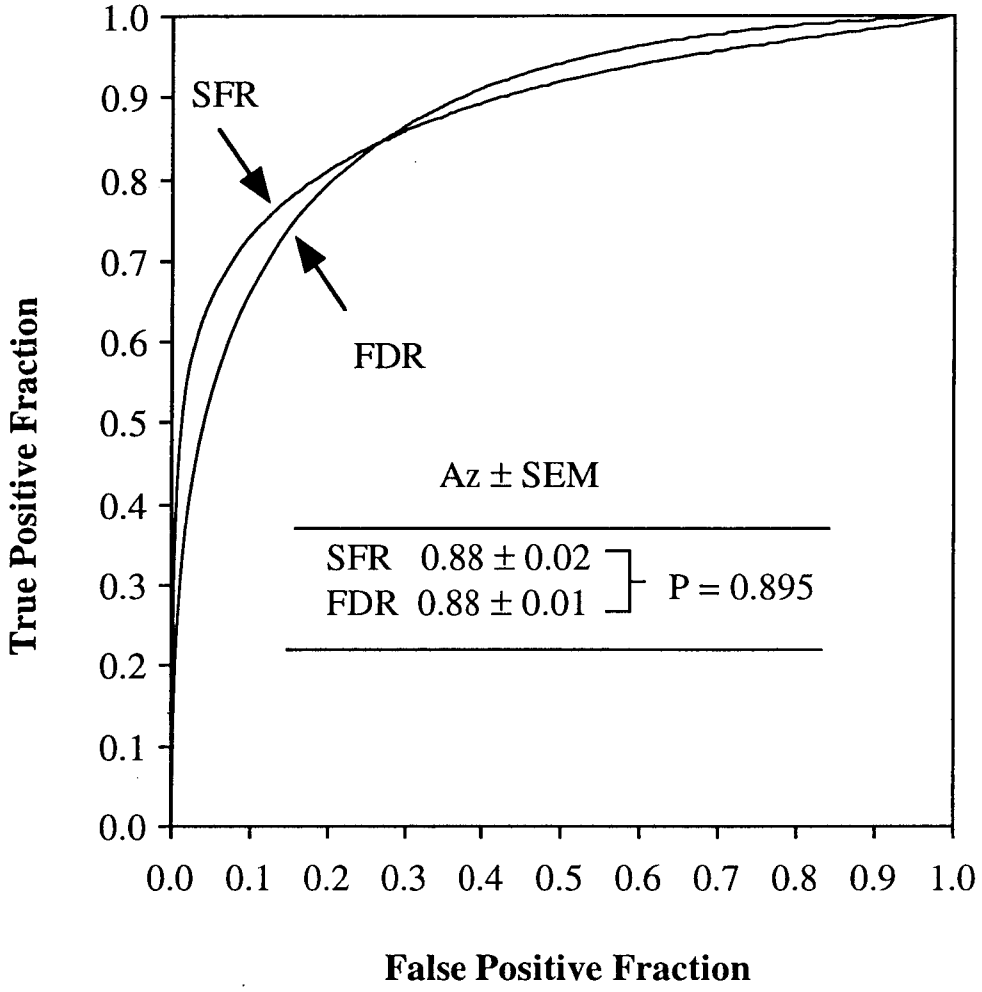

Figure 2.7

Composite ROC curves for the five residents. No significant differences in observer performance were found between SFR and FDR (P = 0.895).

SFR = Screen-film radiography, FDR = film-digitized radiography.

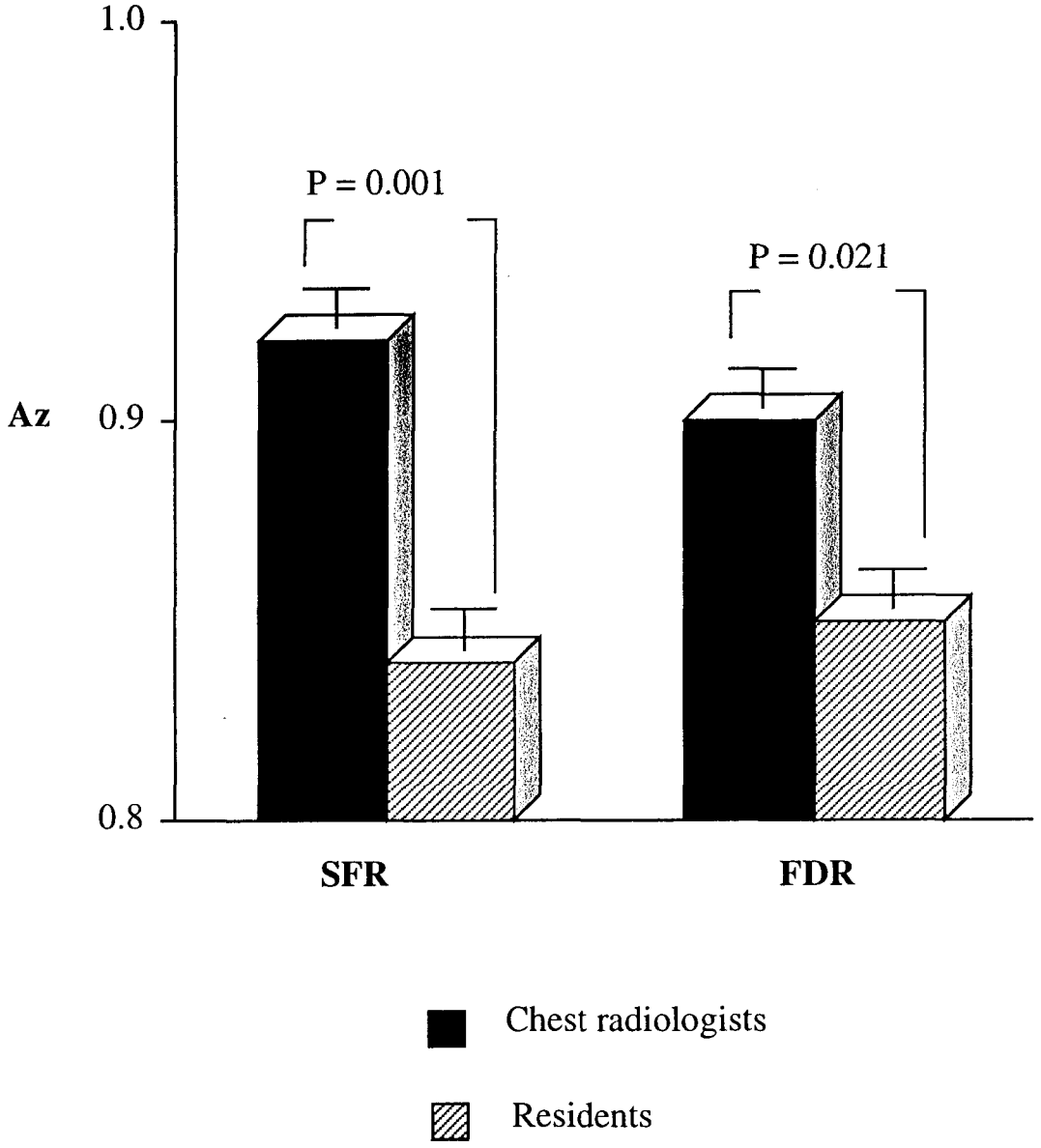

Figure 2.8

Az values for the five chest radiologists and the five residents according to each image modality. Significant differences in the perceptual accuracy between the five chest radiologists and the five residents were found in SFR (P = 0.001), but no significant differences were found in FDR (P = 0.021).

SFR = Screen-film radiography, FDR = film-digitized radiography.

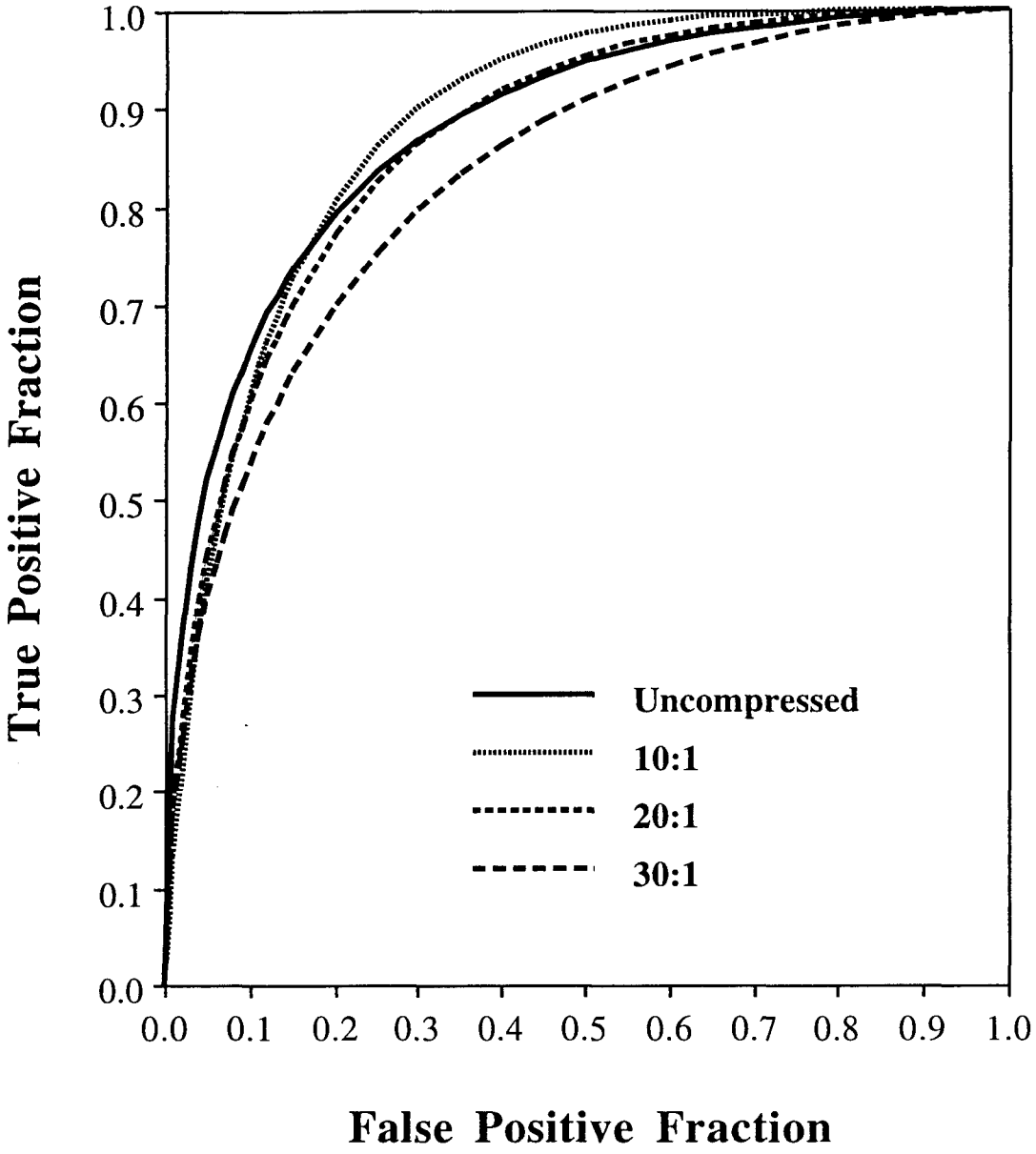

Figure 2.9

Composite ROC curves for the 10 observers. Significant differences in performance were found between uncompressed images and 30:1 compressed images ($P < 0.05$).

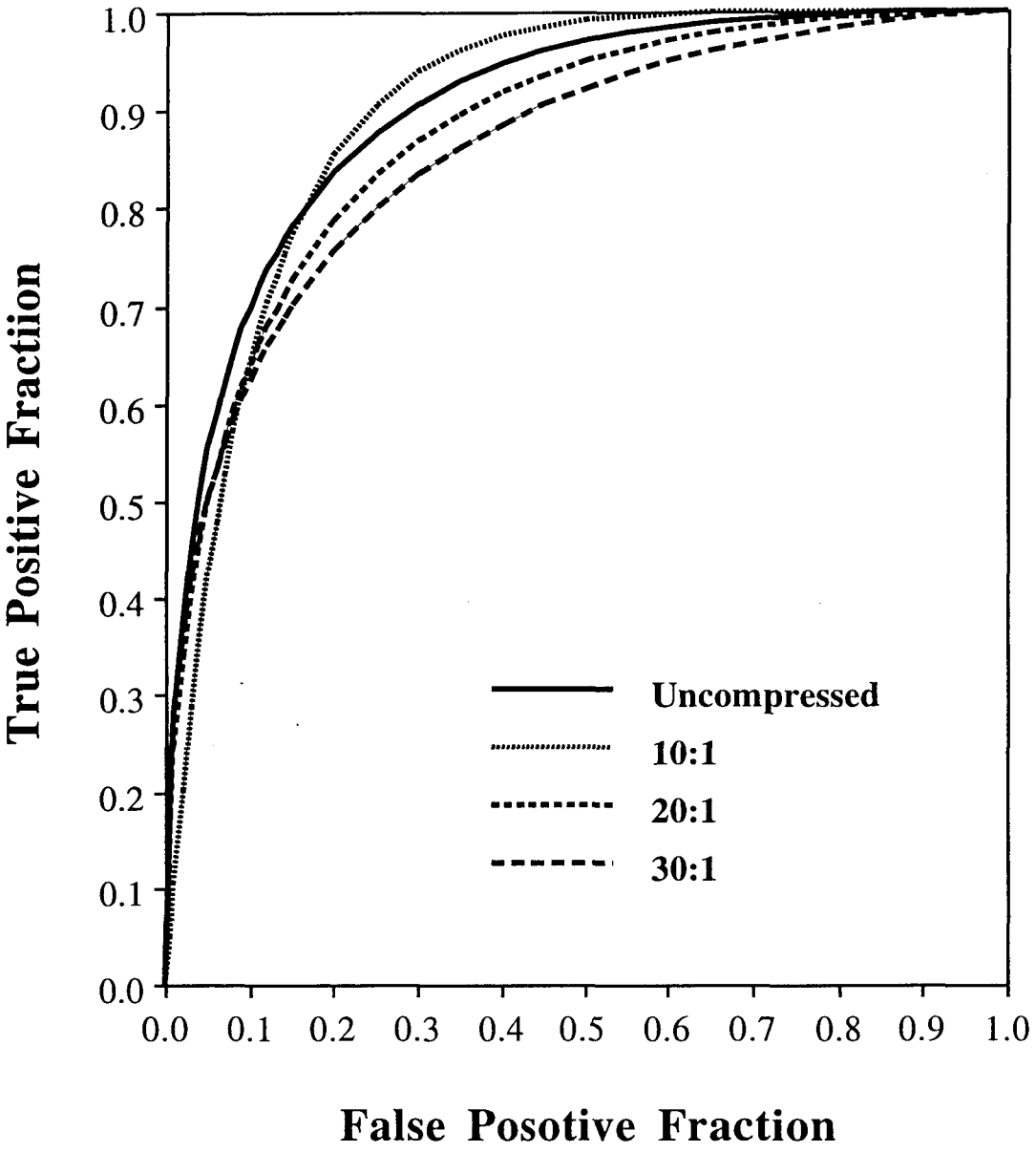

Figure 2.10

Composite ROC curves for the five chest radiologists. Significant differences in performance were found between uncompressed images and 20:1 compressed images ($P < 0.05$) and between uncompressed images and 30:1 compressed images ($P < 0.05$).

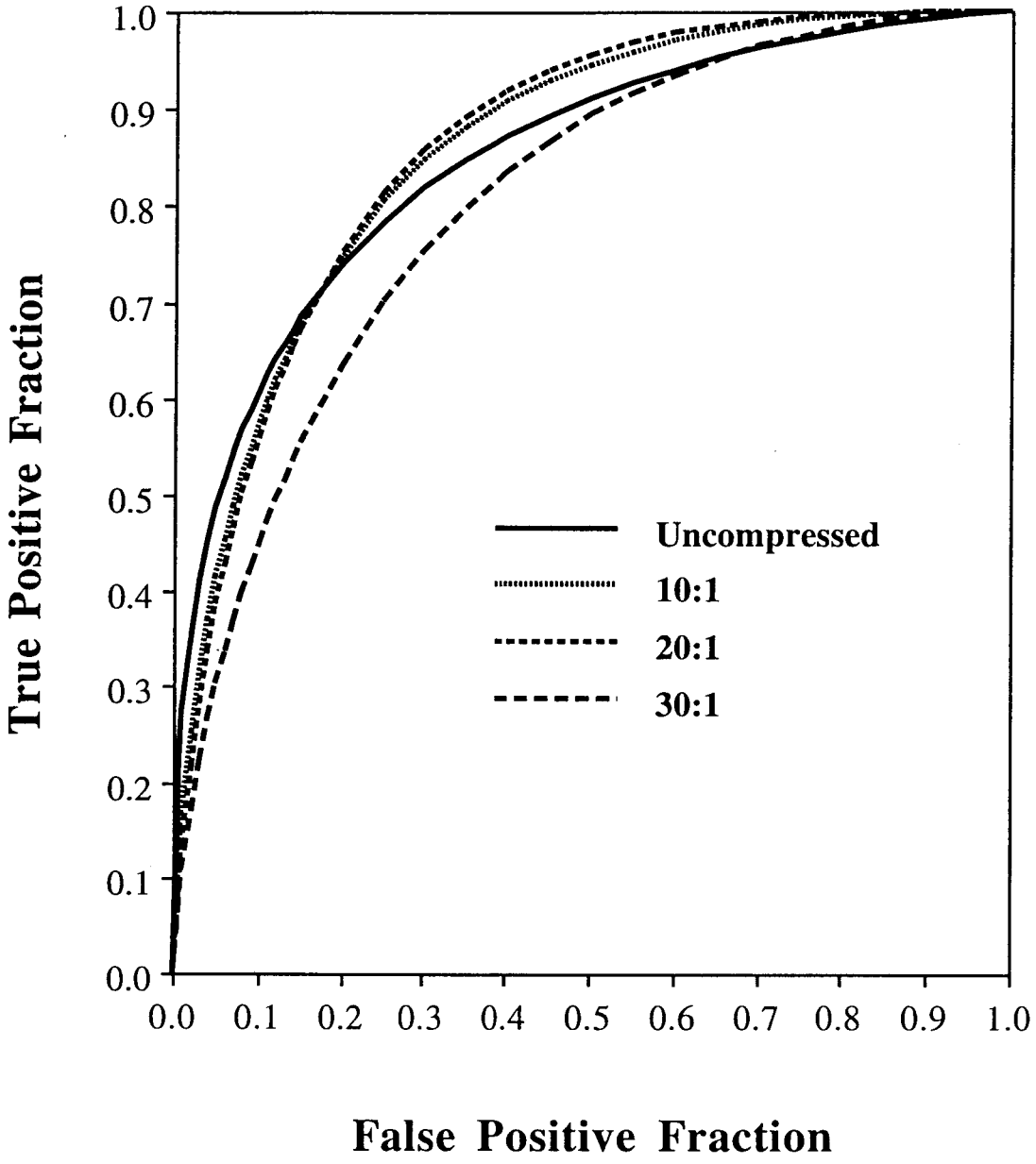

Figure 2.11

Composite ROC curves for the five residents. No significant differences in performance were found between uncompressed images and three formats of compressed images ($P \geq 0.05$).

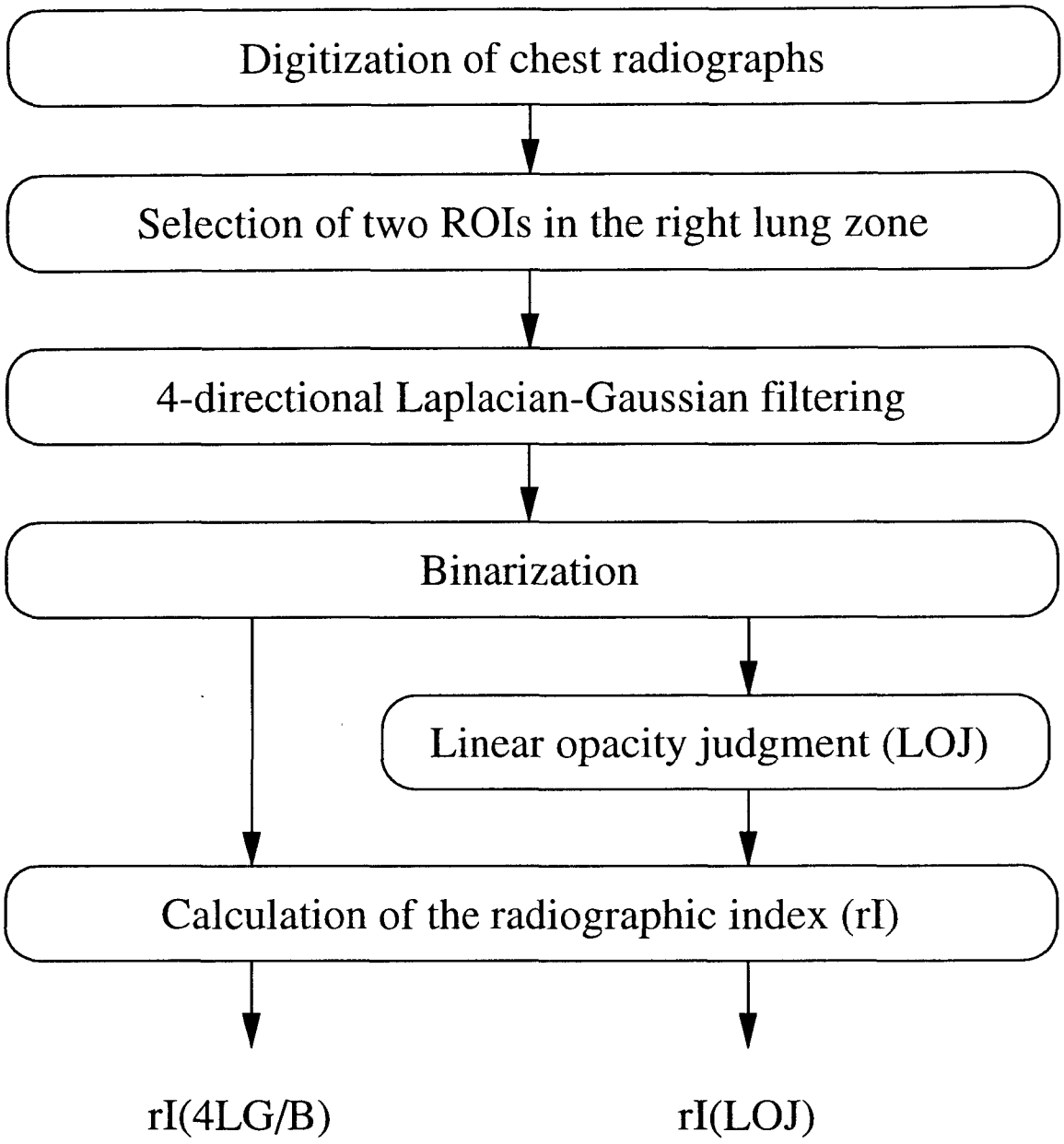

Figure 3.1

Overall scheme of a CAD system for interstitial lung diseases in chest radiography. The radiographic index rI(4LG/B) was obtained from the ROIs processed by 4LG/B. The radiographic index rI(LOJ) was obtained from the ROIs processed by LOJ.

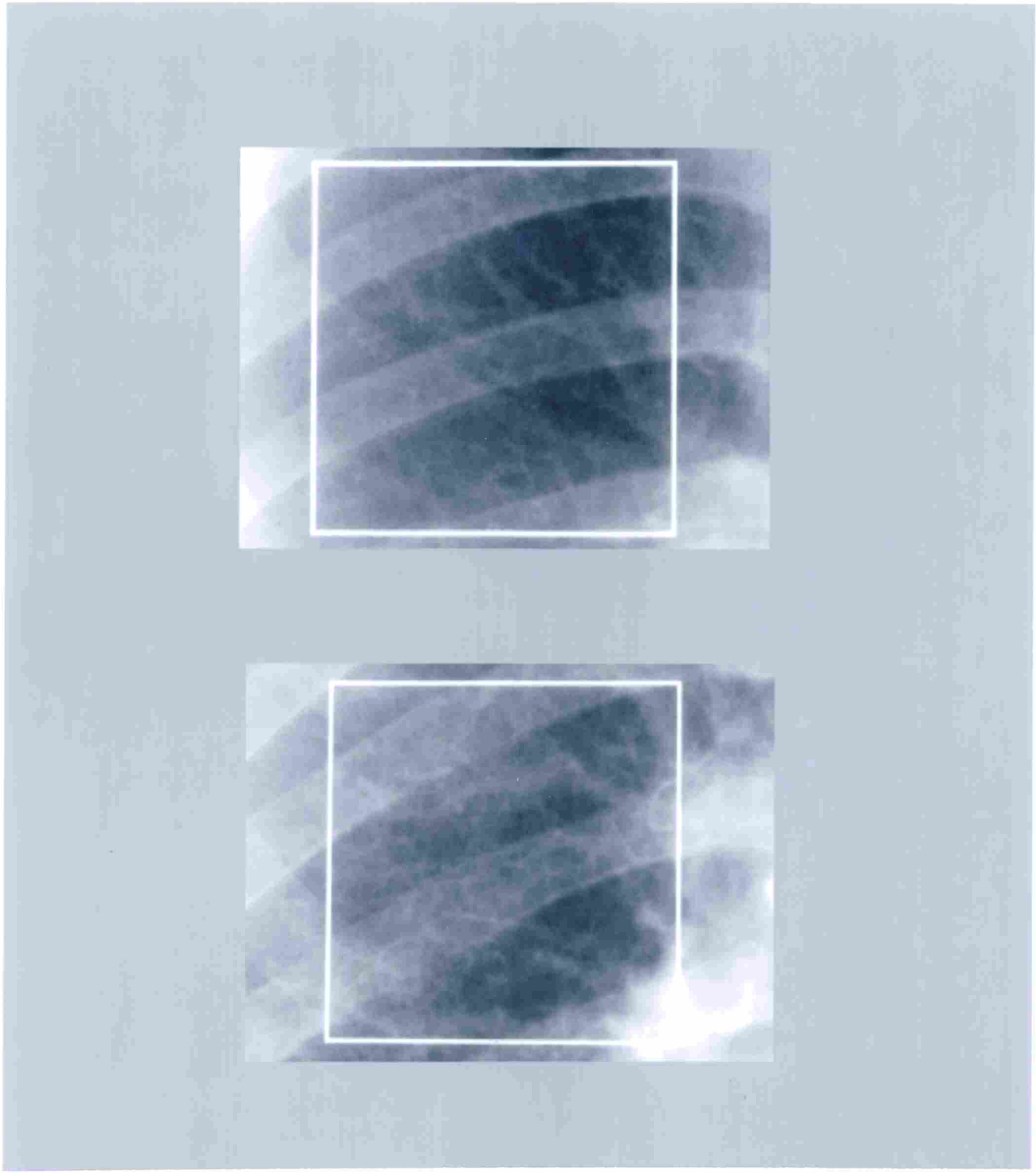

Figure 3.2

Chest radiographs of the right upper lung zones with ROIs. ROIs with 296 x 296 matrix size were selected manually for filtering by 4-directional Laplacian-Gaussian filters. (a) Normal lung **(top)**, (b) abnormal lung **(bottom)**.

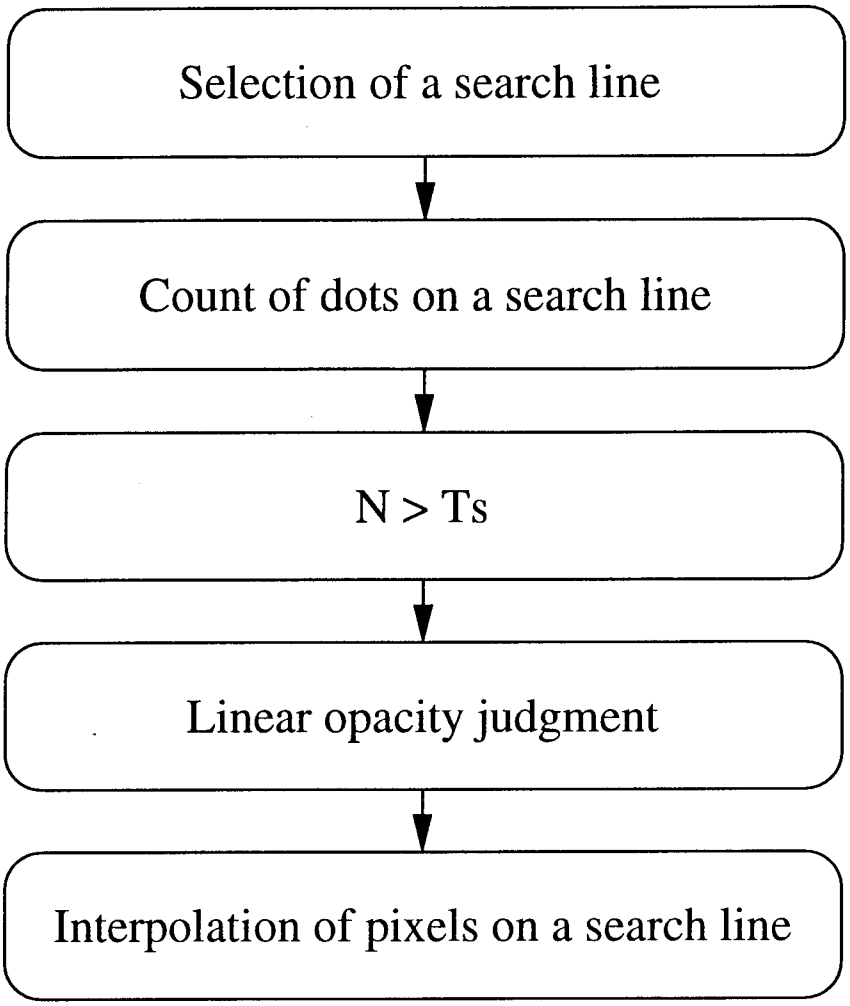

Figure 3.3

Scheme for LOJ processing. The starting point of a search line is selected on all pixels within an ROI, and θ is selected from $\alpha_i - \pi/4$ to $\alpha_i + \pi/4$ for each pixel. N is the total number of pixels on a search line, and Ts is the threshold. If N > Ts, the pixels on a search line are judged to be those of a linear opacity.

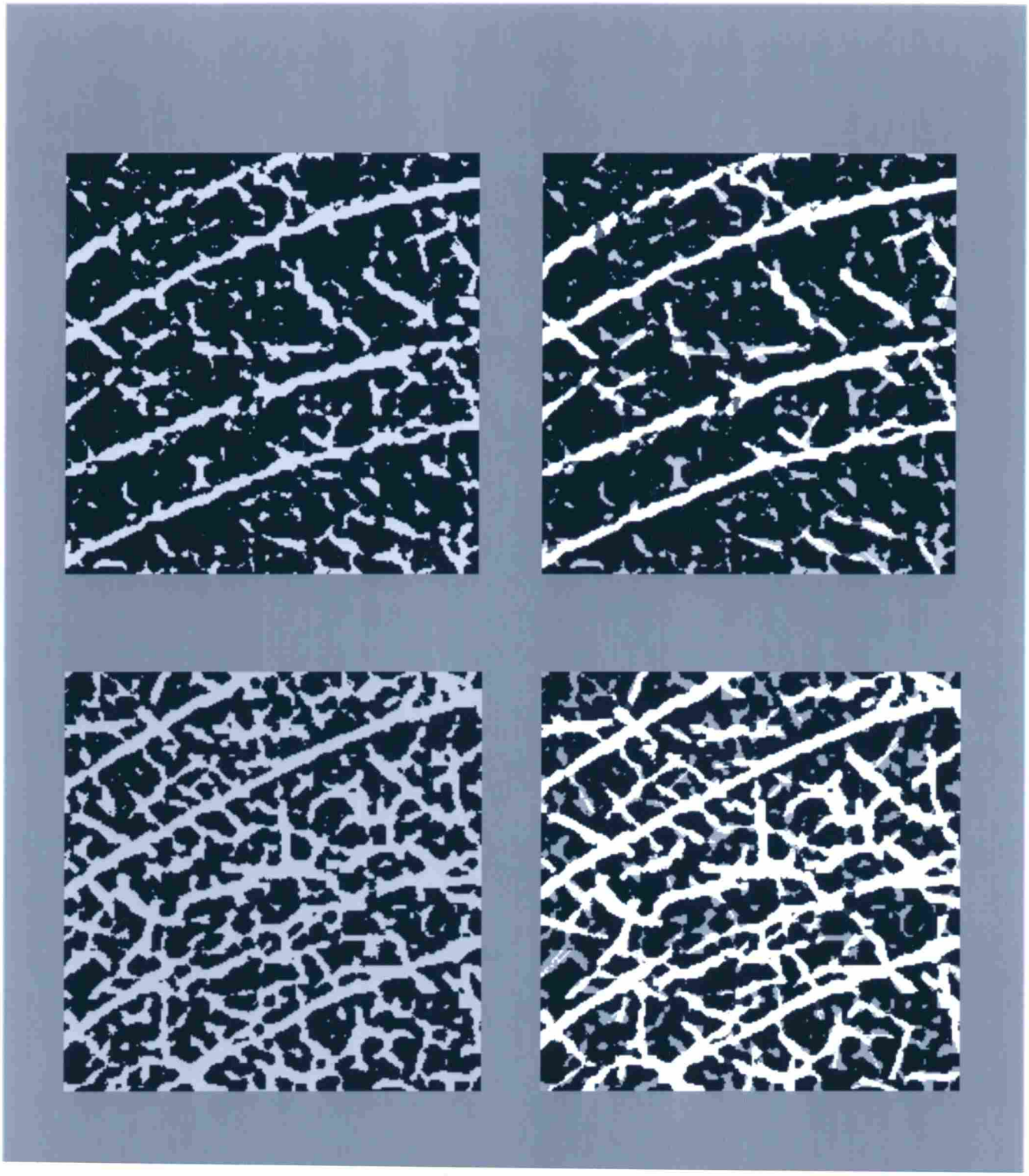

Figure 3.4

Outputs of the selected ROIs (256 x 256 matrix size). (a) Image of the ROI for a normal lung obtained from 4LG/B. Gray regions indicate the 4LG/B outputs. (b) Image of the ROI for a normal lung obtained from LOJ. White and gray regions indicate 4LG/B outputs (including interpolated pixels). White regions are judged to be linear opacities by LOJ. (c) Image of the ROI for an abnormal lung obtained from 4LG/B. (d) Image of the ROI for an abnormal lung obtained from LOJ.

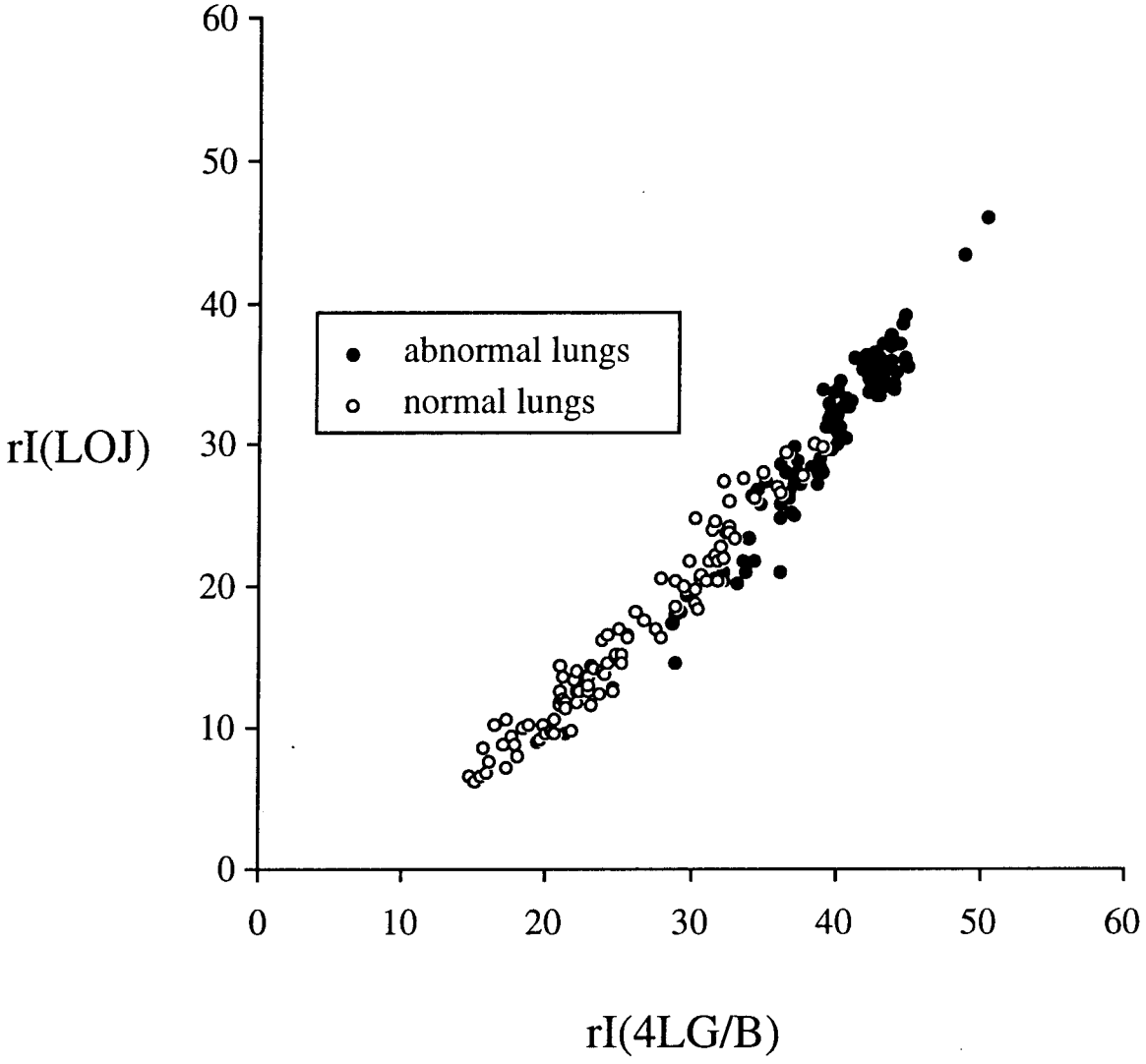

Figure 3.5(a)

Distribution of the two radiographic indices, rI(4LG/B) obtained from the ROIs processed by 4LG/B, and rI(LOJ) obtained from the ROIs processed by LOJ. (a) Comparison of normal and abnormal lungs.

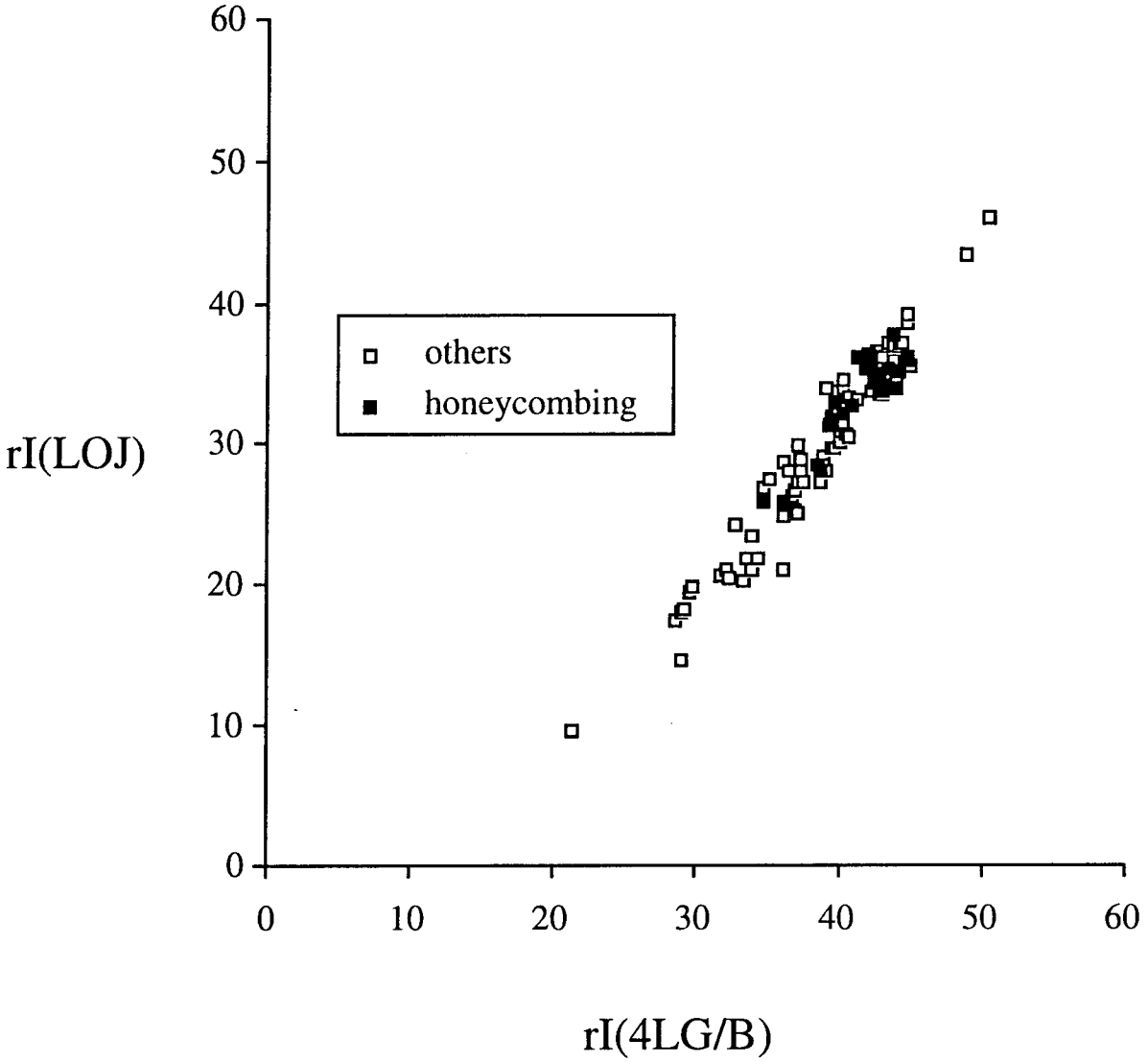

Figure 3.5(b)

Distribution of the two radiographic indices, rI(4LG/B) obtained from the ROIs processed by 4LG/B, and rI(LOJ) obtained from the ROIs processed by LOJ. (b) Comparison of honeycombing and others.

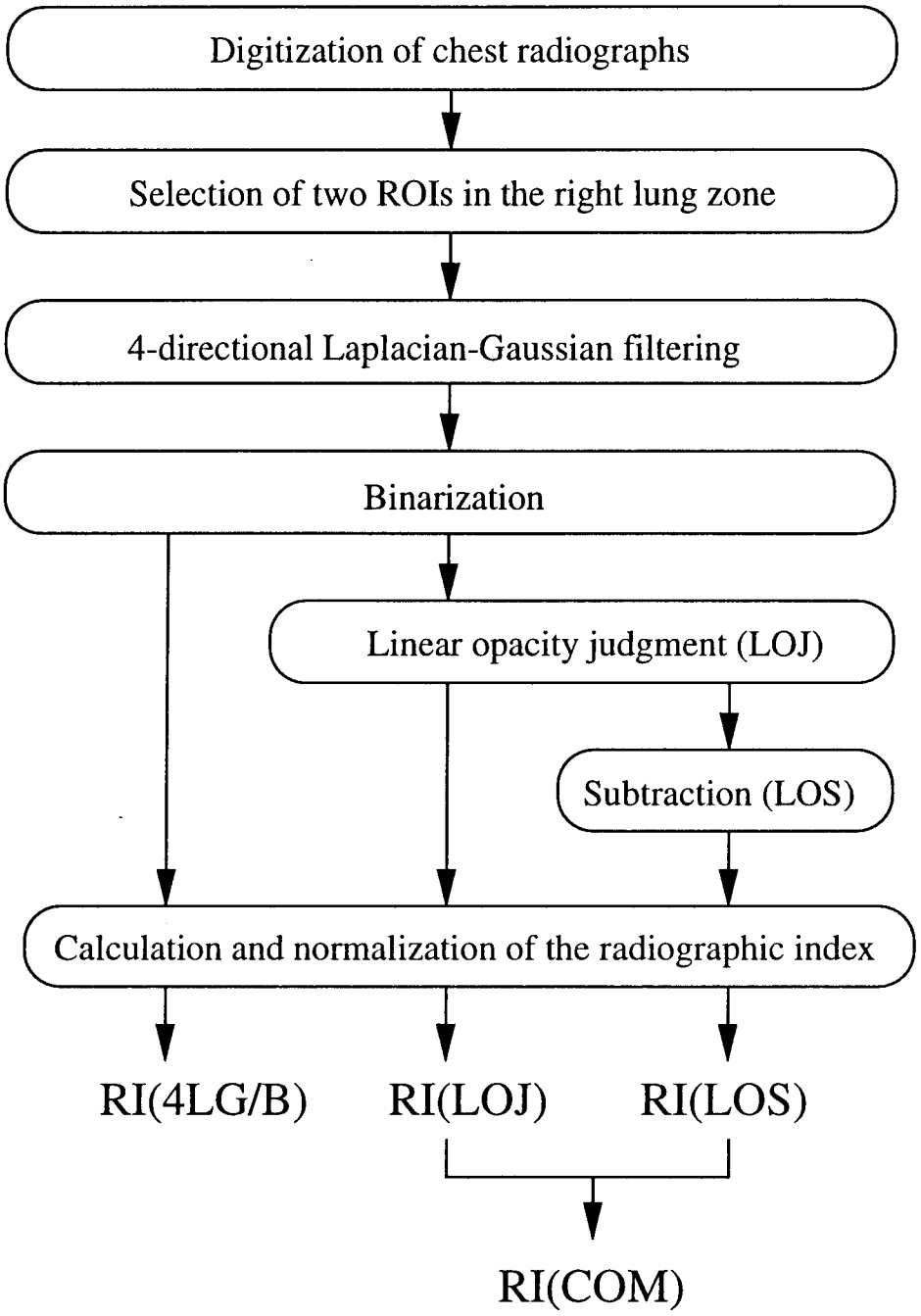

Figure 3.6

Overall scheme for modified CAD system for detection of interstitial lung disease on chest radiographs. Normalized radiographic indices: RI(4LG/B) was obtained from ROIs processed by 4LG/B, RI(LOJ) was obtained from ROIs processed by LOJ, and RI(LOS) was obtained from the ROIs processed by LOS. The combined radiographic index, RI(COM), was obtained from RI(LOJ) and RI(LOS).

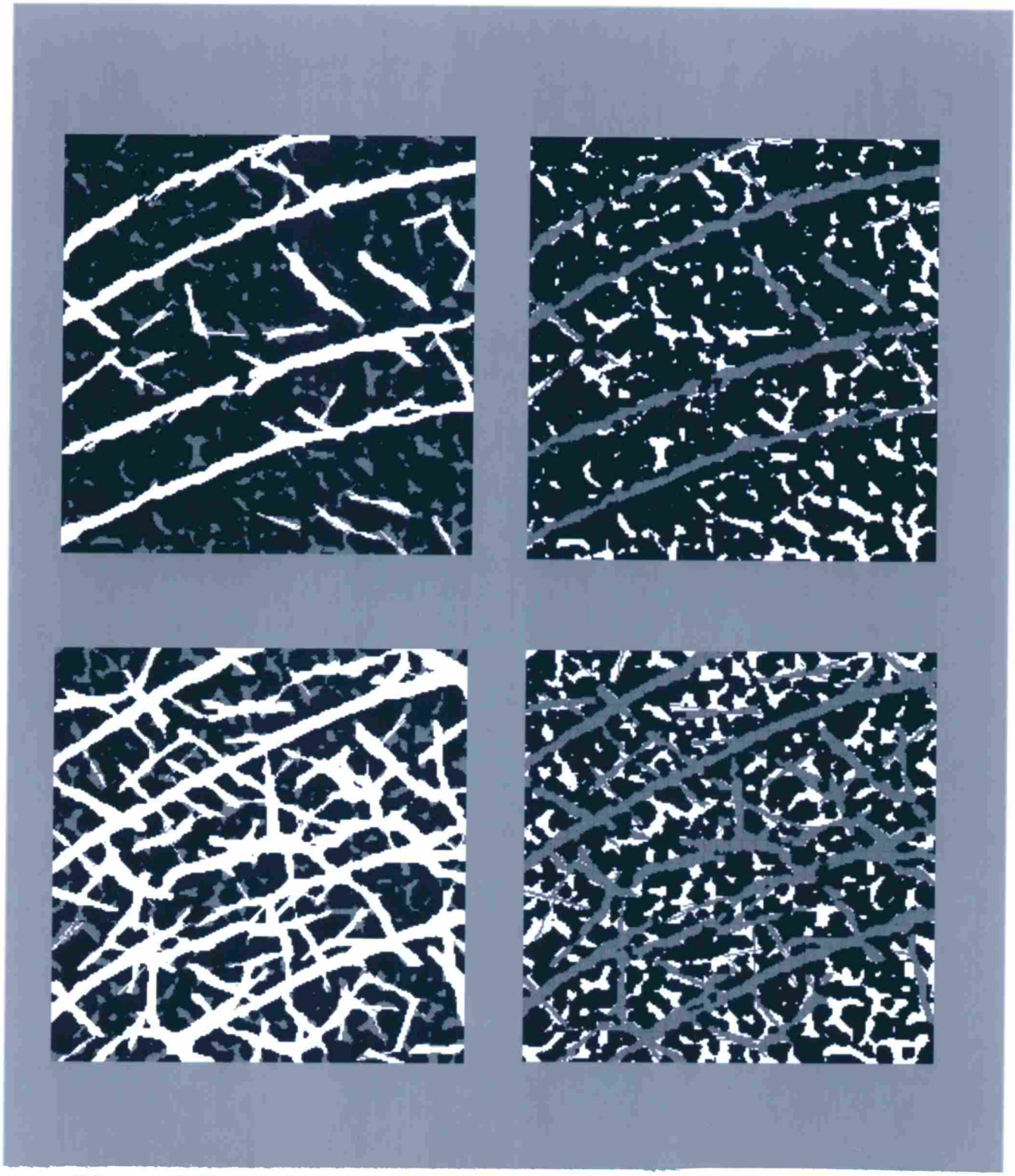

Figure 3.7

Outputs of LOJ and LOS in selected ROIs (256 x 256 matrix size). (a) Image of an ROI for a normal lung, obtained by LOJ. White regions are judged as linear opacities by LOJ (**upper left**). (b) Image of an ROI for a normal lung, obtained by LOS. Gray regions indicate subtracted regions obtained by LOS, and white regions indicate opacities obtained by LOS (**upper right**). (c) Image of an ROI for an abnormal lung, obtained by LOJ (**lower left**). (d) Image of an ROI for an abnormal lung, obtained by LOS (**lower right**).

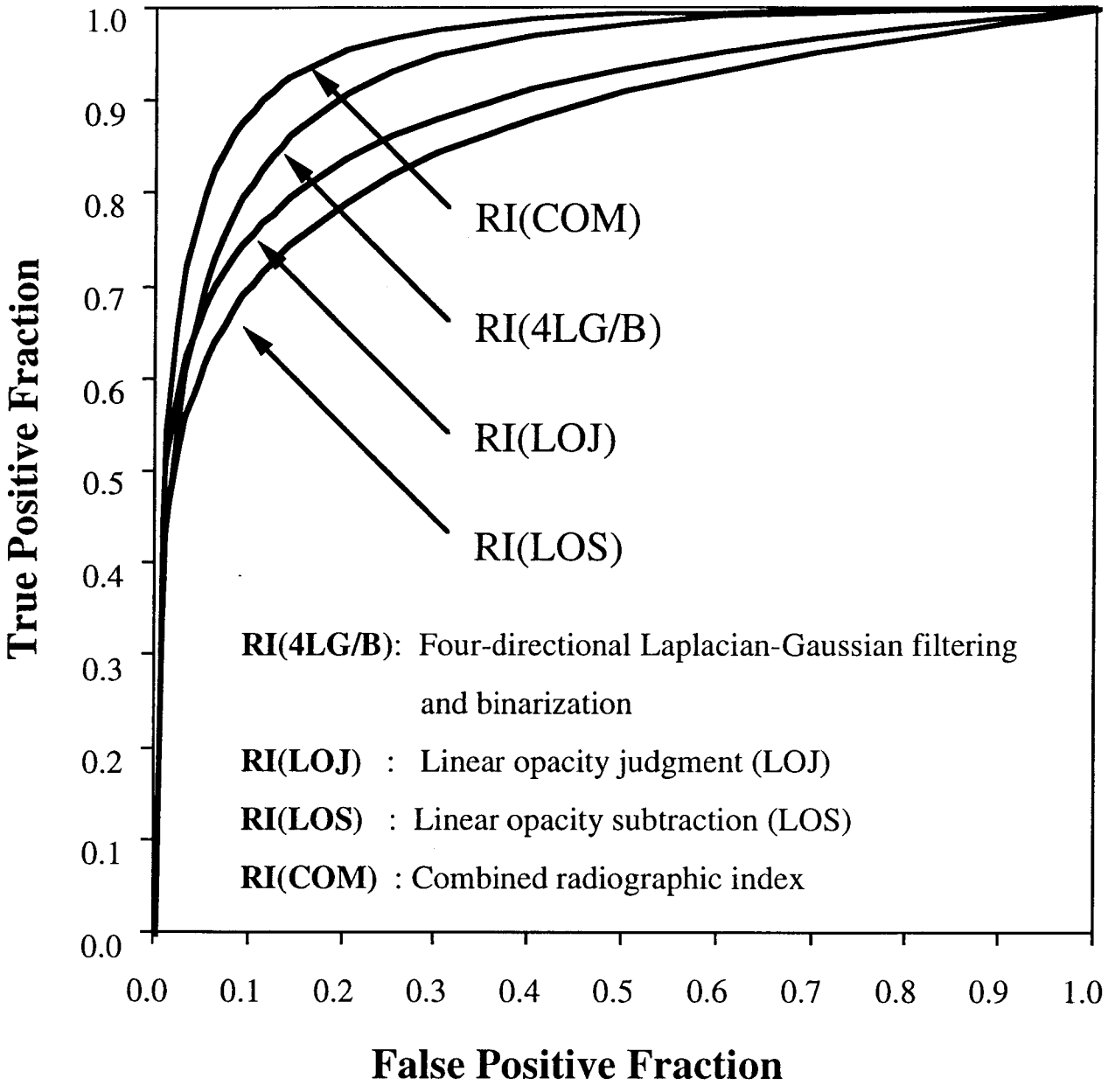

Figure 3.8(a)

Results of evaluation by the CAD system. (a) ROC curves for distinction between ROIs of normal lungs and ROIs with entire interstitial lung abnormalities. RI(COM) is better than the other indices.

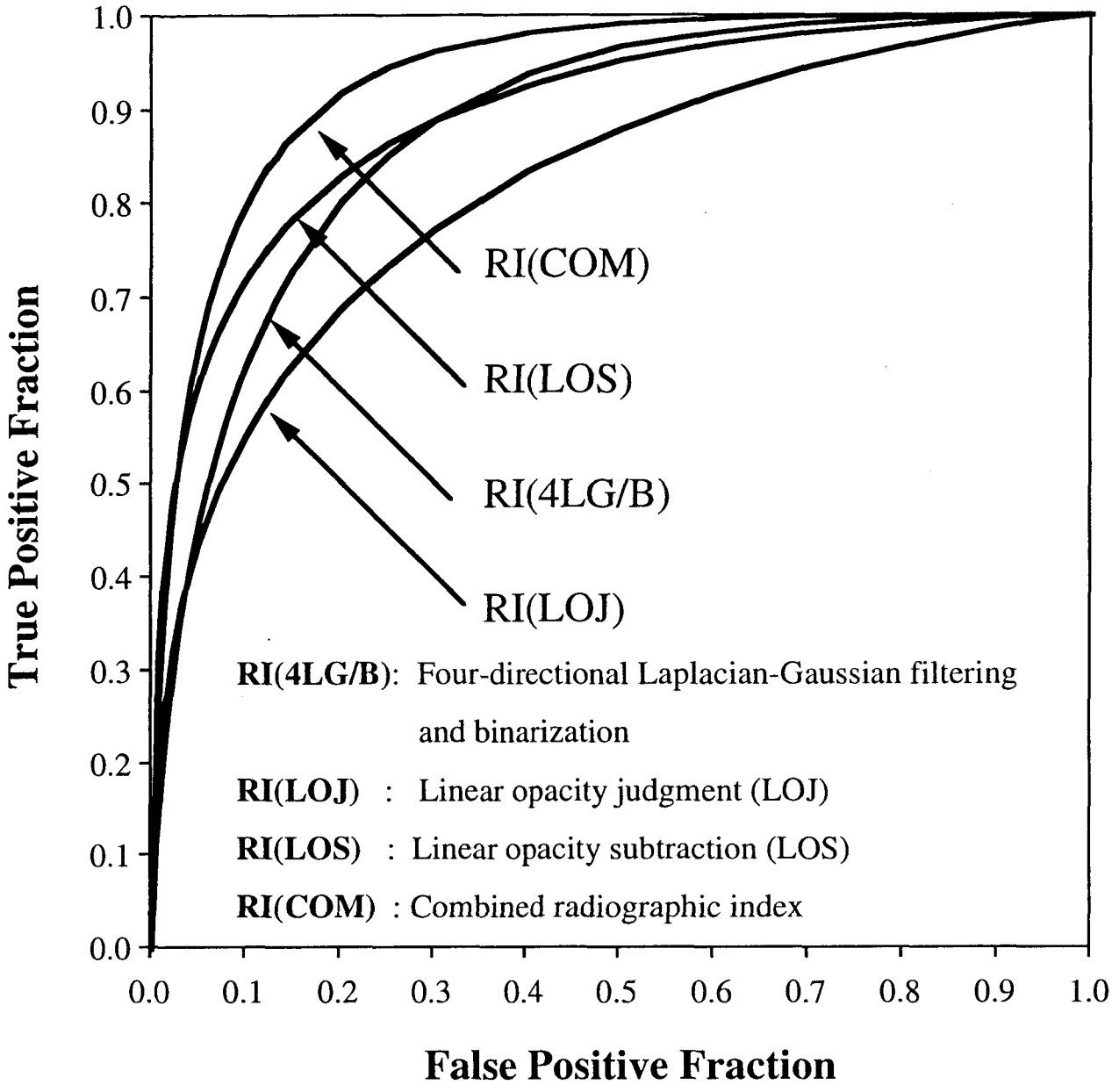

Figure 3.8(b)

Results of evaluation by the CAD system. (b) ROC curves for distinction between ROIs of normal lungs and ROIs with mild interstitial lung abnormalities. RI(COM) is better than RI(4LG/B) and RI(LOJ). ROC curve for RI(COM) is above that for RI(LOS). However, there are no significant differences between RI(COM) and RI(LOS).

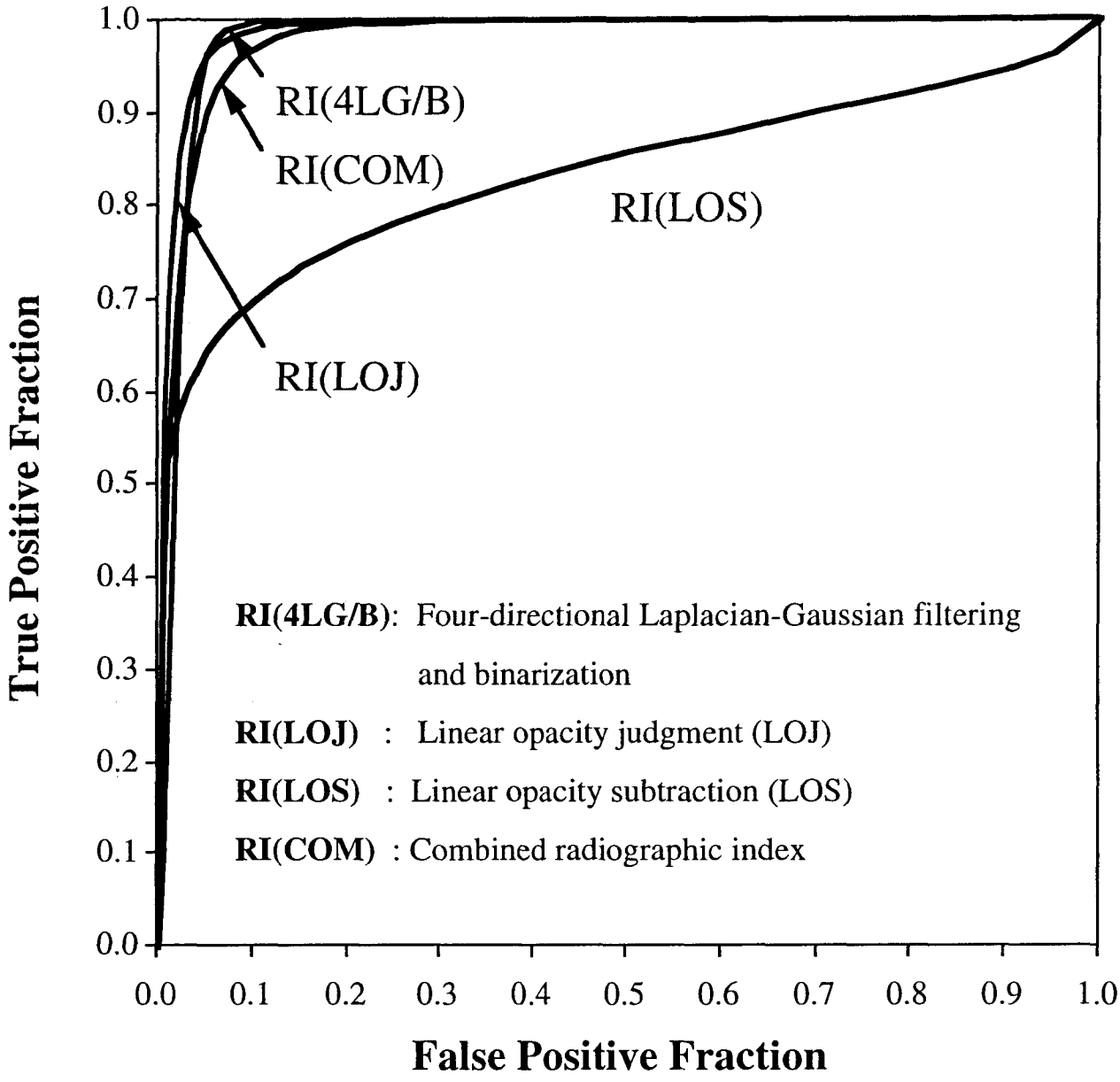

Figure 3.8(c)

Results of evaluation by the CAD system. (c) ROC curves for distinction between ROIs of normal lungs and ROIs with severe interstitial lung abnormalities. There are no significant differences among RI(COM), RI(4LG/B), and RI(LOJ). However, these indices are better than RI(LOS).

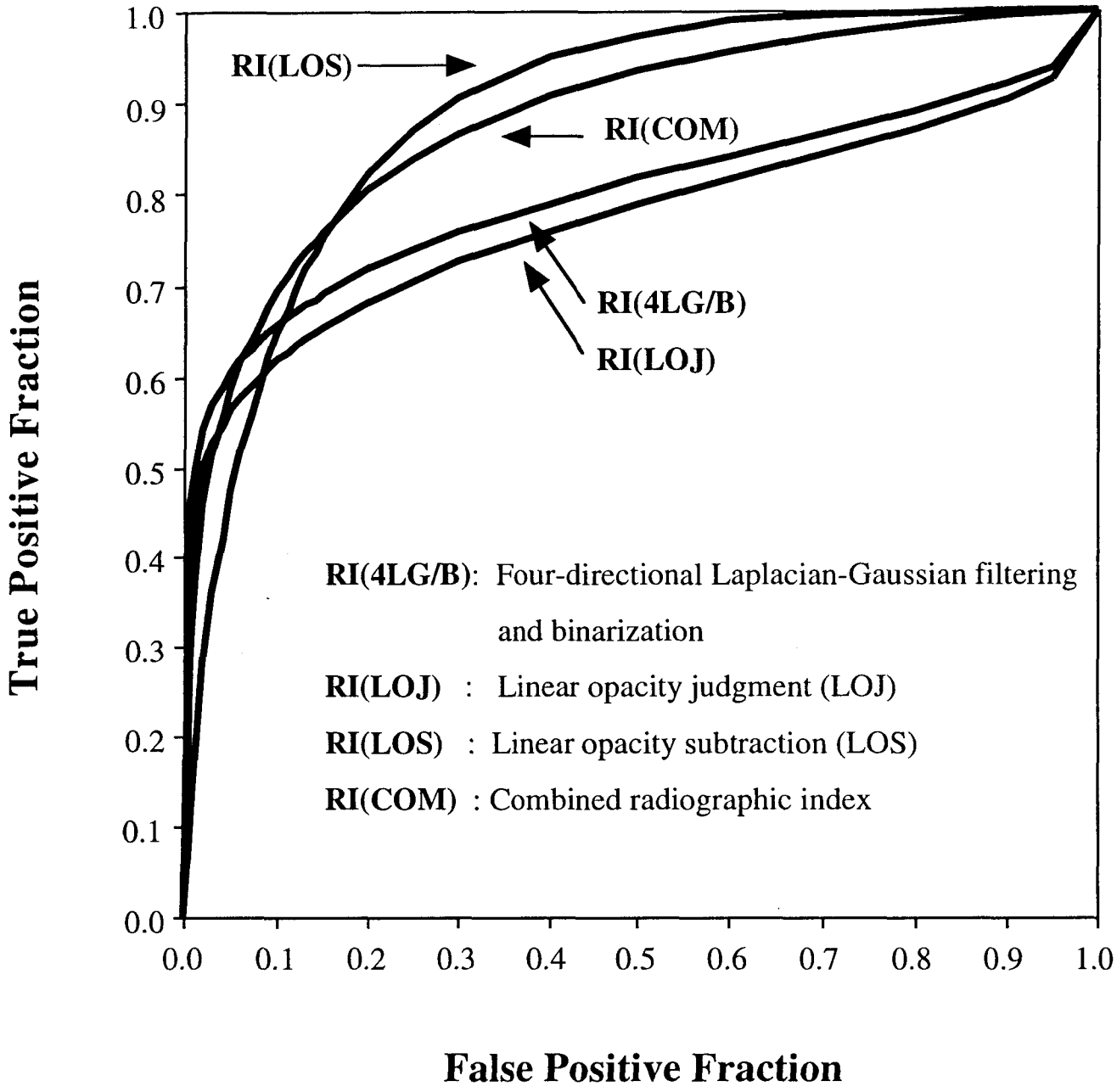

Figure 3.9

ROC curves for the CAD system. RI(4LG/B), RI(LOJ), and RI(LOS) are RIs obtained from the ROIs of 4LG/B, LOJ processing, and LOS processing. RI(COM) is the combined radiographic index obtained from RI(LOJ) and RI(LOS).

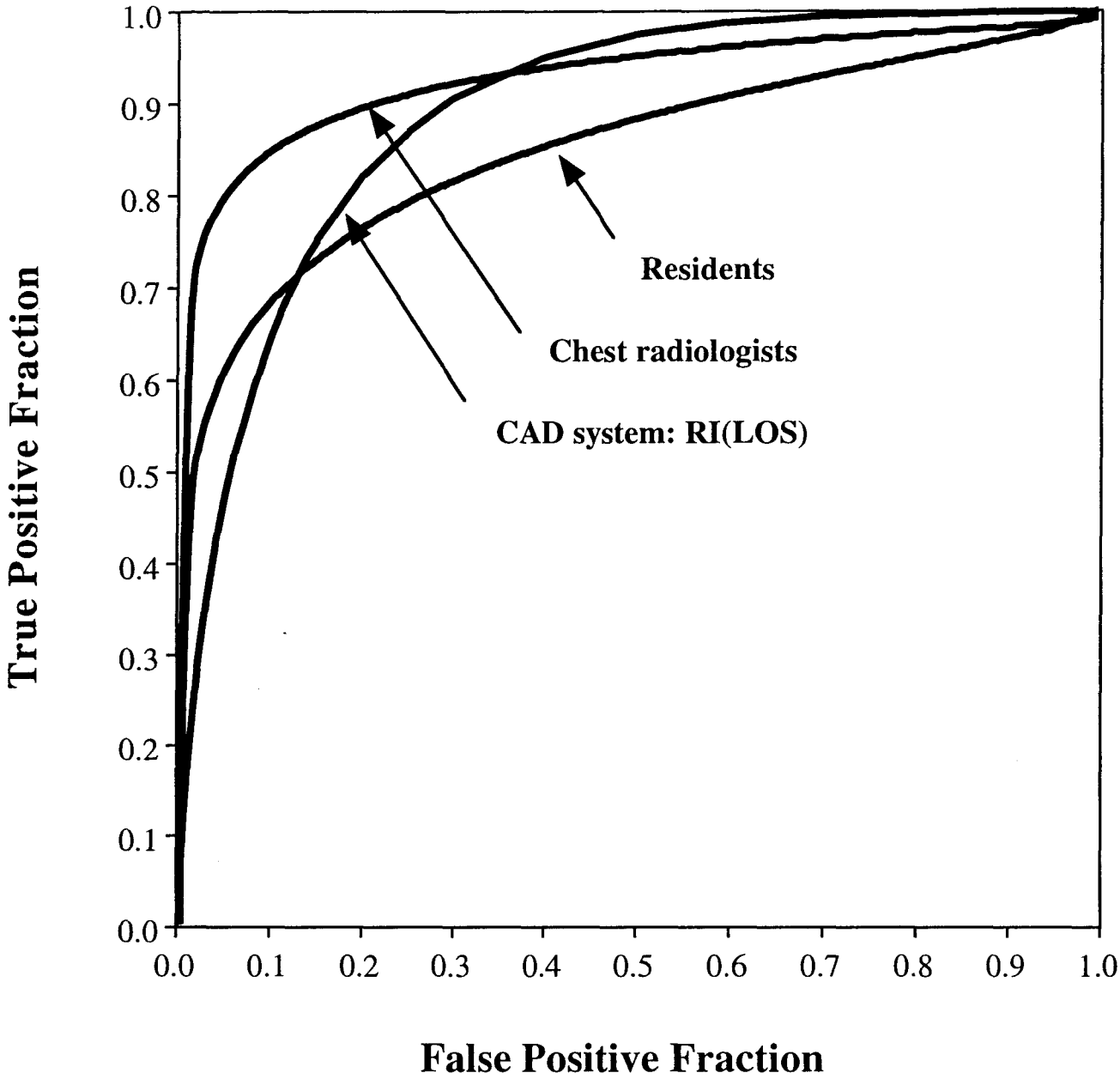

Figure 3.10(a)

ROC curve for the CAD system, and composite ROC curves for 7 chest radiologists and 7 residents. (a) The performance of RI(LOS) is inferior to the mean performance of the chest radiologists (P = 0.0074); however, the performance of RI(LOS) is superior to the mean performance of the residents (P = 0.0024).

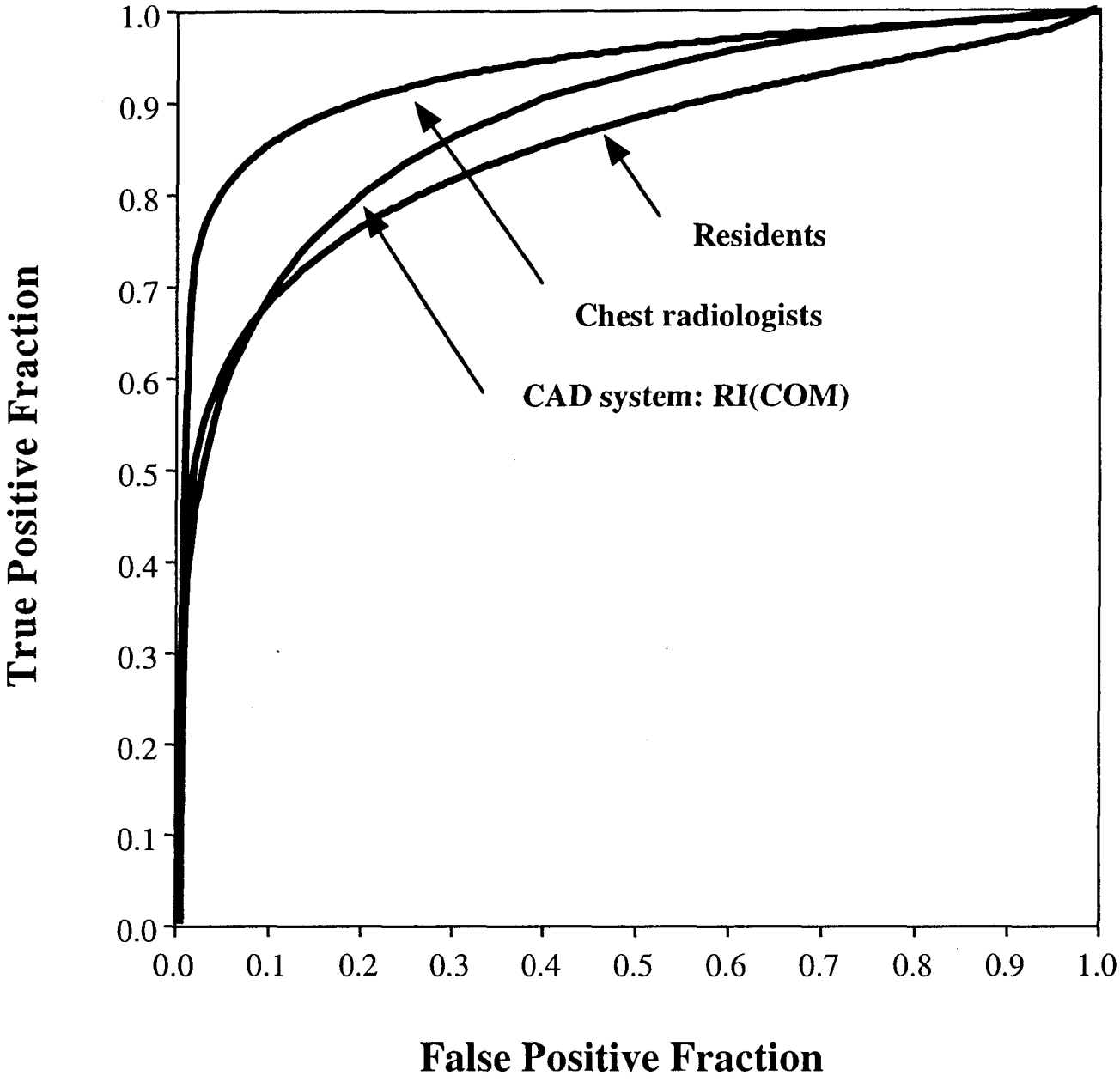

Figure 3.10(b)

ROC curve for the CAD system, and composite ROC curves for 7 chest radiologists and 7 residents. (b) The performance of RI(COM) is inferior to the mean performance of the chest radiologists (P = 0.0035); however, the performance of RI(COM) is superior to the mean performance of the residents (P = 0.0060).

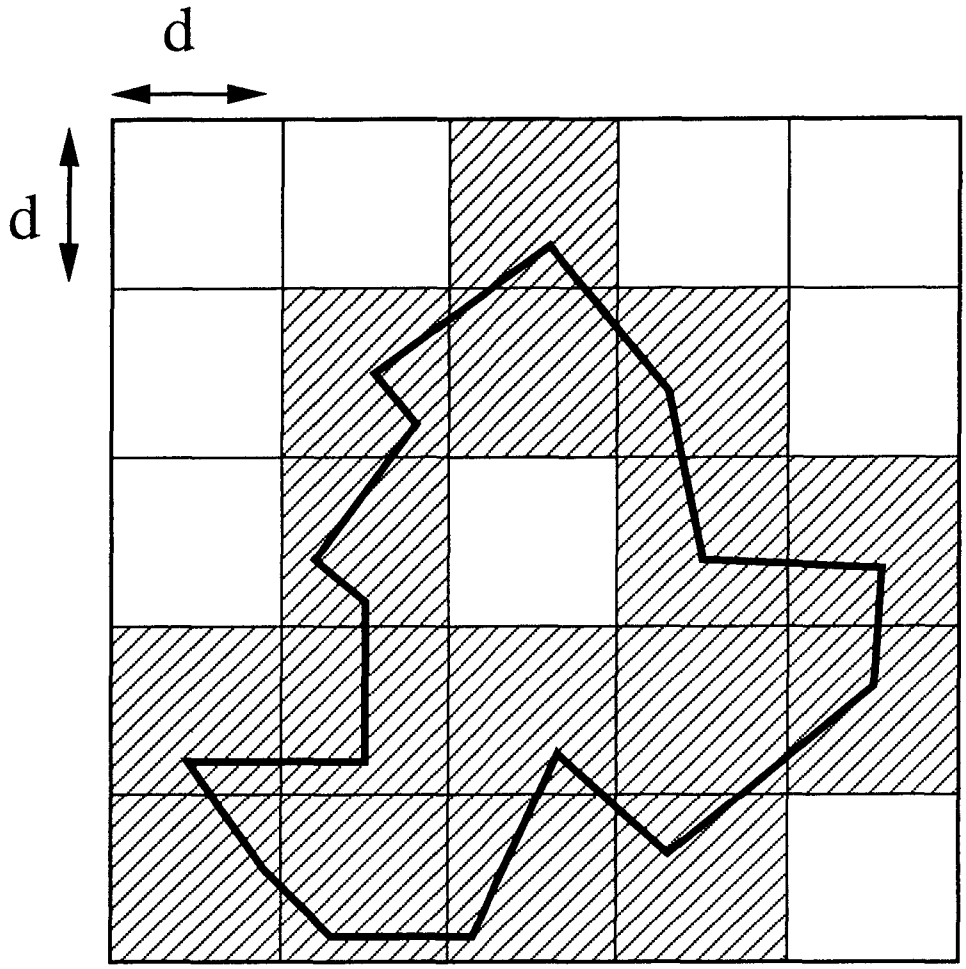

Figure 4.1

A closed curve covered with cubic grids. The size of a box is represented by d. The total number of boxes of size d was 25, and the number of boxes, N(d), required to cover the curve was 16.

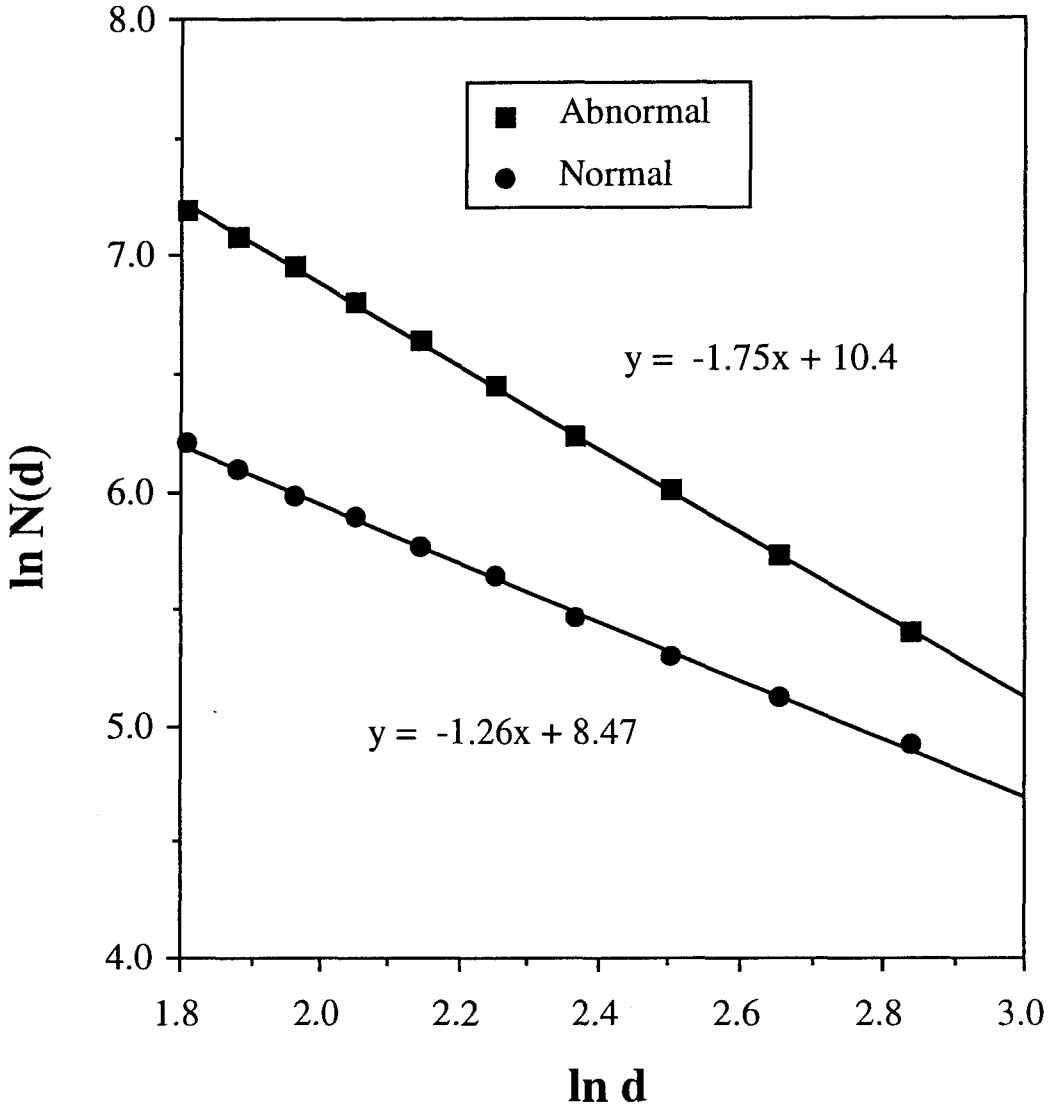

Figure 4.2

Examples of double logarithmic curves of box, d versus the number of boxes, N(d). The FD was calculated from the slope of each curve. The slope of the line for the abnormal case was -1.75, and that for the normal case was -1.26. Therefore, the FD of the abnormal case was 1.75, whereas that of the normal case was 1.26.

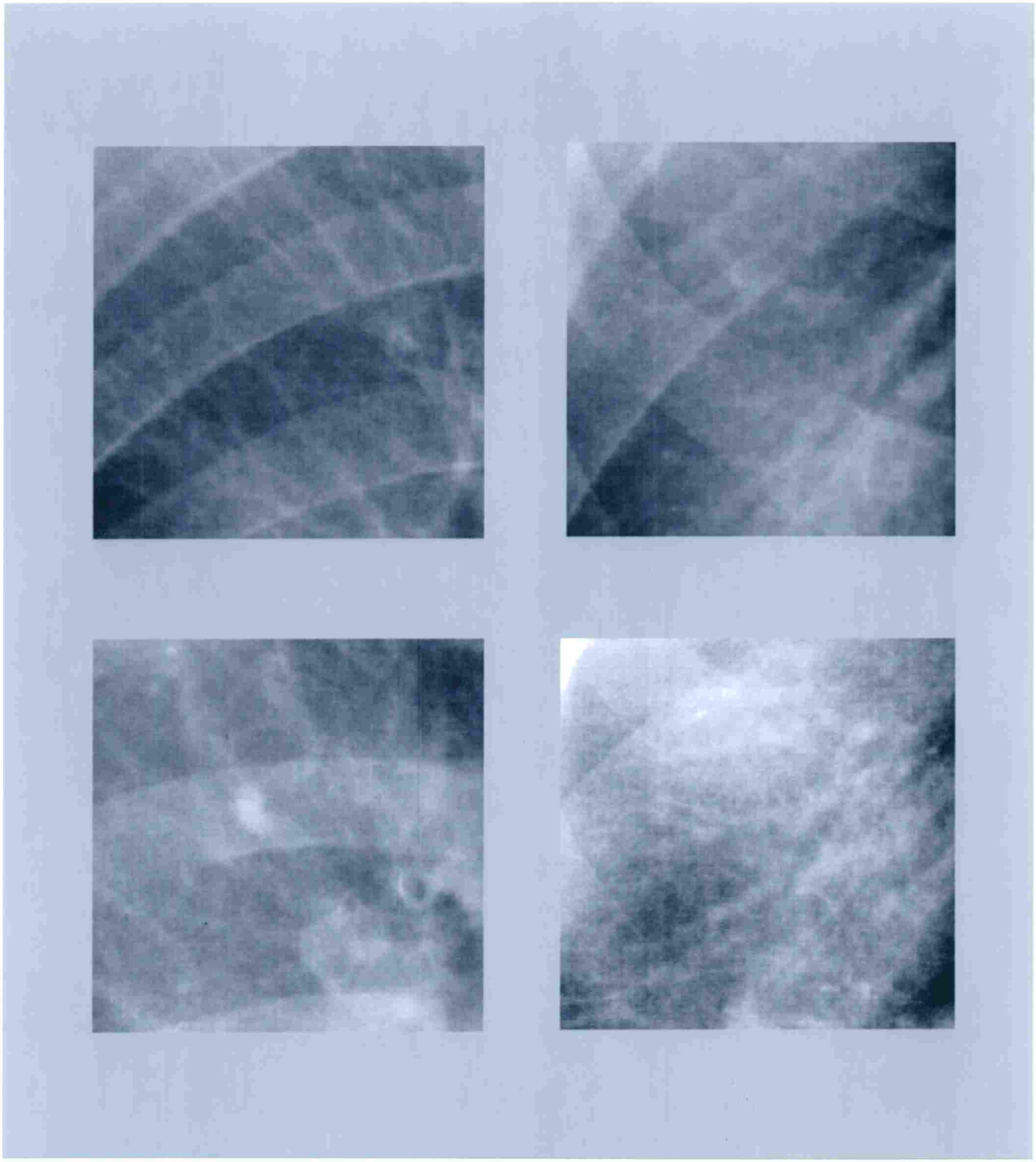

Figure 5.1

Examples of original images for image processing of the selected ROIs (296 x 296 matrix size). (a) Image of the ROI for a patient without MS in the upper lung zone **(upper left)**. (b) Image of the ROI for a patient without MS in the lower lung zone **(upper right)**. (c) Image of the ROI for a patient with MS in the upper lung zone **(lower left)**. (d) Image of the ROI for a patient with MS in the lower lung zone **(lower right)**.

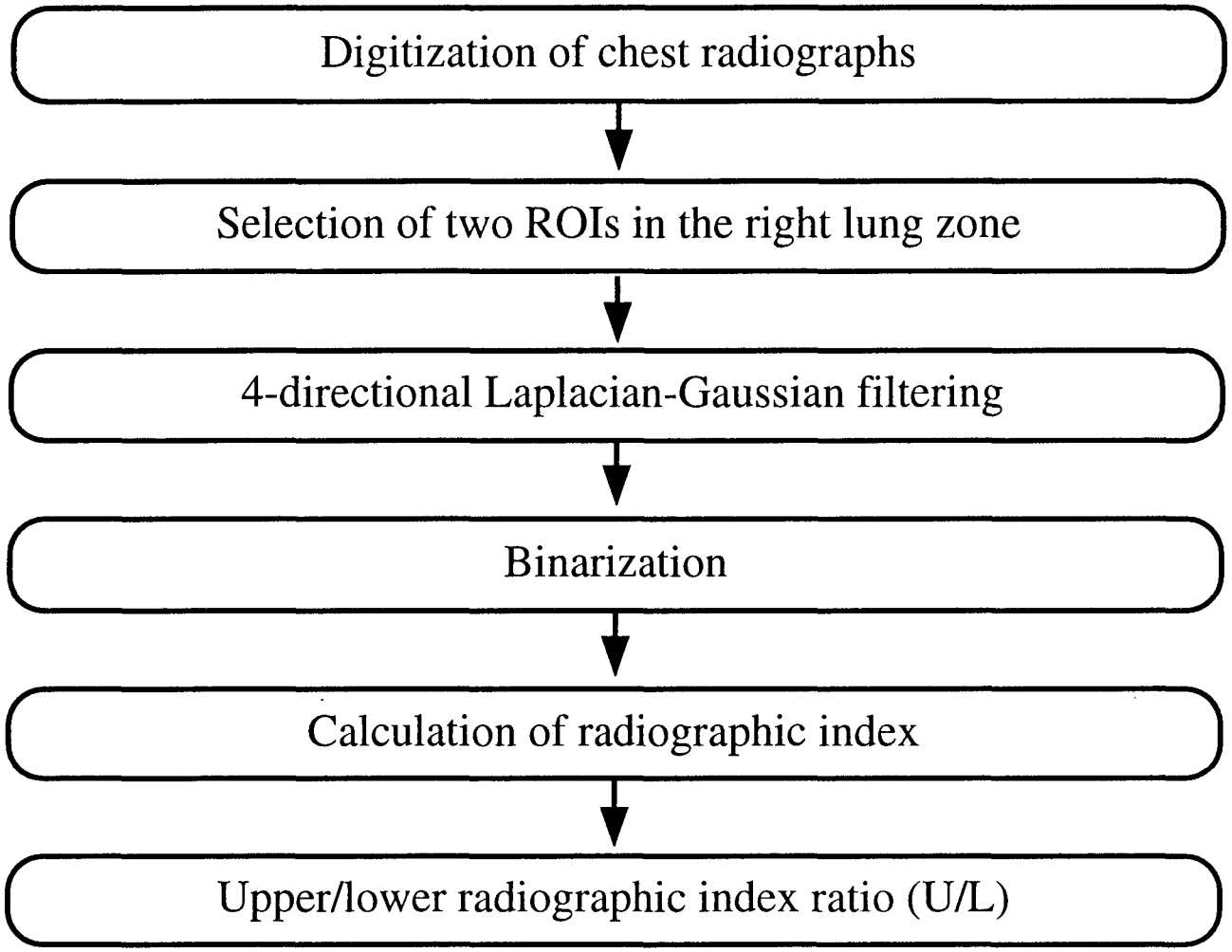

Figure 5.2

Overall scheme of a CAD system for estimating the redistribution of pulmonary blood flow in chest radiographs.

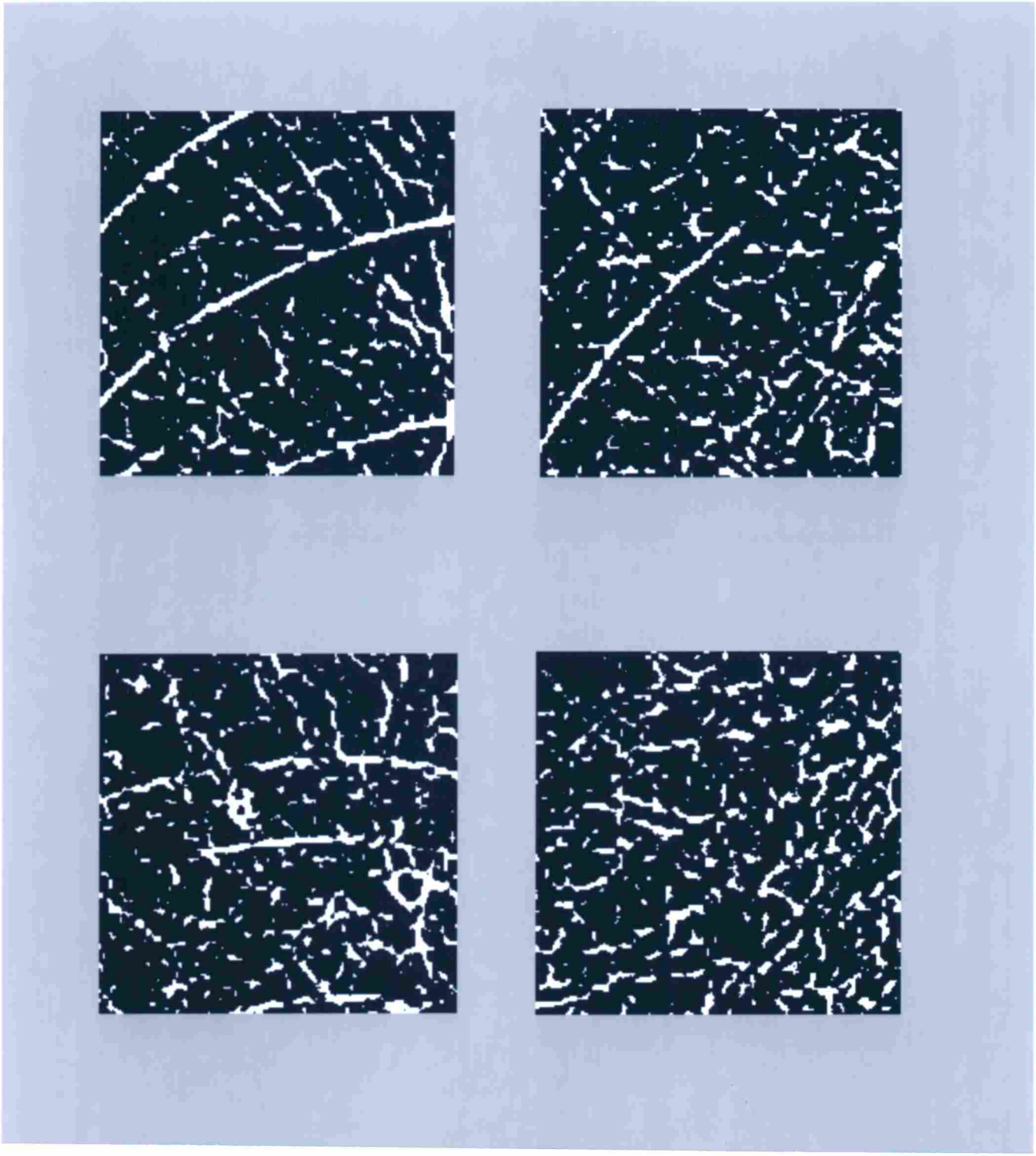

Figure 5.3

Output images of 4LG/B in selected ROIs (256 x 256 matrix size). (a) Image of the ROI for a patient without MS in the upper lung zone, obtained from the summation of 4LG/B. White regions indicate binarization of 4LG/B outputs **(upper left)**. (b) Image of the ROI for a patient without MS in the lower lung zone, obtained from summation of 4LG/B **(upper right)**. (c) Image of the ROI for a patient with MS in the upper lung zone, obtained from summation of 4LG/B **(lower left)**. (d) Image of the ROI for a patient with MS in the lower lung zone, obtained from summation of 4LG/B **(lower right)**.

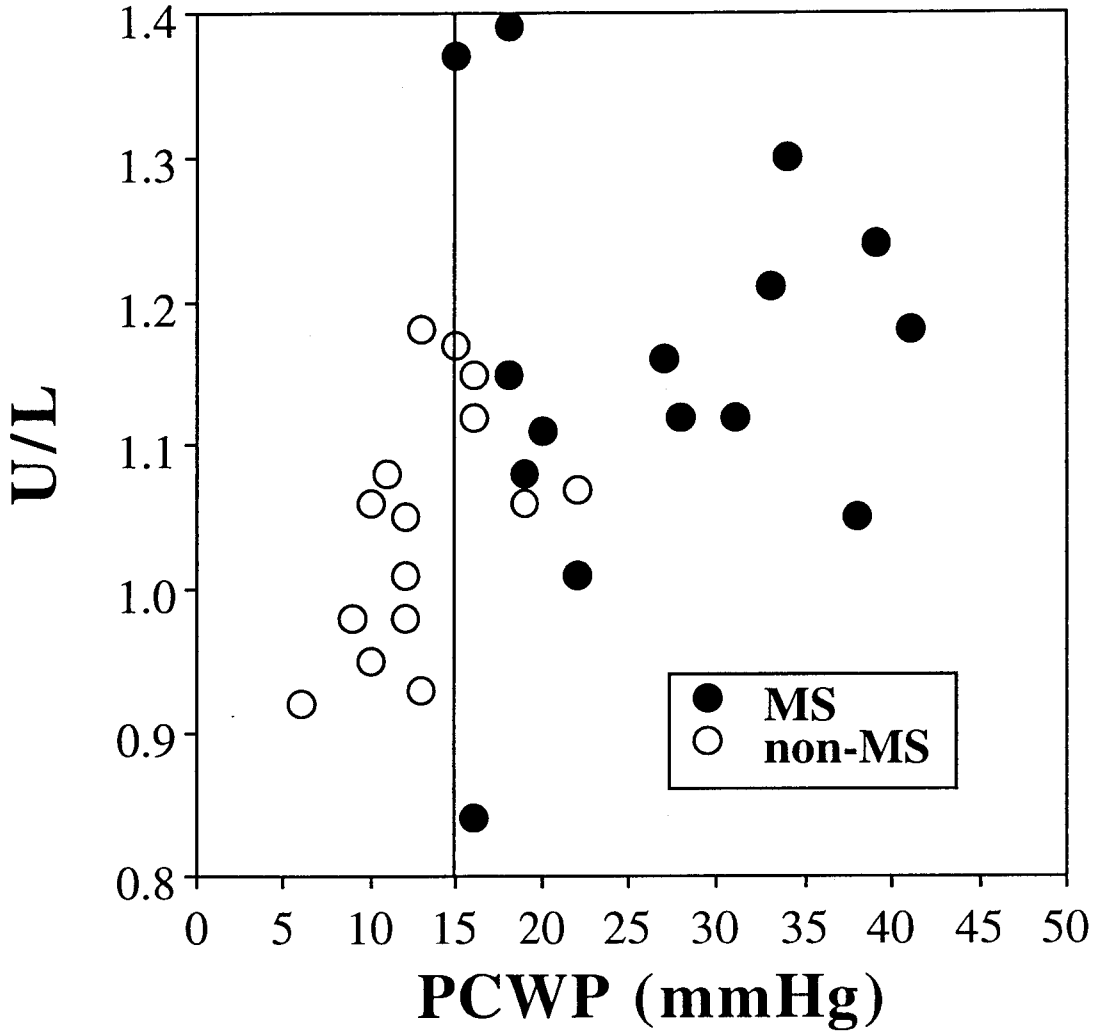

Figure 5.4

Correlation graph of PCWP values and U/L values obtained from the CAD system

References

1. Katsuragawa S, Doi K, MacMahon H. Image feature analysis and computer-aided diagnosis in digital radiography: Detection and characterization of interstitial lung disease in digital chest radiographs. Med Phys 1988;15:311-319.

2. Katsuragawa S, Doi K, MacMahon H. Image feature analysis and computer-aided diagnosis in digital radiography: Classification of normal and abnormal lungs with interstitial disease in chest images. Med Phys 1989;16:38-44.

3. Dwyer SJI, Tempelton AW, Martin NL, et al. The cost of managing digital diagnostic images. Radiology 1982;144:313-318.

4. Fraser RG, Sanders C, Barnes GT, et al. Digital imaging of the chest. Radiology 1989;171:297-307.

5. Sonoda M, Takano M, Miyahara J, Kato H. Computer radiography utilizing scanning laser simulated luminescence. Radiology 1983;148:833-838.

6. Schaefer CM, Greene RE, Oestmann JW, et al. Improved control of image optical density with low-dose digital and conventional radiography in bedside imaging. Radiology 1989;173:713-716.

7. Schaefer CM, Greene RE, Oestmann J, et al. Digital storage phosphor imaging versus conventional film radiography in CT-documented chest disease. Radiology 1990;174:207-210.

8. Schaefer CM, Greene RE, Hall DA, et al. Mediastinal abnormalities: detection with storage phosphor digital radiography. Radiology 1991;178:169-173.

9. Fajardo LL, Hillman BJ, Pond GD, Carmody RF, Johnson JE, Ferrell WR. Detection of pneumothorax: comparison of digital and conventional chest imaging. AJR 1989;152:475-480.

10. Schaefer CM, Greene R, Llewellyn HJ, et al. Interstitial lung disease: impact of postprocessing in digital storage phosphor imaging. Radiology 1991;178:733-738.

11. Elam EA, Rehm K, Hillman BJ, Maloney K, Fajardo LL, McNeill K. Efficacy of digital radiography for the detection of pneumothorax: comparison with conventional chest radiography. AJR 1992;158:509-514.

12. Lams PM, Cocklin ML. Spatial resolution requirements for digital chest radiographs: an ROC study of observer performance in selected cases. Radiology 1986;158:11-19.

13. MacMahon H, Vyborny CJ, Metz CE, Doi K, Sabeti V, Solomon SL. Digital radiography of subtle pulmonary abnormalities: an ROC study of the effect of pixel size on observer performance. Radiology 1986;158:21-26.

14. Kundel HL, Mezrich JL, Brickman I, et al. Digital chest imaging: comparison of two film image digitizers with a classification task. Radiology 1987;165:747-752.

15. Hoffmann KR, MacMahon H, Xu XW, Doi K, Chen X, Yoshimura H. Evaluation of and enhanced digital film-duplication system with ROC analysis (abstr). Radiology 1991;181(P):137.

16. Huang HK, Lo SC, Ho BK, Lou SL. Radiological image compression using error-free irreversible two-dimensional direct-cosine-transform coding techniques. J Opt Soc Am A 1987;4:984-992.

17. Jain AK. Image data compression: a review. Proc. IEEE 1981;69:349-389.

18. Ishigaki T, Sakuma S, Ikeda M, Itoh Y, Suzuki M, Iwai S. Clinical evaluation of irreversible image compression: analysis of chest imaging with computed radiography. Radiology 1990;175:739-743.

19. MacMahon H, Doi K, Sanada S, et al. Data compression: effect on diagnostic accuracy in digital chest radiography. Radiology 1991;178:175-179.

20. Aberle DR, Gleeson F, Sayre JW, et al. The effect of irreversible image compression on diagnostic accuracy in thoracic imaging. Invest Radiol 1993;28:398-403.

21. Lo SC, Huang HK. Radiological image compression: full-frame bit-allocation technique. Radiology 1985;155:811-817.

22. Reeve HCI, Lim JS. Reduction of blocking effects in image coding. Opt Eng 1984;23:34-37.

23. Tasto M, Wintz PA. Image coding by adaptive block quantization. IEEE Trans Commun Technol 1971;COM-19:957-971.

24. Chen WH, Smith CH. Adaptive coding of monochrome and color images. IEEE Trans Commun 1977;COM-25:1285-1292.

25. Wu JK, Burge RE. Adaptive bit allocation for image compression. Computer Graphics and Image Processing 1982;19:392-400.

26. Mettler FA. Diagnostic Radiology: Usage and Trends in the United States, 1964-1980. Radiology 1987;162:263-266.

27. Genereux GP. Pattern recognition in diffuse lung disease. Med Radiogr Photogr 1985;61:2-31.

28. Sutton RN, Hall EL. Texture measures for automatic classification of pulmonary disease. IEEE Trans Comput 1972;21:667-676.

29. Revesz J, Kundel HL. Feasibility of classifying disseminated diseases based on their Fourier spectra. Invest Radiol 1973;8:345-349.

30. Tully RJ, Conners RW, Harlow CA, et al. Toward computer analysis of pulmonary infiltration. Invest Radiol 1978;13:298-305.

31. Kruger RP, Thompson WB, Turner AF. Computer diagnosis of pneumoconiosis. IEEE Trans Syst Man and Cybern 1974;4:40-49.

32. Turner A, Lau F, Jacobson G. A method for the estimation of pulmonary venous and arterial pressures from the routine chest roentgenogram. AJR 1972;116:97-106.

33. Jagoe JR, Paton KA. Reading chest radiographs for pneumoconiosis by computer. Br J Ind Med 1975;32:267-272.

34. Jagoe JR. Gradient pattern coding: An application to measurement of pneumoconiosis in chest X rays. Comput Biomed Res 1979;12:1-15.

35. Katsuragawa S, Doi K, MacMahon H, et al. Quantitative computer-aided analysis of lung texture in chest radiographs. Radiographics 1990;10:257-269.

36. Mandelbrot BB. The fractal Geometry of Nature. New York, NY: W.H. Freeman 1983:1-468.

37. Feder J. Fractals. New York, NY: Plenum Press 1988.

38. Majumdar S, Weinstein RS, Prasad RR. Application of fractal geometry techniques to the study of trabecular bone. Med Phys 1993;20:1611-1619.

39. Caligiuri P, Giger ML, Favus M. Multifractal radiographic analysis of osteoporosis. Med Phys 1994;21:503-508.

40. Honda E, Domon M, Sasaki T. A method for determination of fractal dimensions of sialographic images. Invest Radiol 1991;26:894-901.

41. Honda E, Domon M, Sasaki T, Obayashi N, Ida M. Fractal dimensions of ductal patterns in the parotid glands of normal subjects and patients with Sjogren syndrome. Invest Radiol 1992;27:790-795.

42. Caldwell CB, Stapleton SJ, Holdsworth DW, et al. Characterization of mammographic parenchymal pattern by fractal dimension. Phys Med Biol 1990;35:235-247.

43. Simon M. The pulmonary veins in mitral stenosis. J Fac Radiol 1958;9:25-32.

44. Kerley P. Lung changes in acquired heart diseases. AJR 1958;80:256-263.

45. Milne E. Pulmonary blood flow distribution. Invest Radiol 1977;12:479-481.

46. Savoca C, Gamsu G, Brito A. The effect of acute pulmonary vascular resistance: significance for the interpretation of dilated upper lobe vessels on chest radiographs. Invest Radiol 1977;12:488-495.

47. Milne E. Some new concepts of pulmonary blood flow and volume. Radiol Clin North Am 1978;16:515-536.

48. Baumstark A, Swensson RG, Hessel SJ, et al. Evaluating the radiographic assessment of pulmonary venous hypertension in chronic heart disease. AJR 1984;142:877-884.

49. Kido S, Ikezoe J, Takeuchi N, et al. Interpretation of subtle interstitial lung abnormalities: conventional versus storage phosphor radiography. Radiology 1993;187:527-33.

50. Dorfmann DD, Alf EE. Maximum likelihood estimation of parameters of signal detection and determination of confidence intervals: rating method data. J Math Psychol 1969;14:109-121.

51. Swets JA. Analysis applied to the evaluation of medical imaging techniques. Invest Radiol 1979;14:109-121.

52. Metz CE. ROC methodology in radiologic imaging. Invest Radiol 1986;21:720-733.

53. Hanley JA, McNeil BJ. The meaning and use of area under a receiver operating characteristic (ROC) curve. Radiology 1982;143:29-36.

54. Kido S, Ikezoe J, Takeuchi N, et al. Interpretation of subtle interstitial lung abnormalities: conventional versus film-digitized radiography. Radiology 1994;192:171-6.

55. Kido S, Ikezoe J, Kondoh H, et al. Detection of subtle interstitial abnormalities of the lungs on digitized chest radiographs: acceptable data compression ratios. AJR 1996;167:111-5.
56. Ahmed N, Natarrajan T, Rao KR. On image processing and a discrete cosine transform. IEEE Trans Computer 1974;C-23:90-93.
57. Yonekawa H, Ishimitsu Y, Akune J, Takeuchi H. Adaptive block cosine transform coding using a new quantization algorithm. Proc SPIE 1989;1093:474-485.
58. Dorfman DD, Berbaum KS, Metz CE. Receiver operating characteristic rating analysis. Generalization to the population of readers and patients with the jackknife method. Invest Radiol 1992;27:723-731.
59. Fraser RG, Paré JAP, Paré PD, et al. Roentgenologic signs in the diagnosis of chest disease. In: Diagnosis of diseases of the chest 1988;Philadelphia,Saunders:458-687.
60. Kido S, Ikezoe J, Naito H, Masuike M, Tamura S, Kozuka T. An image analyzing system for interstitial lung abnormalities in chest radiography. Detection and classification by Laplacian-Gaussian filtering and linear opacity judgment. Invest Radiol 1994;29:172-177.
61. Marr D, Hildreth E. Theory of edge detection. Proc Royal Soc London, B 1980;207:187-217.
62. Tamura S, Uga M, Ono T. Straight line extraction for wafer alignment. Proc IEEE Computer Vision and Pattern Recognition 1983;83:285-290.
63. Kido S, Ikezoe J, Tamura S, Nakamura H, Kuroda C. A computerized analysis system in chest radiography: evaluation of interstitial lung abnormalities. J Digit Imaging 1997;10:57-64.
64. Kido S, Tamura S, Nakamura H, Kuroda C. Interstitial lung diseases: evaluation of the performance of a computerized analysis system

versus observers. Computerized Medical Imaging and Graphics 1999;23:103-110..

65. Kido S, Ikezoe J, Naito H, Tamura S, Machi S. Fractal analysis of interstitial lung abnormalities in chest radiography. Radiographics 1995;15:1457-64.

66. Morse DR, Lawton JH, Dodson MM, Williamson MH. Fractal dimension of vegetation and distribution of arthropod body length. Nature 1985;314:731-733.

67. Smith TG, Marks WB, Lange WH, Sheriff WHJ, Neal EA. A fractal analysis of cell images. J Neurosci Methods 1989;27:173-180.

68. Horsfield K. Diameters, generations, and orders of branches in the bronchial tree. J Appl Physiol 1990;68:457-461.

69. Weibel ER. Fractal geometry: a design principle for living organisms. Am J Physiol 1991;261:361-369.

70. Kido S, Kuroda C, Tamura S. Quantification of interstitial lung abnormalities on chest radiography: comparison of radiographic index and fractal dimension. Acad Radiol 1998;5:336-343.

71. Kido S, Arisawa J, Ikezoe J, Nakamura H, Kuroda C. Computerized radiographic assessment of pulmonary blood flow in patients with and those without mitral stenosis. Radiographics 1997;17:1269-1275.

72. Ikezoe J, Kohno N, Kido S, et al. Interpretation of subtle interstitial chest abnormalities: conventional radiography versus high-resolution storage-phosphor radiography--a preliminary study. J Digit Imaging 1995;8:31-36.

73. Katsuragawa S, Doi K, Nakamori N, et al. Image feature analysis and computer-aided diagnosis in digital radiography: Effect of digital parameters on the accuracy of computerized analysis of interstitial disease in digital chest radiographs. Med Phys 1990;17:72-78.

List of original publications

I. Related to this thesis

1. Kido S, Ikezoe J, Takeuchi N, et al. Interpretation of subtle interstitial lung abnormalities: conventional versus storage phosphor radiography. Radiology 1993;187:527-533.

2. Kido S, Ikezoe J, Takeuchi N, et al. Interpretation of subtle interstitial lung abnormalities: conventional versus film-digitized radiography. Radiology 1994;192:171-176.

3. Kido S, Ikezoe J, Naito H, Masuike M, Tamura S, Kozuka T. An image analyzing system for interstitial lung abnormalities in chest radiography. Detection and classification by Laplacian-Gaussian filtering and linear opacity judgment. Invest Radiol 1994;29:172-177.

4. Ikezoe J, Kido S, Takeuchi N, et al. Image quality of digital chest radiography: evaluation of subtle interstitial lung abnormalities (preliminary study). Computer Methods and Programs in Biomedicine 1994;43:107-114.

5. Kido S, Ikezoe J, Naito H, Tamura S, Machi S. Fractal analysis of interstitial lung abnormalities in chest radiography. Radiographics 1995;15:1457-1464.

6. Ikezoe J, Kohno N, Kido S, et al. Interpretation of subtle interstitial chest abnormalities: conventional radiography versus high-resolution storage-phosphor radiography -a preliminary study. J Digit Imaging 1995;8:31-36.

7. Kido S, Ikezoe J, Kondoh H, et al. Detection of subtle interstitial abnormalities of the lungs on digitized chest radiographs: acceptable data compression ratios. Am J Roentgenol 1996;167:111-115.

8. Ikezoe J, Takeuchi N, Kido S, et al. Dynamic range control processing of digital chest images: a clinical evaluation. Acta Radiol 1996;37:107-115.
9. Kido S, Arisawa J, Ikezoe J, Nakamura H, Kuroda C. Computerized radiographic assessment of pulmonary blood flow in patients with and those without mitral stenosis. Radiographics 1997;17:1269-75.
10. Kido S, Ikezoe J, Tamura S, Nakamura H, Kuroda C. A computerized analysis system in chest radiography: evaluation of interstitial lung abnormalities. J Digit Imaging 1997;10:57-64.
11. Kido S, Kuroda C, Tamura S. Quantification of interstitial lung abnormalities on chest radiography: comparison of radiographic index and fractal dimension. Acad Radiol 1998;5:336-343.
12. Kido S, Tamura S, Nakamura H, Kuroda C. Interstitial lung diseases: evaluation of the performance of a computerized analysis system versus observers. Computerized Medical Imaging and Graphics 1999;23:103-110.

II. Others

1. Kido S, Ikezoe J, Naito H, et al. Single-exposure dual-energy chest images with computed radiography: evaluation with simulated pulmonary nodules. Invest Radiol 1993;28:482-487.
2. Kido S, Ikezoe J, Naito H, et al. Clinical evaluation of pulmonary nodules with single-exposure dual-energy subtraction chest radiography with an iterative noise-reduction algorithm. Radiology 1995;194:407-412.
3. Kido S, Kuriyama K, Hosomi N, et al. Fractal analysis of pulmonary nodules in thin-section CT: differentiation of malignant nodules and benign nodules. Japanese Journal of Clinical Radiology 1998;43:25-31 (in Japanese).

4. Mihara N, Kuriyama K, Kido S, et al. The usefulness of fractal geometry for the diagnosis of small peripheral lung tumors. Nippon Acta Radiol 1998;58:148-151 (in Japanese).

5. Shikata H, Kido S, Masuyama H. Quantification of pulmonary nodule's border structure by means of Fourier transform by using chest x-ray CT images. Medical Imaging Technology 1998;16:209-214 (in Japanese).

6. Sawada A, Sato Y, Kido S, Tamura S. Detection of pulmonary nodules on lung x-ray images: studies on multi-resolution filter and energy subtraction images. Medical Imaging Technology 1999;17:81-91 (in Japanese).